Fall 2010

Investigation of Network Architecture Development and Properties in Thermoset Matrices

Jeremy Owen Swanson
University of Southern Mississippi

The University of Southern Mississippi

INVESTIGATION OF NETWORK ARCHITECTURE DEVELOPMENT AND PROPERTIES IN THERMOSET MATRICES

by

Jeremy Owen Swanson

Abstract of a Dissertation
Submitted to the Graduate School
of The University of Southern Mississippi
in Partial Fulfillment of the Requirements
for the Degree of Doctor of Philosophy

December 2010

ABSTRACT

INVESTIGATION OF NETWORK ARCHITECTURE DEVELOPMENT AND PROPERTIES IN THERMOSET MATRICES

by Jeremy Owen Swanson

July 28, 2010

Matrices employed in composite materials directly influence overall composite properties. In all thermoset materials, molecular level interactions and transformations during cure result in heterogeneous architecture. Variability in connectivity results from the often dramatic spatial and topological changes that occur during the crosslinking process. Compatibility (fillers, pigments, additives), temperature gradients and reactivity differences in the precursors only serve to increase the complexity of network formation. The objective of the research herein is to characterize and understand the relationships between cure conditions, conversion, connectivity, network architecture and properties in glassy thermosetting matrix resins.

In this research, epoxy and vinyl ester resins (VERs) were characterized to identify controlling factors in the development of network architecture and understand how they affect the mechanical properties. VERs cure under low temperature conditions (< 50 °C) via redox catalysis resulted in vitrification limiting conversion with resulting glass transition temperatures (T_gs) approximately 15 °C above the cure temperature. Subsequently, *in situ* ligand exchange altered the activity of the metal catalyst, and the reduced connectivity

of the resulting networks translated into a 30% reduction in stiffness above T_g. Network architecture was further manipulated by changing the chemical composition of the backbone. Incorporation of POSS nanoparticles into VERs resulted in changes to initial network development, with higher levels of conversion prior to vitrification. 3,3'-DDS was cured with a variety of epoxies and examined for conversion, connectivity and mechanical properties. Comparison with 4,4'-DDS revealed significant correlations between molecular level structure and properties.

The research established relationships between cure conditions, conversion, connectivity and properties in glassy thermosetting matrix resins. Specifically, the importance of early stages of network development was correlated to ultimate properties. Network architecture is sensitive to the mobility, concentration and rate of matrix development. These parameters can be altered through changes in temperature or initiating system. Control of the network architecture and ultimately mechanical properties can be achieved by tailoring reaction rate and mobility appropriately. Rapid conversion with inadequate mobility increases heterogeneity and reduces mechanical viability through poor connectivity. Conversion must occur at rates comparable to mobility to ensure high conversion and excellent connectivity to maximize mechanical properties.

The University of Southern Mississippi

INVESTIGATION OF NETWORK ARCHITECTURE DEVELOPMENT AND PROPERTIES IN THERMOSET MATRICES

by

Jeremy Owen Swanson

A Dissertation
Submitted to the Graduate School
of The University of Southern Mississippi
in Partial Fulfillment of the Requirements
for the Degree of Doctor of Philosophy

Approved:

James W. Rawlins
_____
Director

Sergei I. Nazarenko
_____

J. Paige Phillips
_____

Daniel A. Savin
_____

Jeffrey S. Wiggins
_____

_____
Dean of the Graduate School

December 2010

DEDICATION

To Derek, Darrel and Nicole
Never stop dreaming, together there is nothing we cannot accomplish

ACKNOWLEDGEMENTS

I would like to thank my dissertation advisor, Dr. James W. Rawlins, and my committee members, Dr. Sergei I. Nazarenko, Dr. J. Paige Phillips, Dr. Daniel A. Savin, and Dr. Jeffrey S. Wiggins, for their advice and support throughout the duration of this project. Special thanks to Mr. Sharathkumar K. Mendon for his significant time and effort spent assisting in many aspects of this work.

Additional thanks to the Thames-Rawlins Research Group for the collaboration, expertise and resources provided during this work. Appreciation must also be expressed to Dr. Jonathon S. Russel, assistant professor of chemistry at St. Norbert College, for his patience and guidance, as well as to Mrs. Wei Lan Lorber, for without her inspiration this journey would have never begun.

I would like to recognize the countless unnamed individuals that contributed to this work, directly or indirectly. I am extremely grateful for your contributions, as none of this would have been possible without the vast network of intellectual and emotional support developed during this process.

Finally, I would like to thank my parents, Leonard and Sandra Swanson, as well as my family for their patience, guidance, wisdom and support. My accomplishments will never adequately reflect the countless sacrifices made to ensure my success. For this I will always be grateful.

TABLE OF CONTENTS

LIST OF TABLES

LIST OF FIGURES

LIST OF EQUATIONS

CHAPTER I

INTRODUCTION

Polymer Composites

Polymer composites continue to gain importance as structural materials trend towards reduced weight and processing costs with preferential consumption of starting materials derived from renewable resources. Relative to metals, polymer composites often provide dramatic reduction in density with increased strength-to-weight and modulus-to-weight ratios. These features make polymer composites especially desirable for weight-critical components with applications in aerospace, automotive, and construction materials.

Polymer matrix composites are multi-component systems with distinct phases embedded in a polymer matrix.[1-4] Fillers range from the macro-scale (e.g., yarns, woven fabrics) to micro-scale (e.g., rubber-modified) and more recently, focus on the potential of nano-scale reinforcement (e.g., carbon nanotubes, graphene). Table 1 provides a general list of the properties of common reinforcing materials. In an ideal polymer matrix composite, the reinforcement material provides a synergistic effect that offers greater performance enhancement than the additive combination of individual components. However, composite performance is often limited by inefficient dispersion, lack of alignment, and poor interaction between the matrix and the reinforcement.

Table 1

Mechanical Property Comparison of Common Composite Fillers[1,3,4]

Material	Modulus (GPa)	Tensile Strength (GPa)	Density (g/cc)	Diameter
SWCNT/MWCNT	~1000	100-200	0.7-1.7	1-20 nm
CNF	~500	3-7	1.8-2.1	20-200 nm
Graphene	~1000	100-400	1.8-2.2	Platelet
High TS Steel	210	1.3	7.80	---
Carbon Fiber	230	3.5	1.75	5-10 mm
Aramid Fiber	60	3.6	1.44	5-10 mm
Glass Fiber	22	3.4	2.60	5-10 mm

Note. SWCNT = single walled carbon nanotubes; MWCNT = multi-walled carbon nanotubes; CNF = carbon nanofiber; High TS steel = high tensile strength steel

Relative to metals, polymer composites offers distinct advantages such as low thermal expansion coefficients, high damping capacity, and good anti-corrosive characteristics.[1,2] The much lower thermal expansion coefficients confers enhanced dimensional stability and broad application temperatures. Damping relates to the transfer of vibrational energy. The high damping capacity of polymer composites lowers noise and reduces vibration transfer to neighboring structures. [1] Polymer composites also inherently do not corrode, unlike metals where corrosion unavoidably reduces the functional lifetimes of metallic materials in many applications.

Polymer composites also require additional design criteria not typically necessary for traditional metal materials.[1-4] Metals are generally isotropic,

exhibiting uniform properties regardless of testing direction. Polymer composites however, are heavily dependent upon the direction of testing, offering significant enhancement along the fiber orientation and reduction in properties as tests move off the fiber axis. For these reasons, composites are of significant interest as they take advantage of a design structure to provide reinforcement/function in specific orientation and on many length scales.[1,4] Nanoparticles, nanoplatelets, nanotubes and nanofibers are incorporated with macro-scale fillers or fibers to provide multiple levels of structural reinforcement and interaction in so called "hybrid composites." The hybrid composite materials take advantage of interactions in the ternary system to not only provide classic composite property enhancements such as stiffness and dimensional stability, but also provide opportunities for increased functionality that include greater thermal stability, electrical conductivity, sensing and self-healing.

Thermoset Polymer Composite Matrix Materials

Structure-property relationships have traditionally been the cornerstone of engineering polymer components. Polymeric materials, in the broadest sense, are classified into two types, thermoplastics and thermosets.[1,2] Tunable chemical compositions and complex three dimensional architectures are provided by both classes of polymers Thermoplastics exist as linear, branched, hyperbranched or dendritic species and develop performance through chain entanglement, summation of intermolecular forces and the time scale of motion. Properties are manipulated through polymer architecture, chemical composition, molecular weight control and through the use of additives. These characteristics enable

precise control of parameters including glass transition temperature (T_g), modulus and toughness. Thermoset materials are covalently bonded into place and lack the capability to flow and be reformed. The covalent bonding between backbone segments in a thermoset results in enhanced properties such as elevated T_g, improved chemical/solvent resistance as well as increased dimensional and thermal stability. Therefore, it is crucial to understand the development of network architecture in high performance thermoset matrices.

Polymer composite matrices that are solely amorphous solids are devoid of crystalline domains.[1] Depending upon the intended use, such polymer composite matrices often exist as either an amorphous glass or rubber. At low temperatures, amorphous thermoset materials exist as glasses. When heated above the respective T_g, the materials transform into crosslinked rubbers. Compared to thermoplastic materials, crosslinked glassy state polymers are brittle and fracture prior to yielding. Variables during glass formation often result in inhomogeneous densification that results in non-uniform stress concentrations throughout the glassy polymer matrix. More specifically, vitrification is the process of solidification through curing and is a thermally reversible process characteristic of amorphous solids. Many amorphous polymer matrices are formed via a sol-gel process. During polymerization, as the gel or polymer component increases in concentration and the sol or monomer component decreases, the material will have reduced molecular mobility, the system T_g will approach the cure temperature and begin to vitrify. Vitrification often interferes with conversion degree and rates and can be overcome via temperature

increase. Upon cooling, the material will once again vitrify and the conditions under which this occurs often impacts stress concentrations and material performance. The stresses result in void formation and are often associated with the plastic-to-brittle or brittle-to-ductile transition that may result in propagation of internal cracks and poor product performance.

Fracture is affected most significantly by the glass formation process. [1-6] Preferentially, a material will undergo extensive plastic deformation prior to fracture (termed as a ductile fracture). Fracture toughness, evaluated in terms of critical stress intensity factor (K_{IC}) and strain energy release rate (G_{IC}), relates to the necessary force or energy requirements for crack propagation, respectively (Table 2).

Table 2

Mechanical Properties of Various Materials[1]

Material	Young's Modulus (GPa)	G_{IC} (kJ/m^2)	K_{IC} $MPa*m^{0.5}$
Rubber	0.001	13	---
Polyethylene	0.15	20	---
Polystyrene	3	0.4	1.1
Epoxy	2.8	0.1	0.5
Toughened Epoxy	2.4	2	2.2

Table 2 (continued).

Material	Young's Modulus (GPa)	G_{IC} (kJ/m^2)	K_{IC} $MPa*m^{0.5}$
Glass Fiber Reinforced Thermoset	7	7	7
Glass	70	0.007	0.7
Wood	2.1	0.12	0.5
Aluminum Alloy	69	20	37
Mild Steel	210	12	50
Steel Alloy	210	107	150

Glassy polymer matrices are inherently brittle, such that little to no plastic deformation occurs before failure. Toughening mechanisms can be incorporated to improve fracture resistance (e.g., via incorporation of particles that lead to preferential cavitation, crack deflection or shear banding prior to crack propagation).[1] Enhancing a material's ability to dissipate energy via multiple pathways prior to chain scission is crucial to the improvement of fracture toughness but often comes at the expense of static and dynamic mechanical properties and/or thermal stability.

Epoxy/VER Networks

Monomeric, oligomeric, and polymeric epoxides (also known as oxiranes) are one of the most widely used base materials in polymer composite matrices due to their broad range of tunable performance parameters and extensive application potential.[1,2,7] The amorphous thermosetting resins provide excellent mechanical properties and dimensional stability in addition to superior chemical, moisture and corrosion resistance when properly cured.[1,2] Many epoxy resins

are based on bisphenol-A (Figure 1).

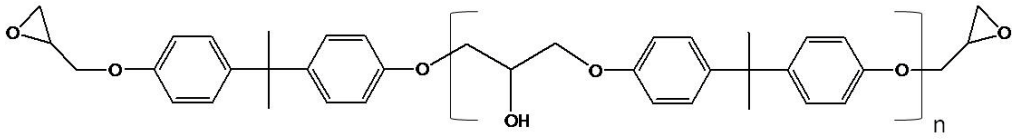

Figure 1. General structure of the diglycidyl ether of bisphenol-A.

Another important feature of these systems is their low shrinkage and lack of volatiles during cure. Curative selection is crucial in determining the processability and ultimate properties of the cured matrix. Epoxy resins cure predominantly via nucleophilic ring opening and offer two functionalities for crosslinking (i.e., the oxirane ring and the secondary hydroxyl produced via the ring opening process). The most commonly used curatives used include amines, phenols, thiols, carboxylic acids and acid anhydrides.[2, 7] A primary amine is difunctional with two active hydrogens, while a secondary amine is monofunctional with one active hydrogen. Tertiary amines are nonfunctional as they lack active hydrogens, but they catalyze the oxirane ring opening. Amine reactivity is generally governed by its nucleophilicity. Aliphatic amines are capable of curing epoxy resins on their own at ambient temperatures. However, aromatic amines require elevated temperatures to affect conversion in reasonable time periods.

One of the major derivatives of epoxies are vinyl ester resins (VERs).[2] VERs are typically synthesized by reacting methacrylic acid with epoxy resins. Styrene is added to VERs to moderate their viscosity. VERs are cured via the use of peroxide initiators to initiate free-radical reactions between the C=C bonds of styrene and the methacrylic functional epoxy. Additionally, transition metal

catalysts are often used to promote peroxide decomposition and permit low temperature cure.

The choice of the epoxy resin used for VER synthesis has a major influence on its performance properties. The diglycidyl ether of bisphenol-A (DGEBA) is the most commonly employed epoxy resin for general applications, while epoxy novolacs are preferred for applications that require high temperature resistance or enhanced solvent resistance. Brominated epoxy species are chosen for applications requiring improved fire retardancy. Recently, natural products such as epoxidized soy oil are being utilized as a greener alternative to petrochemical-based VERs.[8-10]

Gelation and vitrification play a significant role in epoxy and VER systems.[1,7] Gelation refers to a non-reversible, conversion dependent event commonly labeled as the liquid-to-rubber transition. Vitrification is a thermo-reversible process relating to the liquid/rubber-to-glass transition. Significant research efforts have been expended to better understand the complex kinetic transition from chemical control to diffusion control.[12-18] While the mobility of a given matrix often correlates to the onset of diffusion control, the crossover point is rather difficult to discern. Dusek and coworkers observed no spatial segregation in simple epoxy-amine systems as they exhibited fracture surfaces similar to other amorphous polymers.[12] In contrast, Shibayama and Ikkai commented on the heterogeneous nature of polymer gels in terms of spatial, topological and connective inhomogeneities with good agreement between theoretical and experimental data (Figure 2). [13]

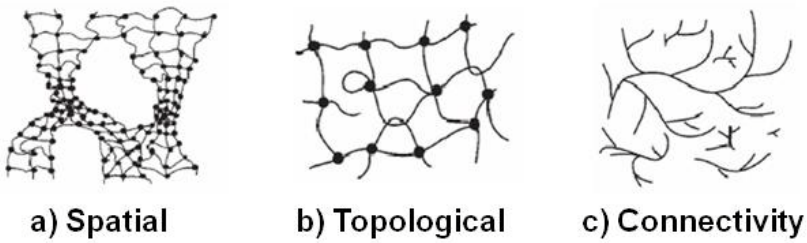

Figure 2. Types of inhomogeneity in crosslinked networks.[13]

Lange et al. used calorimetric and rheological methods to identify variation in vitrification processes and its inherent competition with gelation.[14] Prolongo et al. developed an approach to better approximate the onset of diffusion control and ultimately vitrification.[15] Meng and Simon delineated differences between mobility and diffusion, noting that the two are not equal since the transition from chemically controlled to diffusion controlled kinetics does not necessarily occur at vitrification.[16] Zhang and coworkers investigated the correlation of microgel formation to radical concentration in VERs, and good experimental agreement with their model suggested that control over microgel formation impacts overall conversion and connectivity.[17,18] A thorough understanding of these principles is necessary to further enhance composite performance.

Molecular level architecture of epoxy and VER networks are determined by the chemical structures of the starting materials.[1,2,7] Functionality and chemical structure of the monomeric and oligomeric species directly correlate to performance. The wide variability in available chemical structures is advantageous while tailoring structure-property relationships for specific applications. Designing the distance between crosslink junctions allows many macroscale properties to be altered. A generalized two-dimensional network architecture with defects is represented in Figure 3. Molecular weight between

crosslinks (M_c) and crosslink density are used to define the spatial distance between crosslink junctions as derived from rubber elasticity theory.[1,11]

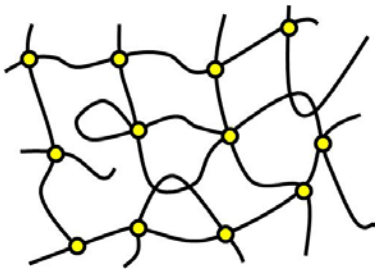

Figure 3. A crosslinked network with defects. M_c is evaluated as the distance between junctions, wavy lines represent polymer and crosslink points are represented by circles.[1]

Managing the network architecture to enhance control of mechanical properties has been the focus of much research.[19-35] Lesser and coworkers correlated network architecture to macroscale properties in terms of stiffness, cohesive energy density and yield.[19,20] Good correlation of well-defined architectures is observed, but inhomogeneous molecular level architecture results in deviation from the predicted model characteristics (Figure 4).

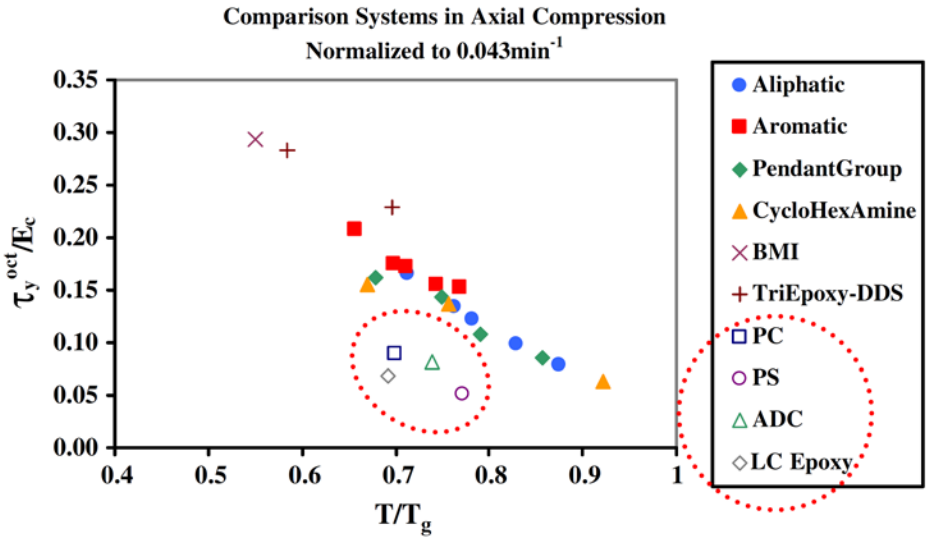

Figure 4. Molecular level architecture correlation to mechanical performance.[20]

Sambasivam et al. investigated molecular level parameters with individual chain scission events, and provided an insight to the development of fracture resistant and self-healing materials.[21] Haris and coworkers altered network architecture by blending different molecular weight precursors to yield a miscible system that exhibited increased fracture toughness without significant impact on glassy modulus (Figure 5).[23,24] The addition of a longer linear segment resulted in a bimodal network architecture and increased fracture toughness at high loading levels.

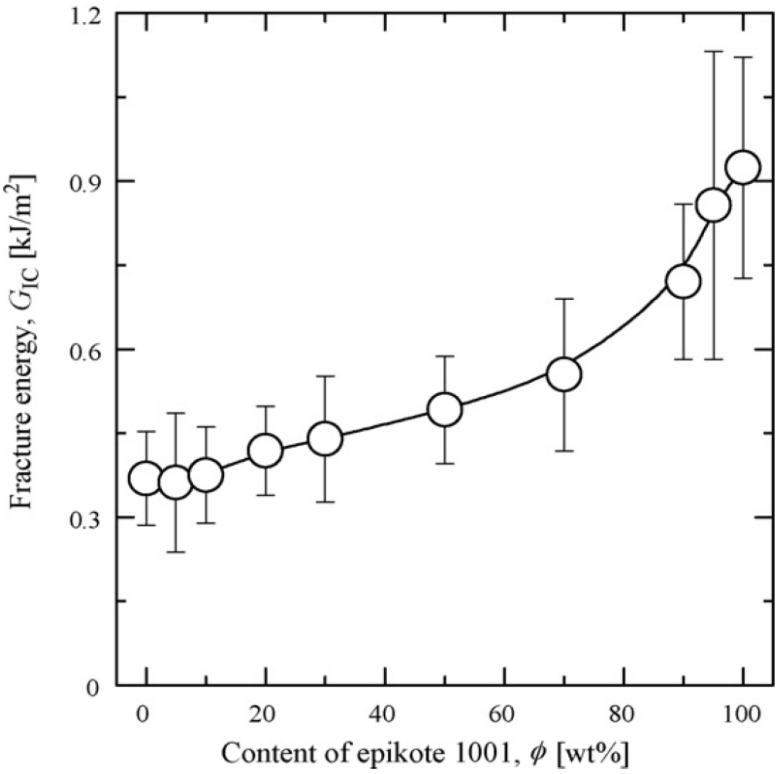

Figure 5. Increasing fracture toughness with increasing amounts of high molecular weight linear segment.[24]

Flexible diamines of various molecular weights have been blended to enhance fracture properties of epoxy resins.[25,26] Sherman et al. took advantage of the etherification side reaction to form epoxy thermosets with improved

thermo-mechanical behavior, correlating excess epoxy conversion at high temperatures to elevated stability.[28] Many of the same architectural control options have been investigated with VERs to provide enhanced understanding of copolymerization effects on macroscopic performance.[33-35]

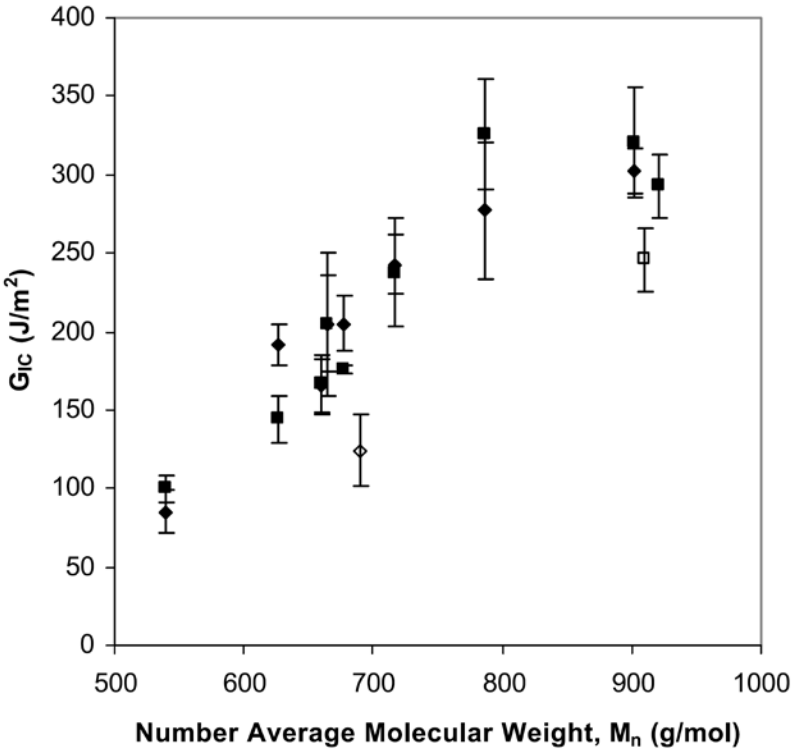

Figure 6. Increases in fracture energy are observed with increasing molecular weight of the dimethacrylate starting material for VERs.[35]

A more comprehensive understanding of molecular level network architecture is essential to ultimately broaden control over vital structure parameters such as crosslink density, morphology, residual stress and ultimate performance. However, the inherent brittleness of highly crosslinked materials limits their ability to be tough materials. Most often, secondary mechanisms of energy dissipation must be employed to maximize the potential of composite matrices within realistic design parameters.

Fracture Toughness

A commonly utilized approach to enhance the performance of brittle glassy matrices is via the addition of microparticles. Introduction of a second phase, and an interface, dramatically alters the stress transfer dissipation mechanisms within a system. The ability to increase material toughness can be achieved with both rigid and soft particles. Toughening mechanisms have been summarized by Zhao and Hoa.[36] Crack pinning occurs when the propagating crack tip is directed between two particles. Microcracking, as an energy dissipation mechanism, results in effective reduction in modulus near the frontal zone of the propagating crack tip due to void formation and expansion while simultaneously reducing stress intensity. Another energy dissipation mechanism, shear banding, incorporates shear yielding of the matrix along with cavitation within rubber particles. The combined response to the propagating crack tip results in plastic deformation that can dissipate energy associated with higher energy loads prior to failure. Particle bridging stems from rigid and flexible particles playing separate roles, i.e., the rigid particle provides compressive reinforcement while the flexible particle undergoes plastic deformation providing crack shielding. Determining the dominant mechanism and tailoring the material to that mechanism is essential for maximizing fracture resistance. Lee and Yee reported that increased shear yielding is a major mechanism of energy absorption. [37] The study evaluated increases in molecular weight between crosslinks in addition to incorporation of glass beads. Although the inherent matrix toughness played its role, the ability of the glass beads to alter the

deformation mechanism led to the largest gains in toughness.

Traditionally, toughening has been achieved through the use of elastomers. Pearson and Yee investigated mechanisms of enhancing toughness via rubber particle addition.[38-41] An order of magnitude increase in fracture toughness was observed over neat epoxy resins with the addition of carboxyl terminated butadiene nitrile rubber (CTBN). The rubber particles enhanced shear yielding while simultaneously dissipating bulk strain energy.[38] Additionally, the effect of crosslink density and T_g were deemed negligible in regards to rubber toughening, provided the matrix was sufficiently capable of yielding.[40-44] Rubber toughening exhibits a drastic increase in fracture toughness due to a change in fracture mechanism compared to the neat resin, regardless of molecular weight (Figure 7). An important point to note is that the effect of elastomer addition on toughening is amplified with increased matrix ductility.

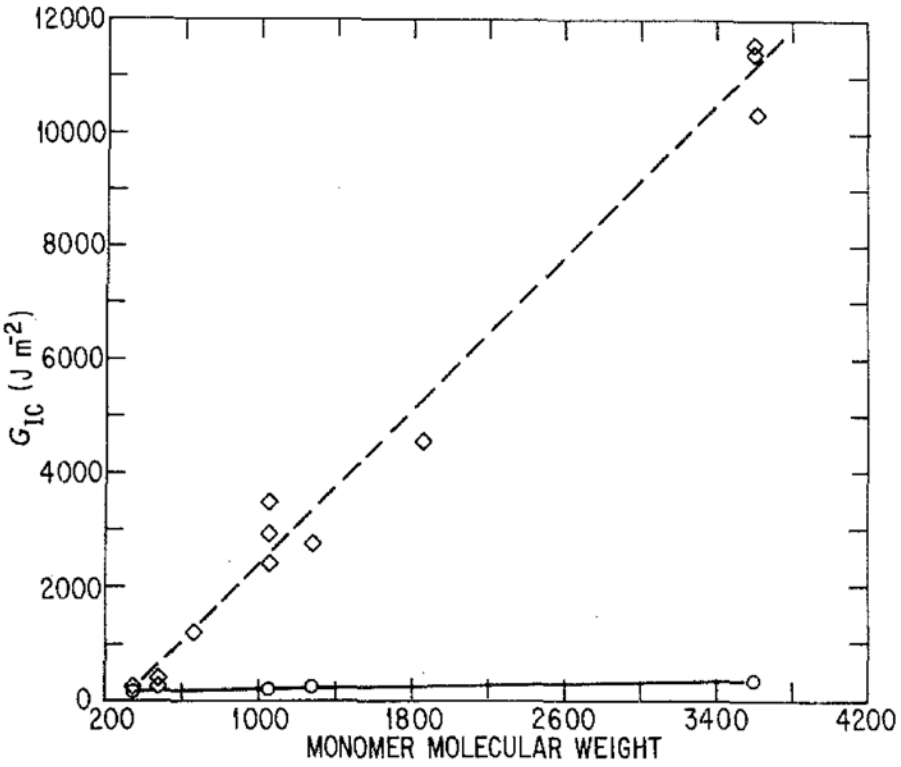

Figure 7. Modest increases are observed by altering monomer molecular weight, while the addition of an elastomer greatly enhances fracture toughness.[40]

Kinloch and Hunston also noted that toughness was not related to rubber loading, thus identifying the necessity for the matrix to preferentially yield.[45] Kim et al. isolated particle size effects on rubber toughening and delineated the importance of interparticle distance for adequate stress transfer.[46] Also, highly crosslinked systems only increase in toughness from cavitation in the rubber particle as shear yielding cannot occur prior to failure. Bagheri and Pearson also addressed this, concluding that cavitation of rubber particles does not increase toughness in highly crosslinked systems; rather their purpose is to alleviate plane strain conditions and permit plastic deformation of the matrix.[47]

CTBN-based toughening continues to be one of the most utilized toughness enhancement technologies despite issues with dispersion, mechanical property

reduction and thermal stability. To address the thermal instability of butadiene based elastomer toughening agents, Ratna evaluated liquid rubber-modified epoxies based on an acrylate alternative.[48,49] The change in elastomer to a carboxyl-terminated poly(2-ethylhexylacrylate) had little effect on toughness as compared to the CTBN based systems, but played a significant role in the development of the thermoset network and cure times. The investigation into more adaptive, multifunctional materials takes advantage of nanoscale materials and their unique performance opportunities. Hsieh *et al.* demonstrated the potential increase in toughness for "hybrid" materials containing silica nanoparticles and CTBN macroparticles.[50] By combining the benefits of conventional macroparticle rubber toughening and silica nanoparticles, these materials were successful in increasing fracture toughness of both the neat resin and a fiber reinforced laminate without reduction in other properties. Nanomaterials offer several potential advantages for enhancing toughness without sacrificing other properties including the opportunity to emulate natural materials in regards to the many hierarchical levels of architectural design.

Trends toward Nanocomposites

Toughness improvements via nanoparticles is of significant interest and is still in its early developmental stages, simplistically based upon the concept of more is better when the materials are smaller. Nanocomposites face several technical challenges from disparity in testing protocols to lack of theoretical models to explain similarity and differences in performance with macro and micro reinforcement and rubber toughening. Judging from particle-polymer

interactions, nanoparticles have a much greater influence on the interfacial region between bulk polymer matrix and nanoparticles than macroscale particles. Enhanced interfacial interactions result in improved stress transfer and increased strength/stiffness, provided the materials have uniform dispersion.[51,52] Additionally, the required loading levels for property improvement tend to decrease with smaller particle size. Bucknall and Paul developed a new model for particle size dependence, concluding that cavitation is possible in particles between 30-80 nm with increasing toughness as particle size increases.[53] However, larger particles simultaneously reduce energy requirements for craze initiation, leading to brittle failure prior to sufficient yielding of the matrix and only a minor increase in toughness. Utility of block copolymer self assembly to enhance fracture toughness without sacrificing modulus or T_g is of current interest.[54-56] Micelle forming block copolymers self-assemble during polymerization, providing enhancement to fracture toughness (Figure 8). Block copolymers provide toughness enhancement and improve processability without significantly sacrificing thermal properties. Additionally, incorporating a matrix-soluble block permits better interaction between the matrix and particle, thus reducing the negative impact on modulus and T_g.

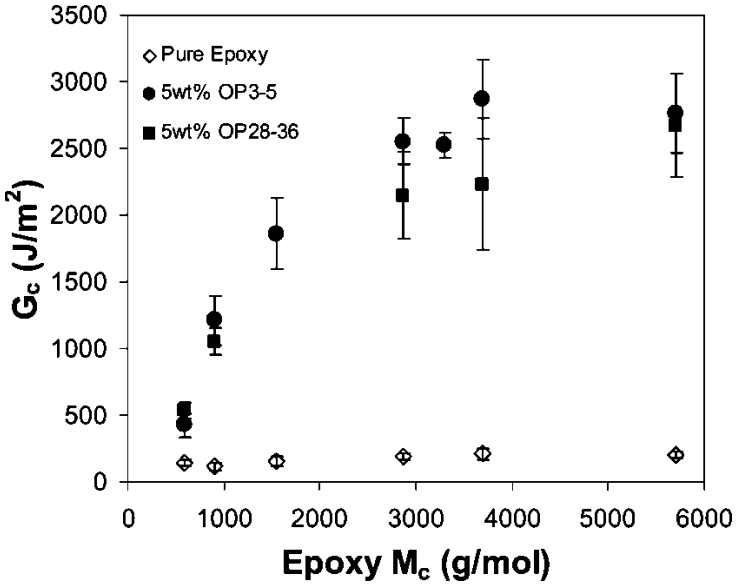

Figure 8. Addition of block copolymers results in increased toughness regardless of the block copolymer molecular weight. OP3-5 and OP28-36 refer to different compositions and molecular weights of a poly(ethylene oxide)-*b*-poly(ethylene-*alt*-propylene) block copolymer. As noted earlier, higher toughness is attained through decreased T_g and modulus, i.e., higher matrix ductility.

Traditional polymer nanocomposites are based upon reinforcements such as aluminum, carbon, clay, silica or titanium, with at least one dimension at the nanometer scale.[1,4] Nanocomposites have the potential to drastically improve mechanical properties while also imparting multifunctionality to materials, such as electrical, thermal, and optical properties not typical of current and classical composites. The promise of nanocomposites include potential performance improvements at a much lower volume fraction of filler, mainly on the basis of increased surface area-to-volume differences and improved interaction.[1,3] Nanoparticles exist in a variety of morphologies including spherical, platelet, fiber/fibrous and tubule.

Montmorillonite nanoclays have been investigated for a variety of applications, including enhanced mechanical properties, increased barrier

performance and catalysis. Nanoclays exist as aggregated platelets stabilized by counterions in the gallery spacing. Exchanging the counterions enables the basal spacing of the aggregated sheets to be adjusted and allows for a variety of dispersion/exfoliation techniques to be used for incorporation into the polymer matrix. Nanoclays have been shown to provide increased fracture toughness, although they are more beneficial in maintaining modulus and strength in hybrid clay-rubber particle reinforced materials.[57] Marouf et al. determined that a hybrid clay-core shell rubber nanocomposite was more detrimental to fracture toughness than a rubber particle modified system, possibly due to competition between energy absorption mechanisms.[58]

Carbon nanotubes exist primarily as single and multiwall materials and are challenged only by graphene in terms of tensile modulus and strength.[59-61] Other morphologies include nanowhiskers, nanobuds, nanotorus and cupstacked carbon nanotubes. Crystallographic defects are detrimental to carbon nanotubes performance in terms of mechanical properties as well as thermal and electrical conductivity, but are often utilized during functionalization to enhance dispersion within a given polymer matrix. [61] Alignment of carbon nanotubes is of considerable interest.[62-64] Garcia et al. used aligned nanotubes to reinforce and enhance prepreg interfacial adhesion, leading to much greater fracture resistance than the control, with crack bridging being evident from fracture micrographs.[64]

Graphene sheets have been investigated for performance improvements.[65-72] Graphene is a single atom thick, planar sheet of sp^2-bonded

carbon atoms. Much like carbon nanotubes, graphene often requires oxidation and functionalization to aid dispersion. However, this directly affects the mechanical, electrical and thermal potential of graphene. Graphene has shown immense potential by increasing fracture toughness by 60% at only 0.1 weight% loading in an epoxy matrix, which is significantly higher than that offered by clays or carbon nanotubes and at much lower loadings.[72]

Polyhedral oligomeric silsesquioxanes (POSS) are nanoparticles of significant interest due to their nanometer dimensions, uniform structure and wide range of chemical functionality. POSS incorporation has shown potential in enhancing T_g, surface characteristics, thermal stability, barrier properties and flame retardance.[73-76] POSS also has the ability to enhance T_g without increasing crosslink density or modulus.[73] POSS dispersion is enhanced with increased functionality, but mechanical properties rely heavily on POSS-POSS interactions.[74] Highly functional POSS reactivity affects several thermal and viscoelastic properties simultaneously.[76] Despite these successes, the true potential of POSS-based nanocomposites has not been realized, and these materials will continue to garner significant attention.

References

1. Sperling, L. H. *Introduction to Physical Polymer Science*, 4th Ed.; John Wiley & Sons, Inc.: New Jersey, 2006.
2. Dostal, C.A. *Engineered Materials Handbook. Vol 2. Engineering Plastics.* CRC Press LLC: 1988.
3. Dostal, C.A. *Engineered Materials Handbook Vol 1. Composites*. CRC Press LLC: 1987.
4. Mallick, P.K. *Fiber Reinforced Composites, 3rd Ed.* Taylor & Francis Group, LLC: Florida, 2008.
5. Krishnamachari, S.I. *Applied Stress Analysis of Plastics, A Mechanical Engineering Approach*. Van Nostrand Reinhold: New York, 1993.
6. (a)Van der Sanden, M.C.M., Meijer, H.E.H., Lemstra, P.J. *Polymer,* **1993,** 34, 2148; (b)Van der Sanden, M.C.M., Meijer, H.E.H., Tervoort, T.A. *Polymer,* **1993**, 34, 2961; (c)Van der Sanden, M.C.M., Meijer, H.E.H. *Polymer*, **1993**, 34, 5063; (d)Van der Sanden, M.C.M., Meijer, H.E.H *Polymer,* **1994**, 35, 2774; (e)Van der Sanden, M.C.M., Buijs, L.G.C., de Bie, F.O., Meijer, H.E.H. *Polymer,* **1994**, 35, 2783; (f)Van der Sanden, M.C.M., Meijer, H.E.H. *Polymer*, **1994**, 35, 2774.
7. May, C.A. *Epoxy Resins Chemistry and Technology, 2nd Ed*. Marcel Dekker, Inc.: New York, 1988.
8. Capanella, A., La Scala, J., Wool, R. *Polymer Engineering and Science*, **2009**, 49, 2384.
9. Lu, J., Wool, R. *Composites Science and Technology,* **2008**, 68, 1025.

10. Lu, J., Wool, R. *Polymer Engineering and Science,* **2007**, 47, 2384

11. Dusek, K., Duskova-Smrckova, M. *Progress in Polymer Science*, **2000**, 25, 1215.

12. Dusek, K., Plestil, J., Lednicky, F., Lunak, S. *Polymer,* **1978**, 19, 393.

13. Ikkai, F., Shibayama, M. Jo*urnal of Polymer Science: Part B: Polymer Physics,* **2005**, 43, 617.

14. Lange, J., Altmann, N., Kelly, C.T., Halley, P.J. *Polymer*, **2000**, 41, 5949.

15. Prolongo, S.G., Mikes, F., Cabanelas, J.C., Paz-Abuin, S., Baselga, J. *Journal of Materials Processing Technology,* **2003**, 143, 546.

16. Meng, Y., Simon, S. L. *Thermochimica Acta,* **2005**, 437, 179.

17. Zhang, Y., Kranbuel, D., Sautereau, H., Seytre, G., Dupuy, J. *Macromolecules,* **2008**, 41, 708.

18. Zhang, Y., Kranbuel, D., Sautereau, H., Seytre, G., Dupuy, J. *Macromolecules,* **2009**, 42, 203.

19. Crawford, E., Lesser, A.J. *Journal of Polymer Science: Part B: Polymer Physics,* **1998**, 36, 1371.

20. Calzia,K.J., Lesser, A.J. *Journal of Materials Science,* **2007**, 42, 5229.

21. Sambasivam, M., Klein, A., Sperling, L.H. *Journal of Applied Polymer Science,* **1997**, 65, 1001.

22. Vakil, U.M., Martin, G.C. *Journal of Applied Polymer Science,* **1992**, 46, 2089.

23. Haris, A., Adachi, T., Araki, W. *Materials Science and Engineering A,* **2008**, 496, 337.

24. Haris, A., Adachi, T., Araki, W. *Journal of Material Science,* **2008**, 43, 3289.

25. Shan, L., Verghese, K.N.E., Robertson, C.G., Reifsneider, K.L. *Journal of Polymer Science: Part B: Polymer Physics*, **1999**, 37, 2815.

26. Yang, G., Fu, S.-Y., Yang, J.-P. *Polymer,* **2007**, 48, 302.

27. Calventus, Y., Montserrat, S., Hutchinson, J.M. *Polymer,* **2001**, 42, 7081.

28. Sherman, C.L., Zeigler, R.C., Verghese, N.E., Marks, M.J. *Polymer,* **2008**, 49, 1164.

29. Harismendy, I., Miner, R., Valea, A., Llano-Ponte, R., Mujika, F., Mondragon, I. *Polymer*, **1997**, 38, 5573.

30. Zhang, S.-Y., Ding, Y.-F., Li, S.-J., Luo, X.-W., Zhou, W.-F. *Corrosion Science,* **2002**, 44, 861.

31. Marks, M.J., Verghese, N.E., O'Connell, C.L., Mansour, A.S. *Journal of Polymer Science: Part B: Polymer Physics,* **2009**, 47, 72.

32. Jain, P., Choudhary, V., Varma, I.K. *European Polymer Journal,* **2003**, 39, 181.

33. Scott, T.F., Cook, W.D., Forsythe, J.S. *European Polymer Journal,* **2008**, 44, 3200.

34. Ganglani, M., Carr, S.H., Torkelson, J.M. *Polymer,* **2002**, 43, 2747.

35. La Scala, J.J., Orlicki, J.A., Winston, C., Robinette, E.J., Sands, J.M., Palmese, G.R. *Polymer*, **2005**, 45, 2908.

36. Zhao, Q. & Hoa, S.V. *Journal of Composite Materials,* **2007**, 41, 201.

37. Lee, J., Yee, A. *Polymer*, **2000**, 41, 8375.

38. Yee, A.F., Pearson, R.A. *Journal of Materials Science,* **1986**, 21, 2462.

39. Yee, A.F., Pearson, R.A. *Journal of Materials Science,* **1986**, 21, 2475.

40. Yee, A.F., Pearson, R.A. *Journal of Materials Science,* **1989**, 24, 2571.

41. Pearson, R.A., Yee, A.F. *Journal of Materials Science,* **1991**, 26, 3828.

42. Levita, G., De Petris, S., Marchetti, A., Lazzeri, A. *Journal of Materials Science,* **1991**, 26, 2348.

43. Iljima, T., Naoto, Y., Tomoi, M. *European Polymer Journal, **1992***, 28, 573.

44. Mafi, E.R., Ebrahimi, M., Moghbeli, M.R. *Journal of Polymer Engineering*, **2009**, 29, 293.

45. Kinloch, A.J., Hunston, D.L. *Journal of Materials Science Letters,* **1987**, 6, 131.

46. Kim, D.S., Cho, K., Kim, J.K., Park, C.E. *Polymer Engineering and Science,* **1996**, 36, 755.

47. Bagheri, R., Pearson, R.A. *Polymer,* **2000**, 41, 269.

48. Ratna, D. *Polymer*, **2001**, 42, 4209.

49. Ratna, D., Banthia, A.K. *Polymer International,* **2000**, 49, 281.

50. Hsieh, T.H., Kinloch, A.J., Masania, K., Lee, J.S., Taylor, A.C., Sprenger, S. *Journal of Materials Science*, **2010**, 45, 1193.

51. Ruiz-Perez, L., Royston, G.J., Fairclough, P.A., Ryan, A.J. *Polymer,* **2008**, 49, 4475.

52. Sun, L., Gibson, R.F., Gordaninejad, F., Suhr, J. *Composites Science and Technology,* **2009**, 69, 2392.

53. Bucknall, C.B., Paul, D.R. *Polymer,* **2009**, 50, 5539.

54. Dean, J.M., Verghese, N.E., Pham, H.Q., Bates, F.S. *Macromolecules,* **2003**, 36, 9267.

55. Thompson, Z.J., Hillmyer, M.A., Liu, J., Sue, H.-J., Dettloff, M., Bates, F.S. *Macromolecules*, **2009**, 42, 2333.

56. Liu, J., Sue, H-J., Thompson, Z.J., Bates, F.S., Detloff, M., Jacob, G., Verghese, N., Pham, H. *Macromolecules,* **2008**, 41, 7616.

57. Subramaniyan, A.K., Sun, C.T. *Composites: Part A,* **2007**, 38, 34.

58. Marouf, B.T., Pearson, R.A., Bagheri, R. *Materials Science and Engineering,* **2009**, 49, 515.

59. Coleman, J.N., Khan, U., Blau, W.J., Gun'ko, Y.K. *Carbon*, **2008**, 44, 1624.

60. Bose, S., Khare, R.A., Moldenaers, P. *Polymer,* **2010**, 51, 975.

61. Tasis, D., Tagmatarchis, N., Bianco, A., Prato, M. *Chemical Reviews*, **2006**, 106, 1105.

62. Zhu, Y-F., Ma, C., Zhang, W., Zhang, R-P., Koratkar, N., Liang, J. *Journal of Applied Physics,* **2009**, 105.

63. Ma, C., Zhang, W., Zhu, Y., Ji, L., Zhang, R., Koratkar, N., Liang, J. *Carbon*, **2008**, 46, 706.

64. Garcia, E.J., Wardle, B.L., Hart, J.A. *Composites: Part A,* **2008**, 39, 1065.

65. Yan, J., Wei, T., Shao, B., Fan, Z., Qian, W., Zhang, M., Wei, F. *Carbon*, **2010**, 48, 487.

66. Hong, W., Bai, H., Xu, Y., Yao, Z., Gu, Z., Shi, G. *Journal of Physical Chemistry: Part C,* **2010**, 114, 1822.

67. Yan, J., Wei, T., Fan, Z., Qian, W., Zhang, M., Shen, X., Wei, F. *Journal of Power Sources,* **2010**, 195, 3041.

68. Kim, H., Macosko, C.W. *Polymer,* **2009**, 50, 3797.

69. Xu, Y., Hong, W., Bai, H., Li, C., Shi, G. *Carbon,* **2009**, 47, 3538.

70. Wang, S., Tambraparni, M., Qui, J., Tipton, J., Dean, D. *Macromolecules*, **2009**, 49, 5251.

71. Liu, J., Yan, W., Tao, L., Li, D., Boyer, C., Davis, T.P. *Journal of Polymer Science: Part A: Polymer Chemistry,* **2010**, 48, 425.

72. Rafiee, M.A., Rafiee, J., Wang, Z., Song, H., Yu, Z-Z., Koratkar, N. *ACS Nano,* **2009**, 3, 3884.

73. Lee, A., Lichtenhan, J. *Macromolecules,* **1998**, 31, 4970.

74. Strachota, A., Kroutilova, I., Kovarova, J., Matejka, L. *Macromolecules,* **2004**, 37, 9457.

75. Glodek, T., Boyd, S., McAninch, I., LaScala, J. *Composites Science and Technology,* **2008**, 68, 2994.

76. Ragosta, G., Musto, P., Abbate, M., Scarinzi, G. *Polymer,* **2009**, 50, 5518.

CHAPTER II

RESEARCH PREVIEW

Polymeric Network Architecture

Matrices in composite materials directly influence overall composite properties. In all thermoset materials, heterogeneities or inhomogeneities exist as a consequence of molecular level interactions and cure related material property transformations. The characteristics are increasingly complex as the average functionality increases. Hierarchical control of network architecture development at many length scales is of significant fundamental interest as it provides the opportunity to engineer performance above current attainable levels, and multiple levels of function (e.g., sensing, self-healing and energy harvesting). The objective of the research herein is to characterize and understand the relationships between cure conditions, conversion, connectivity, network architecture and properties in glassy thermosetting matrix resins.

In theory, a homogenously connected network allows chains to deform uniformly and within critical stress limitation, thus affording relaxation and maximizing energy requirements for degradation/failure almost regardless of mode (e.g., chemical, thermal, mechanical). However, practical network formation conditions often lead to irregularity in network architecture through sol-gel solubility parameter differences, thermal gradients (via exothermic or endothermic reactions) and varying rates of conversion.

Depending on the polymerization type and parameters, each material develops a unique network structure. Variability is due to several factors related

to the crosslinking process such as excluded volume effects, diffusion limits, solubility variations and substrate interactions. Compatibility (fillers, pigments, additives), temperature gradients and reactivity differences in the precursors play an important role in the level of inhomogeneous architectural development. Variability may produce macroscopic flaws in the system or subtle nodular variations on a scale from 10-50 nm and lead to drastic differences in network properties based on the work of Shibayama and Ikkai discussed in the introduction. Spatial inhomogeneities result from the non-uniform spatial distribution of crosslinks, while topological inhomogeneities are due to trapped entanglements, loops and dangling chain ends. Connectivity inhomogeneities are directed by the size and distribution of nodes within the system. Each of these deviations from ideal network architecture is a result of changes in reaction conditions, conversion, functionality and diffusion within a given system. Network defects lead to architectural stresses, drastically affecting properties and potentially catalyzing failure and/or degradation. Inhomogeneous networks, however, maintain stress concentrations and have higher potential for catastrophic degradation. Simultaneously, variability in network architecture may result in improved properties (ultimate tensile strength, fracture toughness, etc.) in static testing but suffer dramatically when tested under dynamic conditions such as fatigue loading. The failure of polymeric materials initiates at the weakest linkages according to theory, yet very little experimental data exists to produce a clear understanding of molecular force distribution under mechanical load for glassy polymeric materials. Flaws occurring during network formation

promote degradation pathways of these materials and yet represent potential dissipation mechanisms. Higher stress concentrations result from the inability of individual chains to relax to the same extent as neighboring chains or highly reactive sites and produce inhomogeneities and weak points within the network.

Network Structure, Yield, and Fracture

Material failure is a direct result of molecular level degradation, albeit very difficult to capture, quantify, and identify at the bond dissociation level. Network failure results when the individual chains are unable to adequately respond to the applied deformation or energy. Unlike metals, polymer networks are not typically able to exhibit plastic deformation while maintaining performance, consequently, the energy is released through another mechanism, such as chain scission. An elevated stress concentration results in higher probability for continued scission and ultimately leads to catastrophic failure.

Chain pullout and chain scission are two types of energy dissipation mechanisms within polymer networks. Chain pullout occurs when polymer chains are able to slide or retract from the stressed location rather than break. Dangling chain ends and physical entanglements within the network structure often provide energy release in this manner. Both pathways result in loss of dimensional stability. Chain scission (i.e., bond rupture) is the primary means of molecular failure within polymer networks, and can be initiated through any of the forces discussed above. Activation energy of covalent linkages must be overcome for chain scission to occur and yet the reported energy values required for these events on a molecular level varies dramatically in the published

literature. This energy requirement may be lowered significantly by the existence of network defects, including spatial and topological gradients in chemical structure as well as residual catalysts, dissolved oxygen and other activated species that may promote degradation. From an engineering standpoint, conventional thermosetting polymers are extremely brittle for use as matrices in composites applications. This has important consequences as polymer composites seek to replace metals in many applications. Metals can often sustain significant plastic deformations prior to failure while maintaining performance. On the other hand, many composites suffer brittle failure in the polymer matrix prior to any plastic deformation. If the polymer matrix cannot yield to accommodate the stress, energy cannot be dissipated via plastic deformation and the result is catastrophic failure.

Mechanisms may be introduced to enhance the energy absorption/dissipation capabilities of a given polymer matrix. Toughening methods include reducing crosslink density and/or the use of elastomeric phases. However, many of these methodologies result in performance reductions (e.g., reduced modulus and lower T_g that limit their application).

This research seeks to define key parameters of network development related to cure conditions, conversion, connectivity, network architecture and properties.

- Understanding the variability associated with networks and network formation is of key interest, as initial development of network connectivity and morphology controls ultimate properties.
- Secondly, understanding the impact of polymer composition on

properties allows accurate design of high performance materials.

- Thirdly, control over network connectivity and architecture will enhance the inherent toughness of polymer matrices without sacrificing other performance parameters.

Combining these aspects of polymer network architecture provides the framework for intelligent design of multifunctional polymer matrices to hasten the evolution of composite materials.

Research Objectives

The research objective is to develop a fundamental understanding of network architecture development in thermoset polymers and the relationships and impact on mechanical performance. Specifically, the impact of cure environment, chemistry and chemical structure of high performance composite matrices will be investigated to develop the groundwork for engineering polymeric materials capable of fulfilling several functions (i.e., enhanced mechanical performance/longevity, sensing, self-healing and energy harvesting).

Research Overview

Chapter III lists the experimental reagents used in network synthesis and formulation along with a brief description of the research methods. Network formation was characterized using Fourier transform infrared (FTIR) and near infrared spectroscopy (NIR), differential scanning calorimetry (DSC) and dynamic mechanical analysis (DMA). Polymer networks were characterized before and after post-cure to determine crosslink density, transition temperatures, modulus and fracture through spectroscopic, thermal and mechanical techniques.

Chapter IV investigates the role of temperature in the development of network architecture for free radical cure starting materials. Neat resins were cured at a series of low temperatures using a standard redox initiation package. The samples were quantified for conversion via FTIR and DSC before and after post-cure. DMA was used to establish correlations between conversion and network morphology development before and after post-curing. Additionally, tensile testing determined the effect of temperature on mechanical response of the resins before and after post-curing.

Chapter V focuses on understanding the impact of ligand exchange on the redox reaction of VER cure. VERs commonly employ redox initiators that involve peroxide decomposition using a metal ion catalyst at ambient temperatures. Redox initiation proceeds through multiple reversible steps whose relative rates depend upon the redox potential of the metal ion and the ligands involved. Cobalt naphthenate was exchanged *in situ* with varying levels of 2,4-pentanedione, and the impact on conversion and mechanical property development was investigated. Neat resin samples were evaluated for conversion via DSC before and after post-cure. DMA was employed to compare network development and morphology upon the addition of 2,4-pentanedione. Tensile testing was employed to determine the effects of 2,4-pentanedione addition on the mechanical response of the resins before and after post-curing.

Chapter VI compares the structural differences between three different VERs (i.e., standard, brominated and impact modified). Bromine is commonly used to impart thermal stability and flame resistance to composite matrix resins.

The impact of bromine substitution and incorporation of a secondary phase were compared to a standard bisphenol-A based species. Secondary phases, typically utilizing low T_g elastomeric components, were employed to provide greater toughness of composite matrices. The materials compared were studied as neat resins and as materials normalized by styrene concentration.

Chapter VII examines POSS nanoparticles for improving composite matrix properties. POSS incorporation has shown potential to increase T_g and improve surface characteristics, thermal stability, barrier properties and flame retardance. Functional and nonfunctional versions of POSS were evaluated for their impact on conversion, network architecture and mechanical performance at low loadings.

Chapter VIII expands the investigation to a variety of epoxy-amine species. Molecular weight, average functionality, and chemical composition were explored to establish a baseline of mechanical performance parameters for utilization in future investigations for multifunctional (e.g., sensing, self-healing) materials. The impact of subtle changes to chemistry and functionality on conversion and mechanical properties are discussed.

Chapter IX summarizes the major findings of this research and explores future extensions of the work. Design and control of network architecture is known to be affected by the early stages of polymerization in high performance composite matrices. Temperature, polymerization rate and structure were correlated to structure property relationships and the impact of initial network architecture was determined for VERs. Epoxy-amine networks exhibited

significant differences in mechanical properties despite subtle changes in molecular level architecture as investigated between a *meta*- and *para*-substituted crosslinker. The research results support the development of high performance materials with hierarchical control and multifunctional (e.g. sensing, self-healing) capabilities

Finally, extensions of the work are presented with a focus on improved thermomechanical performance in composites . Further investigation of VER cure mechanisms in the presence of long fiber reinforcement is one area of significant interest. Finally, thiol-containing derivatives of typical matrix monomers and a detailed synthesis of tetrafunctional epoxides based on diaminodiphenylsulfone are presented as an option to impart backbone flexibility (improve toughness) without sacrifice of other properties (modulus, T_g).

CHAPTER III

EXPERIMENTAL

Materials

Vinyl Ester Resins

Commercial vinyl ester resins, Derakane® 411-350 (Figure 9), Derakane 510A-40 (Figure 10) and Derakane 8084 (Figure 11), were obtained from Ashland Chemical and used without purification. Styrene was purchased from Sigma Aldrich and used as received (Figure 12).

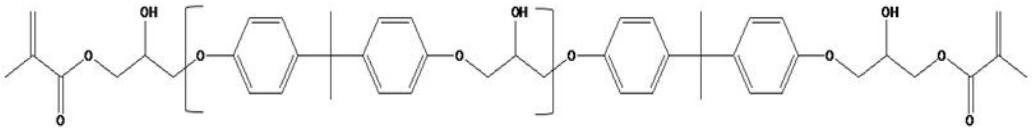

Figure 9. Derakane 411-350 is diluted with 45 wt% styrene.

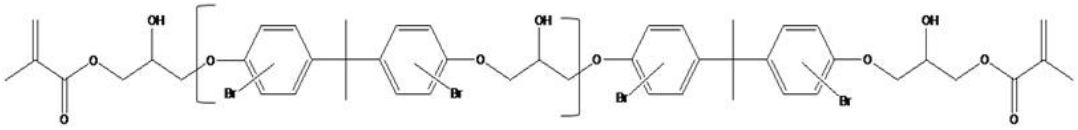

Figure 10. Derakane 510A-40 is diluted with 38 wt% styrene.

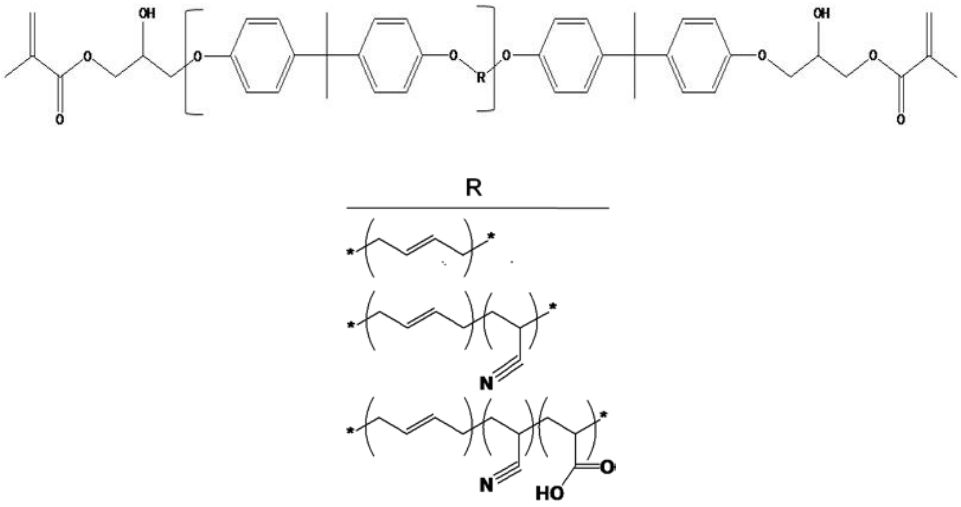

Figure 11. Derakane 8084 is diluted with 40 wt% styrene.

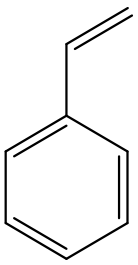

Figure 12. Styrene.

Polyhedral Oligomeric Silsesquioxanes (POSS)

POSS species, isobutylPOSS (Figure 13) and methacrylPOSS (Figure 14) were obtained from Hybrid Plastics, Inc. and used as received.

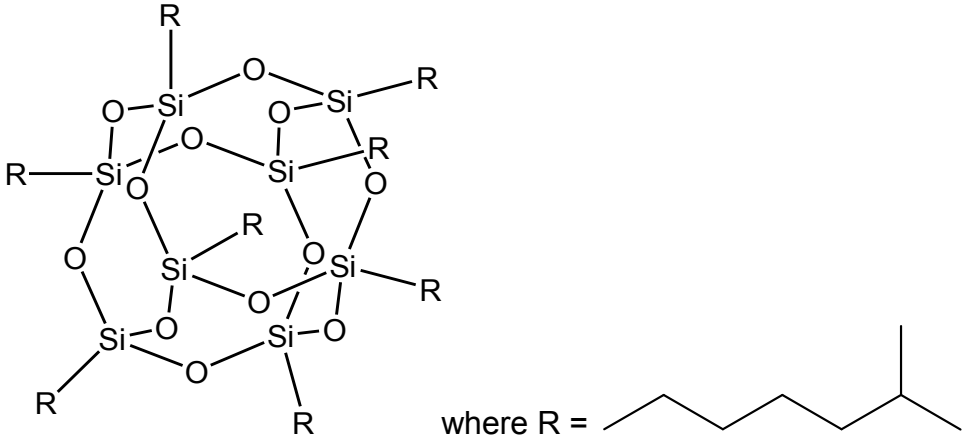

Figure 13. IsobutylPOSS

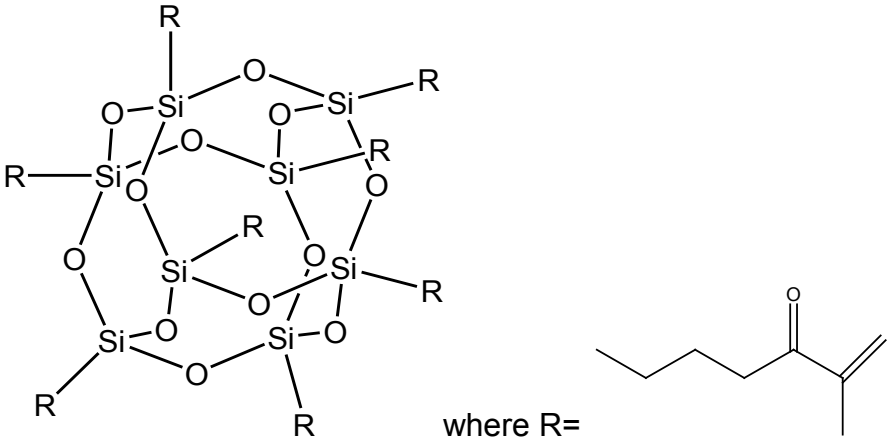

Figure 14. MethacrylPOSS.

Initiators

The free radical initiator methyl ethyl ketone peroxide (MEKP) was purchased from Fibre Glast (Figure 15). Cobalt naphthenate (CoNap) with 6% metal content was procured from OMG Americas, Inc. and used as an accelerator to promote peroxide decomposition under ambient conditions. All initiating system materials were used as received.

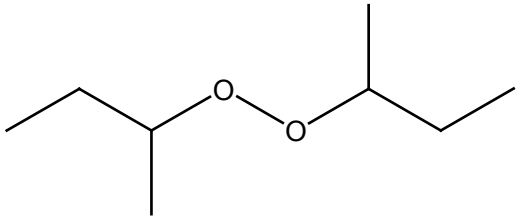

Figure 15. MEKP.

Epoxy Resins

The difunctional epoxy resins used in this work, Epon® 828 and Epon 1001F, are derivatives of diglycidyl ether of bisphenol-A supplied by Hexion Specialty Chemicals, Inc. Trifunctional epoxy resins (Araldite® MY0510, Araldite MY0610) as well as a tetrafunctional epoxy resin (Araldite MY721) were obtained from Huntsman Advanced Materials. 3,3'-diaminodiphenylsulfone (3,3'-DDS, 98%) was purchased from TCI, America. 4,4'-diaminodiphenylsulfone (4,4'-DDS, 97%) was purchased from Sigma Aldrich. All chemicals were used as received.

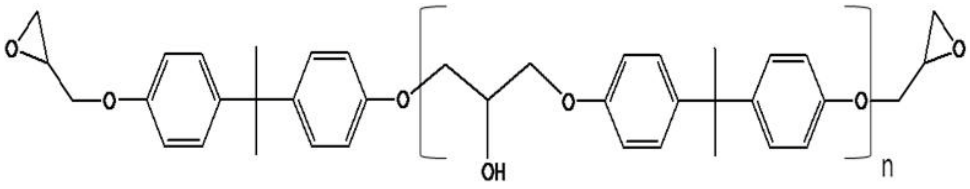

Figure 16. Epon 828 (EEW = 189) and 1001F (EEW = 550).

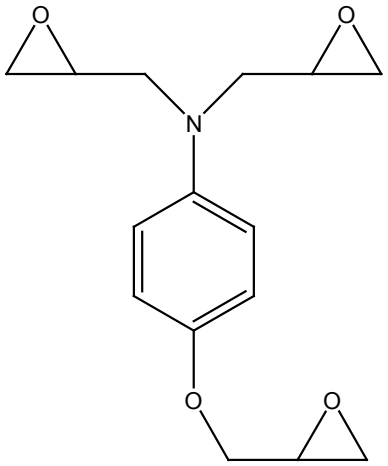

Figure 17. Araldite MY0510.

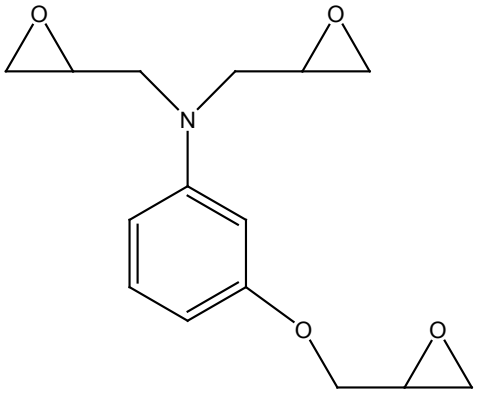

Figure 18. Araldite MY0610.

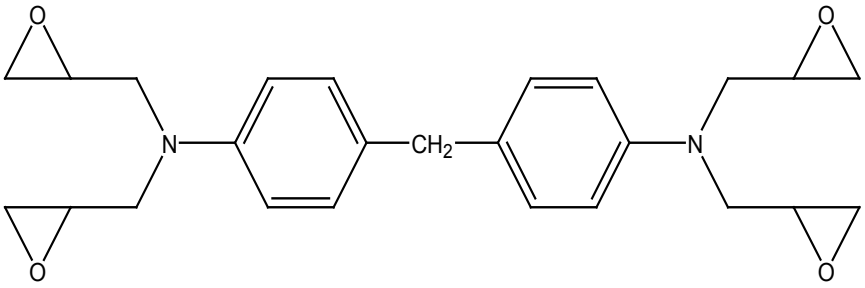

Figure 19. Araldite MY721.

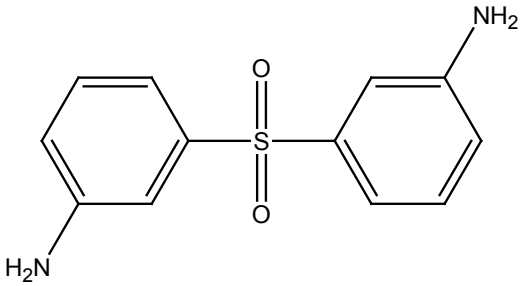

Figure 20. 3,3'-DDS.

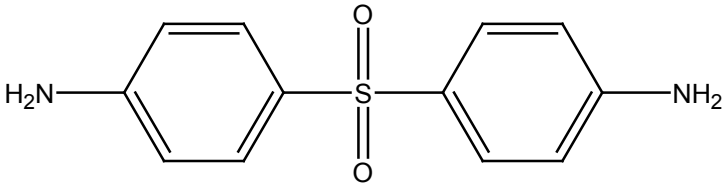

Figure 21. 4,4'-DDS.

Fibers

Fibers studied included 1.5 oz./sq. ft. fiberglass chopped strand mat from Infinity Composites, Inc. and 680GSM unidirectional carbon fiber from Sigmatex.

Resin Analysis

GPC was performed on a Varian PL GPC-50 and autosampler equipped with dual angle light scattering, differential pressure and refractive index detectors. Tetrahydrofuran (THF) was used as the eluent at a flow rate of 0.8 mL/min at 40°C with a series of four Polymer Laboratory columns (three Polypore® and one 50Å PLGel® column).

Matrix Preparation

VERs were blended with 0.2 wt% CoNap until the system was visually homogeneous. 1.0 wt% MEKP was added to the blend and mixed thoroughly until homogeneous. The resins were then transferred to specifically designed

molds for testing (i.e., DMA bars, tensile/compression specimen, fracture bars, etc.), cured for 24 hours under ambient conditions, and post-cured for two hours at 125 °C unless otherwise noted.

Epoxy resins were degassed to remove any volatile materials before formulating with stoichiometric amounts of DDS in an oil bath at 100 °C until the blend turned transparent. The resin mixture was transferred to prepared glass slides or heated molds as described briefly above for subsequent analysis.

IR Spectroscopy

FTIR spectroscopic analysis was conducted on a Nicolet 6700 FTIR from Thermo Scientific. The VERs were sandwiched between two NaCl plates using a polytetraflouroethane (PTFE) spacer to achieve standard sample thickness. A Simplex Scientific temperature controller was used to simulate cure conditions with a cure profile of 12 hours at 125 °C followed by a two hour post-cure at 125 °C and 150 °C for 2 hours to ensure complete conversion. Absorption spectra were taken in the MIR region of 400-4000 cm^{-1} (32 scans, resolution 4 cm^{-1}) with integrating sphere via OMNIC version 7.3 software. Methacrylate and styrene conversions were monitored using corresponding peaks at 945 cm^{-1} and 910 cm^{-1}, respectively. Samples were normalized to the hydroxyether backbone of the VER component at 830 cm^{-1}.

For NIR spectroscopic analysis, the epoxy-amine mixture was sandwiched between two glass slides with a PTFE spacer to achieve a standard sample thickness. NIR spectra were obtained using an Antaris II, FT-NIR Analyzer from Thermo Scientific. Absorption spectra were recorded in the NIR region of 4000-

8000 cm^{-1} (32 scans, resolution 4 cm^{-1}) with integrating sphere via OMNIC version 7.3 software. Epoxy, primary amine, and secondary amine concentrations were calculated from their respective peaks using Lambert-Beer's law while tertiary amine concentration was calculated by subtracting primary and secondary amine concentrations from initial total amine concentration.

Thermal and Mechanical Analysis

DSC studies were conducted on a DSC Q2000 (from TA Instruments, Inc.) via a heat/cool/heat temperature profile in a nitrogen environment. Samples of approximately 5 mg were evaluated over a temperature range of 0 °C to 300 °C with heating and cooling rates of 10 °C/min and 5 °C/min respectively. The multiple scans were evaluated and compared for additional cure exotherms and variations of T_g from the midpoint.

Thermogravimetric (TGA) studies were conducted on a TGA Q5000 from TA Instruments, Inc. The analysis was conducted in dynamic mode over a temperature range of 25 °C to 1000 °C in a nitrogen environment. Samples of ~15 mg were evaluated for mass loss and thermal stability.

DMA studies were conducted on a DMA Q800 from TA Instruments, Inc. under tensile mode using free films (~1 mm thick, ~5 mm wide). The analysis was conducted at a frequency of 1.0 Hz with a heating rate of 2 °C/min from -120 °C to 350 °C in a nitrogen environment using strain control. The materials were monitored for storage modulus, loss modulus, and T_g from the tan δ maxima. Molecular weight between crosslinks (M_c) was calculated to define network connectivity using the theory of rubber elasticity where E' is the rubbery modulus,

ρ is the sample density, R is the ideal gas constant and T is the temperature in Kelvin (Equation 1).

$$M_c = 3\rho RT / E' \quad (1)$$

Uniaxial tension and compression tests were conducted on a MTS 810 Materials Test System from MTS System Corporation. Tensile testing procedures followed the methods set forth in ASTM D 638-08. The samples were carefully aligned in the grips and tensile testing was conducted at a speed of 1.27 mm/min using an MTS 810 servo hydraulic universal test frame fitted with tension clamps supplied from Wyoming Test Fixtures. Compression testing procedures followed the methods set forth in ASTM 695-02a. Cylinders (diameter 0.5 inch, length 1.0 inch) were compressed at a displacement controlled test speed of 0.050 inch per minute on a MTS 810 servo hydraulic universal test frame equipped with a low friction compression sub-press purchased from Wyoming Test Fixtures. Loading data was recorded using a MTS supplied 20,000 lbf capacity load cell at a sampling rate of 10 Hz.

Fracture toughness samples were prepared with width 25.80 (± 0.12) mm, thickness 6.62 (± 0.26) mm, notch length 11.40 mm, and crack length 12.69 (± 0.51) mm. The tests were operated in flexural mode with single edge notch bending geometric arrangement according to ASTM D5045-99, using a load cell of 1000 lbf and cross head speed of 1.27 mm/min. Fracture toughness as determined by the stress intensity factor, K_{IC}, was determined using Equation 2.

$$K_{IC} = \left(\frac{P_Q}{BW^{1/2}}\right) f(x) \quad (2)$$

where P_Q is the peak load (kN), B is sample thickness (cm), W is sample width (cm) and f(x) is the calibration factor that depends on the ratio of crack length to width.

Density

The density of fully cured resins was determined using a Mettler-Toledo XS104 microbalance using a density kit (accuracy 0.002 cm^3/g). A sample of approximately 2 g was serially weighed in air and deionized water at 20 °C.

CHAPTER IV

IMPACT OF CURE ENVIRONMENT ON NETWORK DEVELOPMENT AND MECHANICAL PROPERTIES OF VINYL ESTER RESINS

Introduction

Despite widespread use of composite matrices, many principles of network development are still poorly understood. Network regularity or irregularity, termed heterogeneity, is of primary interest, due to the inconsistent or indirect correlation with mechanical performance in composite systems.[1-4] Significant debate still exists regarding the level of heterogeneity in both cured epoxy and vinyl systems.[3-7] Vinyl ester resins (VERs) (i.e., dimethacrylates based on DGEBA) belong to the category of unsaturated polyester-type thermoset composite matrices, and are widely used due to their inherent versatility associated with free radical cure.[4-12] VER systems often require reactive diluents such as styrene to reduce viscosity to practical levels and control over processability/manufacturing. Properties such as T_g and modulus depend not only on the relative amounts of VERs and reactive diluents, but also on the degree and uniformity of cure and variability in molecular level architecture formed during cure. Conversion is often evaluated as the sole measure of polymer matrix viability. However, connectivity of the molecular level network is vital in determining mechanical properties.

Unlike step growth polymerization processes, free radical crosslinking generates high molecular weight at low conversion. Step growth polymerizations proceed from monomer to dimer, trimer, tetramer, pentamer and so on,

consequently, step growth polymers only achieve high molecular weight polymer at high levels of conversion. On the other hand, free radical processes proceed immediately to polymer and yield high molecular weight polymer at all levels of conversion.[1] Complex polymerization processes generally promote higher levels of heterogeneity in the network architecture. As conversion progresses in glassy materials, polymer chain-chain mobility decreases and diffusional kinetic and conversion control occurs upon the onset of vitrification. Diffusion control of termination leads to the Trommsdorff or "gel" effect. The complexity of these processes results in non-uniform network development with regions of variable conversion/crosslinking such as microgels (typically defined as domains of high crosslink density randomly dispersed in a sea of unreacted monomer). Free radical crosslinking systems are particularly susceptible to this type of morphological heterogeneity and are a direct result of the physical and topological limitations of free radical processes.[5] Low temperature cure conditions tend to promote preferential methacrylate functionality conversion, resulting in drastically different copolymerization behavior and microgel morphology.[6-9]

Initiating radicals can be produced by a variety of thermal, photochemical and redox methods.[1] Redox reactions are practical and of considerable interest for larger structures due to their appreciable rates at low temperatures (< 50 °C) (i.e., without the aid of heat).[1] Vitrification and gelation are directly affected by the reaction conditions, and in turn control/hinder/determine the final properties of the polymer system. The selection of cure conditions is often restricted by

processing or economic limitations despite the potential for serious impact on mechanical properties. As a result, wide variation in properties are observed in commercial matrix resins.[6,7,13-19]

The experiments below focus on understanding the influence of cure temperature on conversion, connectivity and network development. The research goal was to identify T_g and modulus development versus time and as a function of temperature for analogous materials, ultimately isolating the influential molecular level variables responsible for driving or diminishing mechanical performance. By utilizing temperature as the initial variable, it is possible to investigate conversion during the early stages of cure.

Derakane 510A-40 was blended manually with 0.2 phr CoNap for ~ 1 minute and equilibrated at the desired cure temperature (0 °C, 20 °C, 25 °C, 30 °C, and 65 °C). Subsequently, 1.0 phr MEKP was added and blended manually for ~ 1 minute. The blends were then transferred to silicon molds that had also been equilibrated at the planned cure temperature and cured for 24 hours. An additional control set of the same formulation was post-cured for two hours at 125 °C for comparison with vitrification/gelation limited materials.

Resin Conversion

FTIR conversion profiles are shown in Figure 22 and revealed a consistent result (i.e., during ambient temperature cure [~ 25 °C], the initial/early rate of conversion for the methacrylate species was higher than that of styrene). The low cure temperature results in preferential homopolymerization of the methacrylate, resulting in delayed conversion of the styrene monomer. The

particular combination of parameters (i.e., cure temperature, material conversion rate and preferential polymerization of the methacrylate functional groups) result in a clear onset of vitrification occurs after three hours, further limiting the mobility of the propagating radicals and making the transformation to diffusion controlled reaction propagation. At this stage, the styrene conversion continues and the methacrylate conversion is minimal. The conversion of methacrylate functionality is limited to 50-55% for the duration of ambient cure. Upon post-cure, there is a sharp increase in conversion of both species, with styrene approaching full conversion. The dimethacrylate component only achieves 90% conversion, and this has an important consequence in the development of the molecular level network architecture as this portion of the composite matrix is characterized by higher molecular weight and functionality whereas styrene is monomeric and only form a linear polymer in the absence of side reactions.

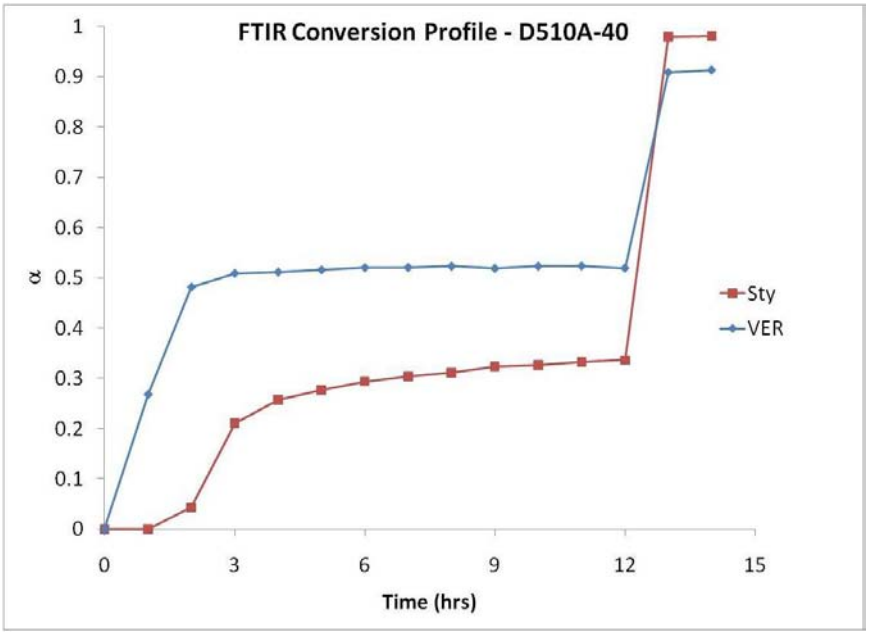

Figure 22. FTIR conversion of Derakane 510A-40 using a 12 hour cure at 25 °C followed by a two hour post-cure at 125 °C.

Samples extracted at predetermined intervals were characterized via DSC and DMA to better understand thermal and mechanical property development. The initial DSC scans are shown in Figure 23. Consistent with literature reports, a non-uniform exotherm exists during the heating scan.[18] The initial low temperature peak is related to the conversion associated with the redox reaction, while the higher temperature shoulder is a consequence of initiation and propagation via thermal dissociation from the remaining peroxide. As reaction time is prolonged, the vitrification onset is driven from 25 °C at two hours to 38 °C at 24 hours validating that propagation continues to occur, albeit slowly, after vitrification. Additionally, the exotherm (via DSC) is reduced as a result of increased conversion that has occurred prior to analysis (Table 3).

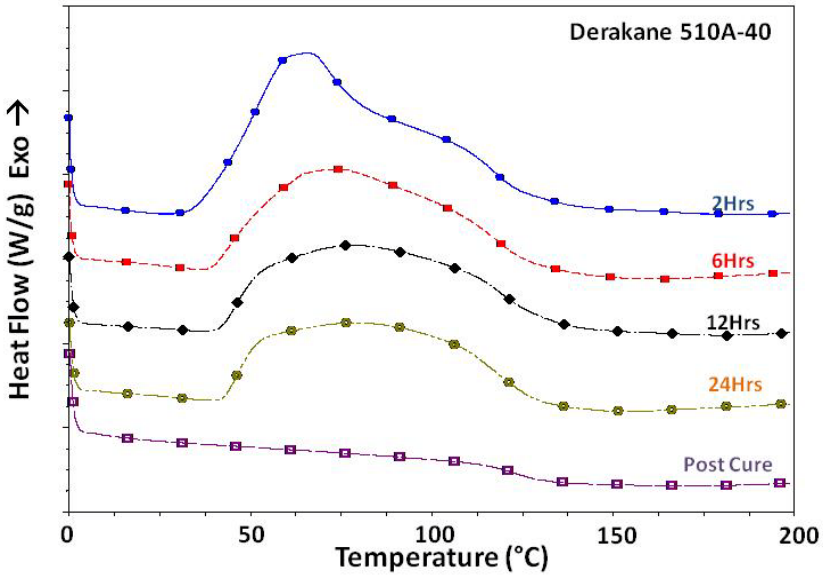

Figure 23. DSC conversion of Derakane 510A-40 with samples being cured at ~ 25 °C for 24 hours then immediately post-cured for two hours at 125 °C.

For the starting point samples, conversion rapidly plateaus, with minimal increase after six hours at ambient. This is similar to the result observed in the previously examined FTIR results. Vitrification limits the conversion and the

reaction pathway changes from chemical control to diffusion control at low temperatures.

Table 3

DSC Conversion Analysis of Derakane 510A-40

Sample	Exotherm Area (J/g)	Conversion (%)	T_g 2nd Heating Cycle (°C)
2 hr	117.4	67.4	119.45
6 hr	89.2	75.2	120.82
12 hr	81.9	77.3	120.88
24 hr	73.9	79.5	119.78
Post-Cure	0.0	100.0	123.53

Note. Post-Cured sample is assumed to reach 100% conversion as there is no detectable conversion during analysis

DMA was utilized to track of mechanical properties at similar intervals. The tensile storage modulus data is shown in Figure 24. After two hours of cure at ambient conditions, the material exhibits softening just below ambient temperature. The combination of low conversion, monomer plasticization and poor network connectivity results in a low modulus, low T_g material that draws significantly during the analysis. Upon heating above ambient temperature, the material exhibits an increase in modulus due to thermally induced conversion as the network increases in connectivity. Similar trends, albeit less pronounced, are observed at 6, 12, and 24 hours. The increase in both onset of softening and modulus for extended cure times is a direct result of increased levels of conversion. Upon post-cure, the sample no longer exhibits the low temperature

softening point related to low levels of conversion and low T_g.

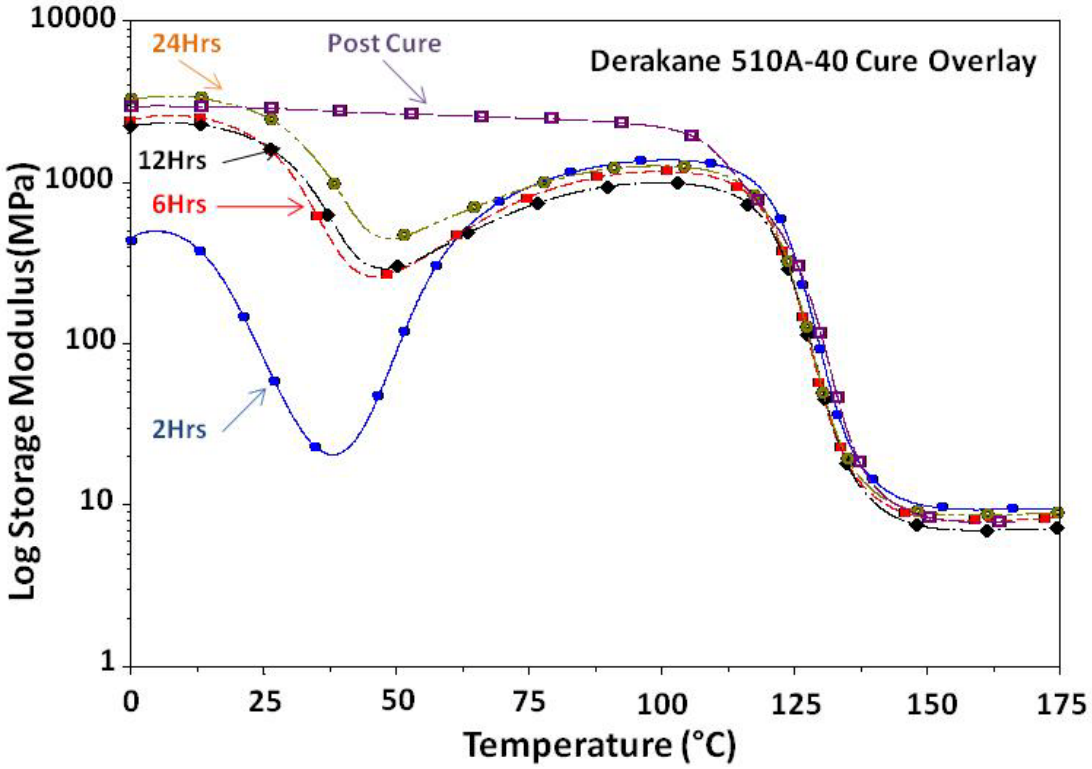

Figure 24. DMA storage modulus development of Derakane 510A-40 with samples being cured at ~ 25 °C for 24 hours then immediately post-cured for two hours at 125°C.

The tan δ data (Figure 25) reveals a decrease in low temperature relaxation as cure advances, which is a direct result of monomer incorporation into the network architecture and reduced monomer plasticization. In the post-cured sample, a low temperature shoulder remains, with an onset temperature of 103.4 °C. This transition correlates to network heterogeneity resulting from trapped monomer, incomplete conversion, and poor connectivity.

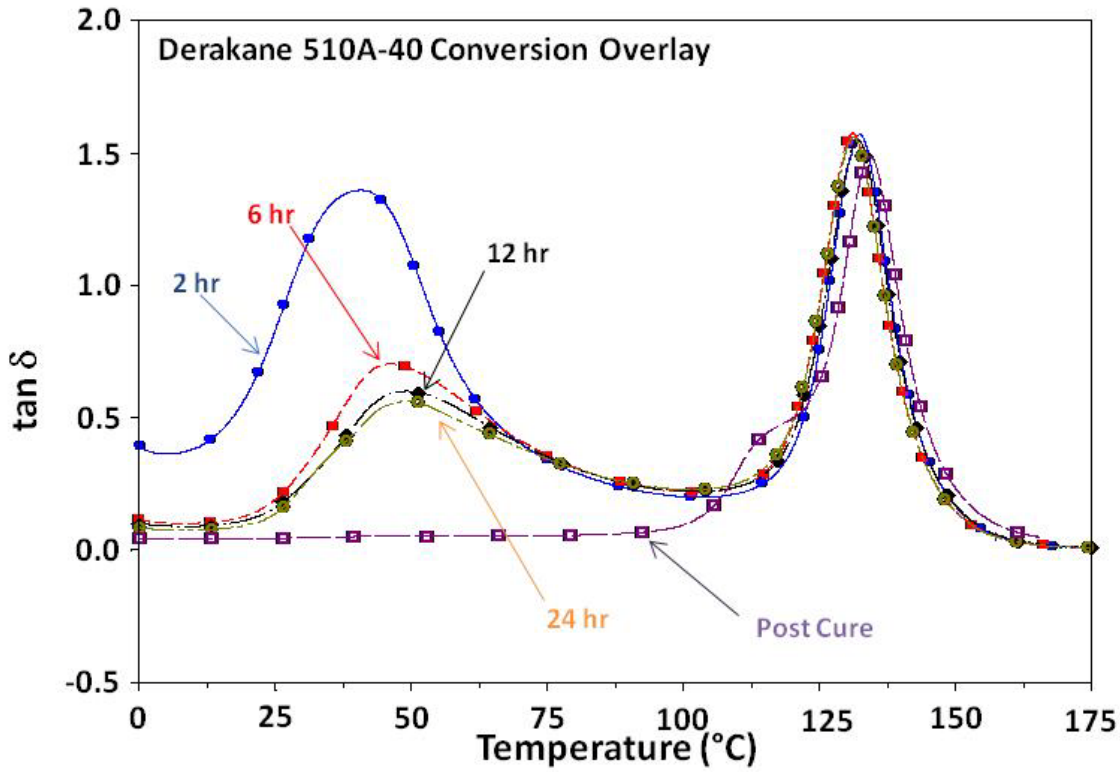

Figure 25. DMA tan δ of Derakane 510A-40 with samples being cured at ~ 25 °C for 24 hours then immediately post-cured for two hours at 125 °C.

Free radical crosslinking of VERs is a complex process that results in heterogeneous morphology early in the polymerization. Early onset of the Trommsdorff effect and transition to diffusion control alters the network architecture dramatically at low temperature. Gelation and vitrification processes alter the properties of the final product. A schematic shown in Figure 26 combines the previously discussed data with microgel theory to depict the early stages of reaction.[1,2]

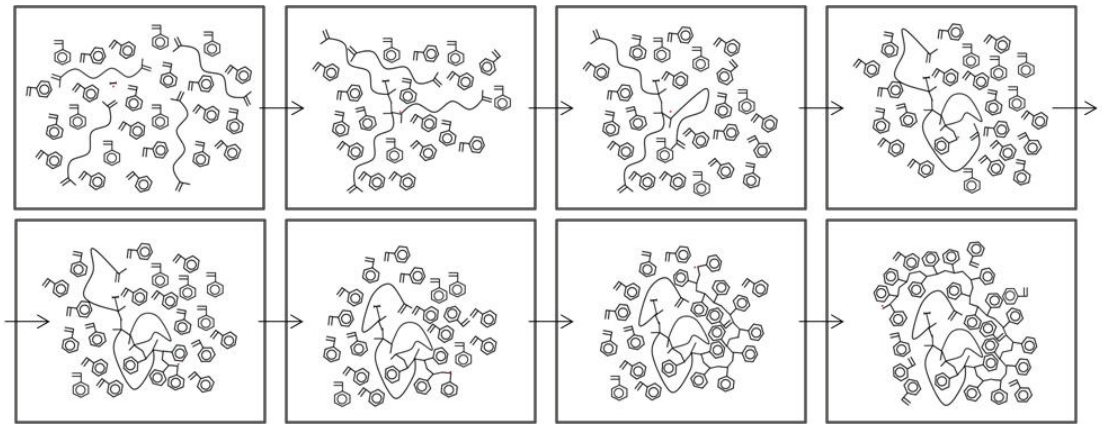

Figure 26. Schematic of the early stages of reaction. Conversion proceeds around a single radical, preferentially methacrylate species are consumed until diffusion control sets in, minimizing termination and accelerating the conversion of local vinyl groups resulting in a microgel domain.

Local production of the microgels results in gelation at low conversion in these systems. As the microgel domains begin to increase in size and interact, a vitrification point is reached. The transition from early conversion to microgels and ultimately a thermoset network is shown in Figure 27.

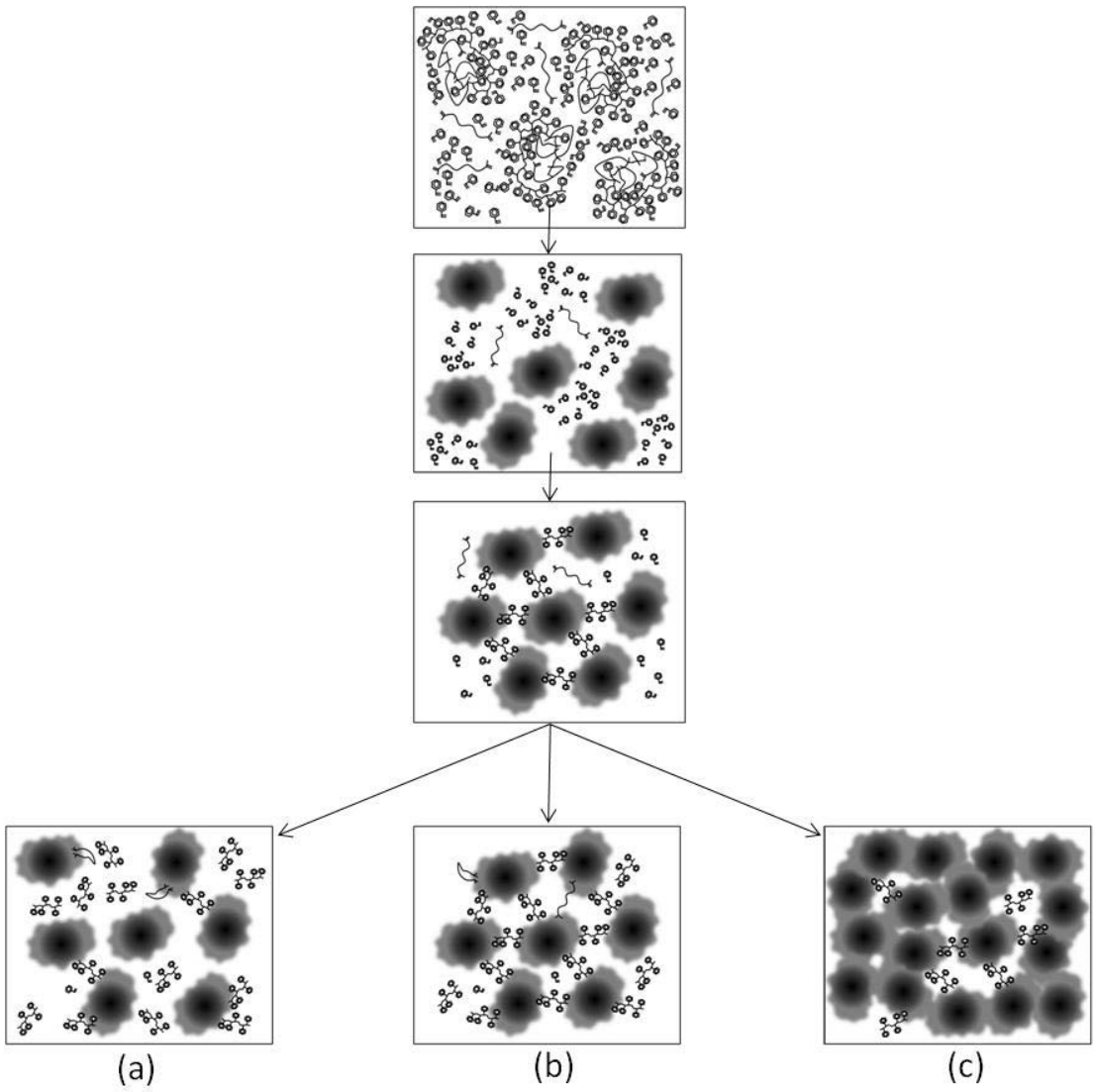

Figure 27. A schematic for microgel association. Initial conversion results in microgel formation. The microgels are surrounded by remaining monomeric species. As cure continues, the microgels continue to consume surrounding monomer, albeit slowly as gelation and vitrification alter kinetics. Depending on the cure conditions, the ultimate morphologies may be drastically altered, resulting in (a) poorly connected, weakly interacting microgel domains, (b) a combination of connected and poorly interacted microgels or (c) a well connected, interactive microgel architecture.

The FTIR, DSC and DMA data support the hypothesis that early in the reaction, polymerization of the methacrylate species produces microgel domains. These domains continue consuming monomer until the point of vitrification, at which point the methacrylate species, reacted and unreacted/initiated but unable

to propagate, becomes primarily trapped in the gel phase. The styrene continues to convert, albeit slowly, as it comprises a majority of the sol phase. Upon post-curing, the remaining sol phase is converted rapidly, connecting the microgels through pendant methacrylate species. The remaining methacrylate functionality is then trapped due to topological restrictions within the network architecture. Mechanical properties are controlled by the connectivity of these microgels, with temperature playing a primary role in the complex relationship between conversion, gelation, and vitrification.

Cure Temperature Evaluation

Low temperature cure environments were used to further investigate the effect of temperature on network development. DSC analysis of the VER systems cured for 24 hours at various temperatures is shown in Figure 28. Vitrification limited the initial conversion of the free films. Upon heating above T_g, the ambient cured systems exhibited a significant exotherm due to continued crosslinking. The non-uniformity can again be attributed to the redox reaction at low temperature and the peroxide thermal decomposition at higher temperatures. The initial vitrification point is directly related to the ambient cure temperature.

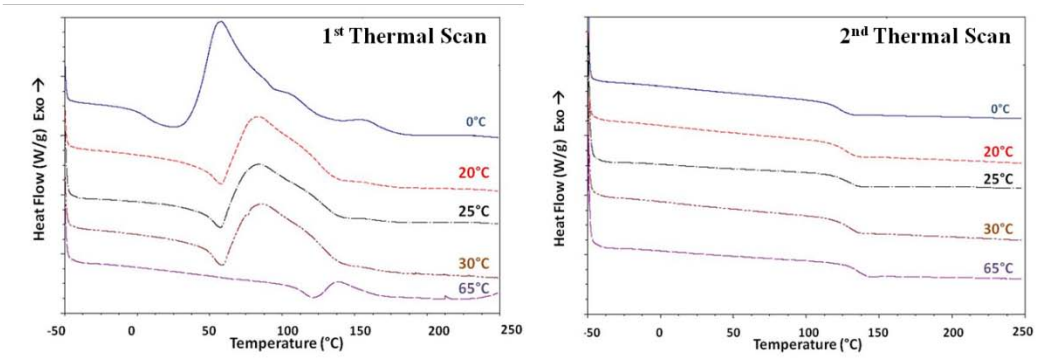

Figure 28. DSC heating scans of VER films cured for 24 hours at the listed temperature.

Dynamic heating scans of the post-cured systems are shown in Figure 29. As anticipated, the post-cured systems exhibited much higher initial conversion. However, the conversion did not proceed to completion. Upon heating to 250 °C, the same materials exhibit characteristics for full conversion, and no apparent exotherms were observed for additional reaction in the second scans of either the ambient or post-cured systems.

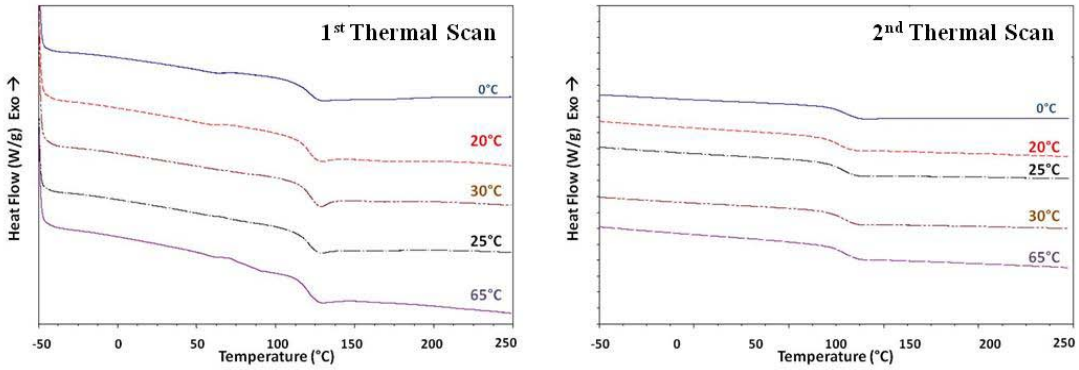

Figure 29. DSC scans of VER films cured for 24 hours at the listed temperature followed by an additional post-cure at 125 °C for 2 hours.

During ambient cure, conversion was limited by early vitrification. Since cure advanced during the first heating cycle, the T_g was determined from the second heating cycle. The residual heat evolved during the crosslinking process was determined by measuring the area under the curve and used to calculate conversion (Table 4). The lowest temperature cure environment (0 °C) was limited to 69.3% conversion while curing at moderate temperatures (20-30 °C) yielded 84% conversion. The sample cured at 65 °C reached near complete conversion by this analysis at 98.4%.

Table 4

DSC Conversion Analysis of Various Initial Cure Temperatures

Sample	Exotherm Area (J/g)	Conversion (%)	T_g 2nd Heating Cycle (°C)
0 °C	69.3	69.3	1226
20 °C	58.7	83.7	125.9
25 °C	58.1	83.9	130.3
30 °C	57.8	84.0	130.7
65 °C	---	100.0	135.2

Note. 65 °C sample is assumed to reach 100% conversion as there is no detectable conversion during analysis

Dynamic Mechanical Analysis

Ambient cure DMA scans shown in Figure 30 indicate that storage modulus increased with increasing cure temperature due to enhanced conversion and connectivity. The VER films exhibited thermal transitions relating to vitrification early in the dynamic scans, with approximate onset temperatures (T_1) listed in Table 5. Early during the reaction, the prevalence of branching and crosslinking results in microdomain formation that limits mobility and raises T_g. Vitrification ensues when the system T_g exceeds the cure temperature. Low temperature cure forces vitrification at low conversion. The onset temperatures are higher than that of the cure environment due to the exothermic nature of the reaction.

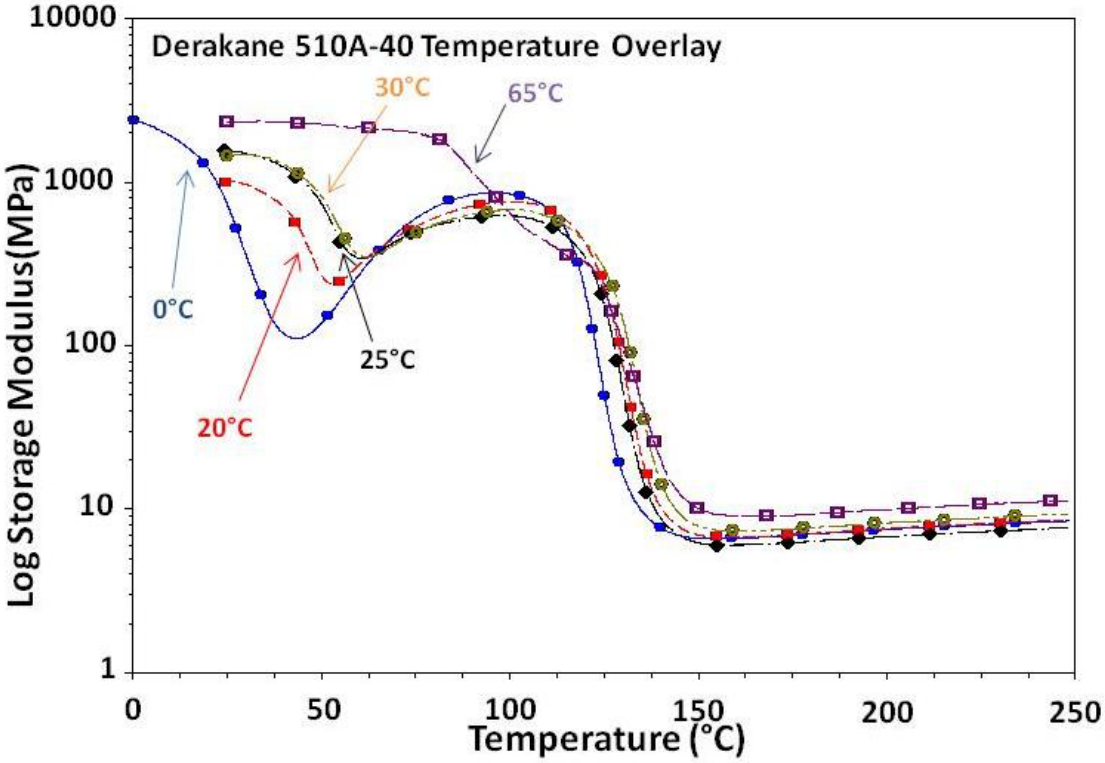

Figure 30. DMA storage modulus of VER films cured for 24 hours at the listed temperature.

An expansion of the rubbery modulus region is shown in Figure 31. The VER film cured at 0 °C exhibits the lowest rubbery plateau modulus, indicative of the lowest degree of crosslinking among all the systems. As the original cure temperature increases, the network connectivity and crosslink density increases consistently to a maximum rubbery plateau modulus. The calculated values also correlate well with literature values for theoretical and measured M_c values. Therefore, while the storage modulus values appear to be similar, rubbery modulus values indicate a detectable and quantifiable difference in molecular level network connectivity, molecular architecture, depending upon the original cure variable, i.e., temperature.

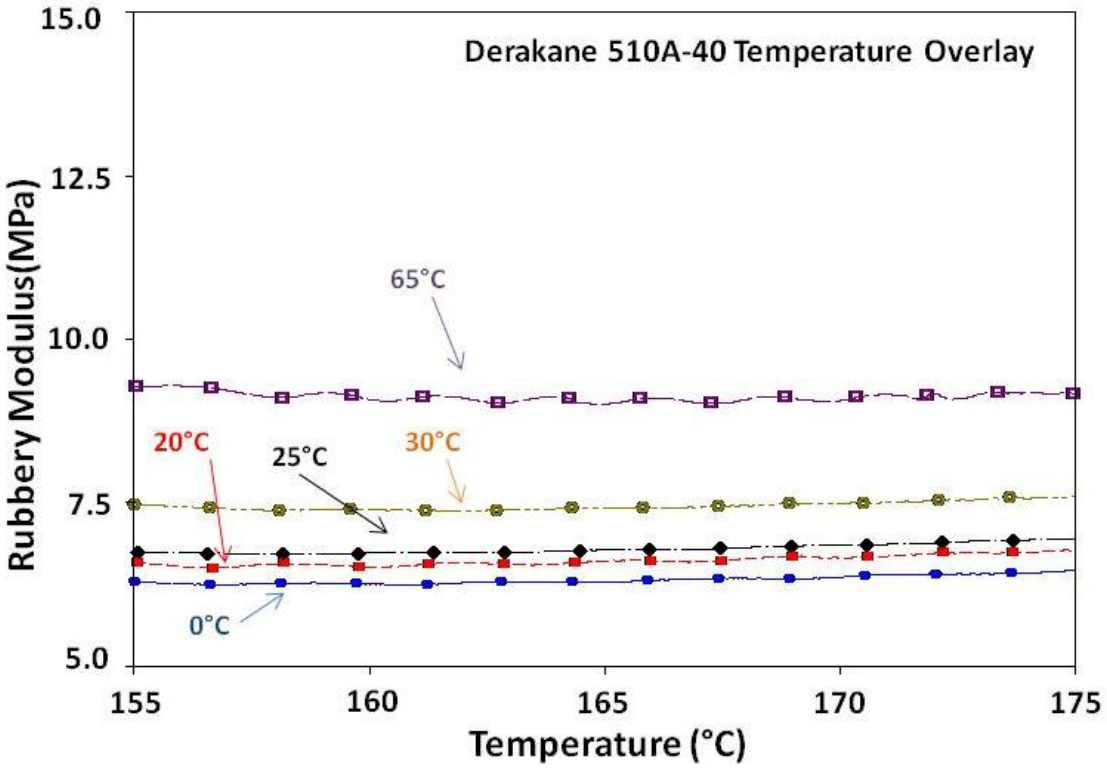

Figure 31. DMA rubbery modulus region of VER films cured for 24 hours at the listed temperature.

The effect of vitrification is more clearly evident in the tan δ data (Figure 32). The low temperature peak correlates to the initial vitrification point. As the cure temperature is increased, the intensity of the low temperature peak is reduced while the onset temperature increases due to increased conversion. Ultimately, the materials achieve high temperature tan δ maxima in the traditional and anticipated range for full conversion, but as discussed earlier with the rubbery modulus evaluation, connectivity is not consistent across the range of temperatures. This is also observed in the T_g data determined from the high temperature maxima of the tan δ.

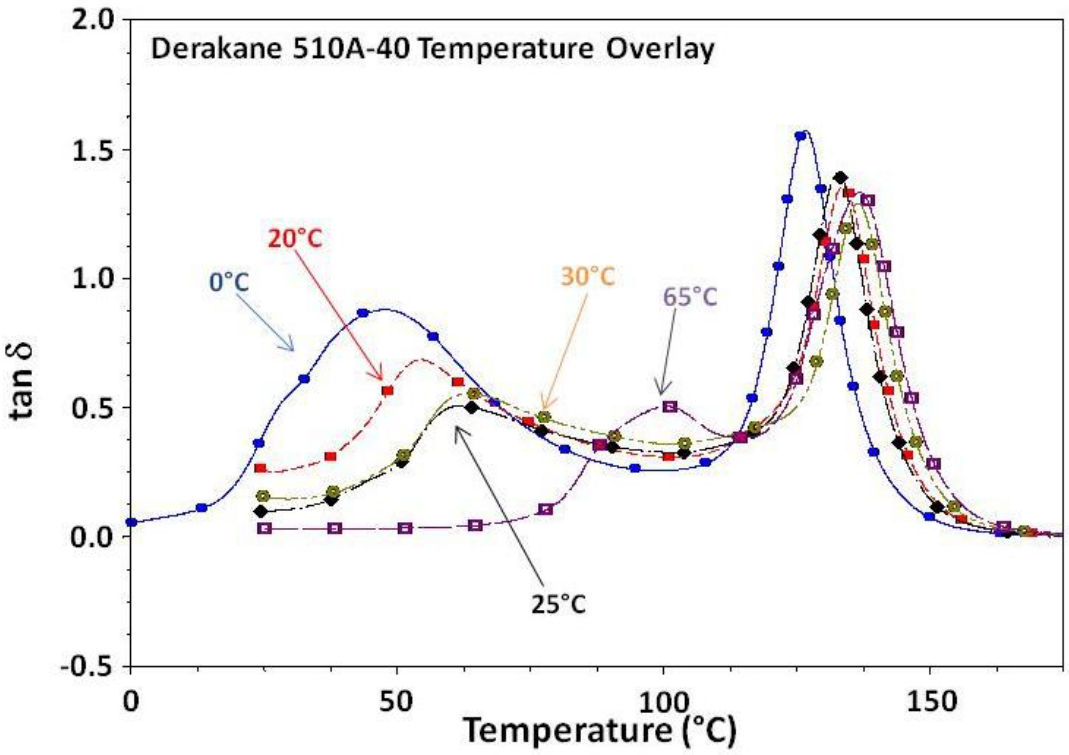

Figure 32. DMA tan δ of VER films cured for 24 hours at the listed temperature.

As the initial cure temperature is raised, crosslink density increases and correlates to a reduction in M_c (Table 5). The increase in connectivity between microgels results in increased T_g and modulus. At sufficiently elevated temperatures, vitrification is overcome by thermal mobility resulting in a less-diffusion limited reaction. At this stage, mobility of remaining functional groups is impaired and connectivity is maximized. VER films cured at 0 °C cure exhibit a slight reduction in T_g compared to the networks cured between 20 °C and 30 °C, but develop similar crosslink density during DMA analysis. Curing at 65 °C increases conversion and connectivity while resulting in a more heterogeneous network architecture as seen by the increase in full width at half height (FWHH) and drop in M_c.

Table 5

Properties of VERs Cured for 24 hours at the Listed Temperature

Sample	Density (g/mL)	T_1 (°C)	T_g (°C)	FWHH	DMA E'_R @ T_g + 40°C (MPa)	DMA M_c (g/mol)
0 °C	1.289	17.12	127.3	14.7	6.41 ± 0.15	833 ± 41
20 °C	1.390	38.32	130.7	16.6	6.88 ± 0.27	856 ± 87
25 °C	1.393	38.38	133.8	16.2	6.90 ± 0.45	856 ± 163
30 °C	1.395	39.44	134.6	15.1	7.49 ± 0.54	789 ± 162
65 °C	1.372	78.14	135.5	20.7	9.05 ± 0.32	643 ± 56

Variation in the glassy storage modulus values of the post-cured films is a consequence of thermal conditioning (Figure 33). The onset of softening is consistent across all cure temperatures. The non-uniform drop in modulus and T_g softening is attributed to the network architectural heterogeneity. The rubbery plateau region exhibits a very uniform modulus range regardless of the original 24 hour cure conditions. Network architecture is homogenized through increased connectivity of the microgel domains during post-cure and subsequent thermal energy provided during DMA analysis (Figure 34).

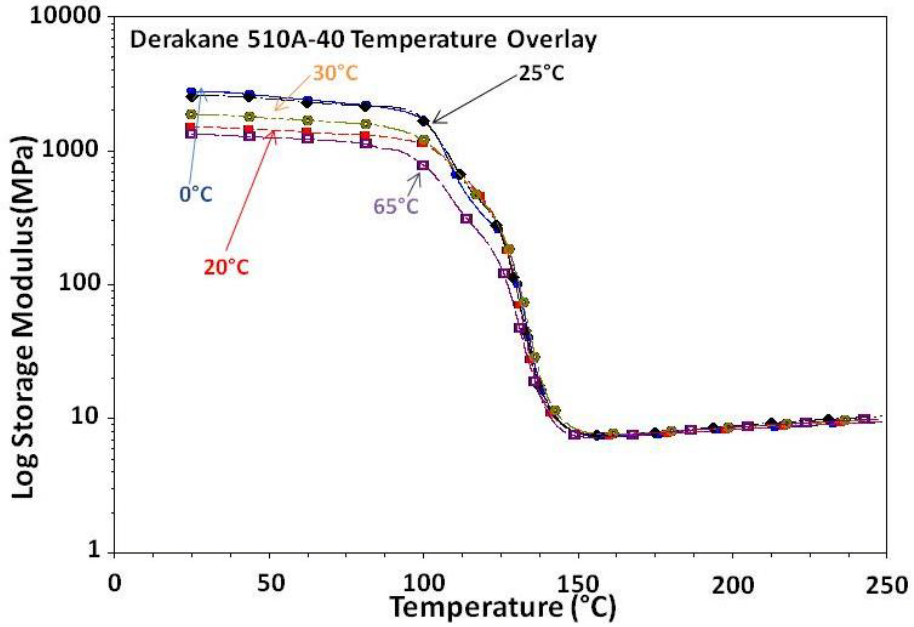

Figure 33. DMA storage modulus of VER films cured for 24 hours at the listed temperature followed by an additional post-cure at 125 °C for 2 hours.

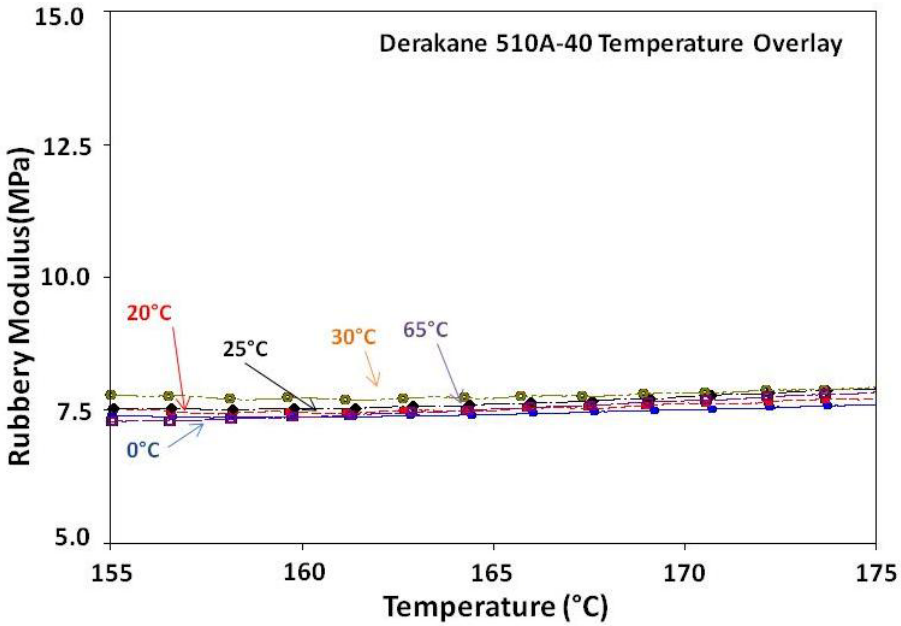

Figure 34. DMA rubbery modulus region of VER films cured for 24 hours at the listed temperature followed by an additional post-cure at 125 °C for two hours.

As observed earlier, the low temperature shoulder of the tan δ peak correlates to incomplete conversion and heterogeneous network architecture. Onset temperatures range from ~ 85 °C to 105 °C, indicative of inadequate

conversion, connectivity and plasticization by remaining monomer/oligomer (Figure 35). Table 4 shows the increased conversion and connectivity with lower M_c values compared to ambient samples. The rubbery plateau region indicates minimal differences in connectivity among post-cured samples even though these same materials were quantifiably different before thermal post curing.

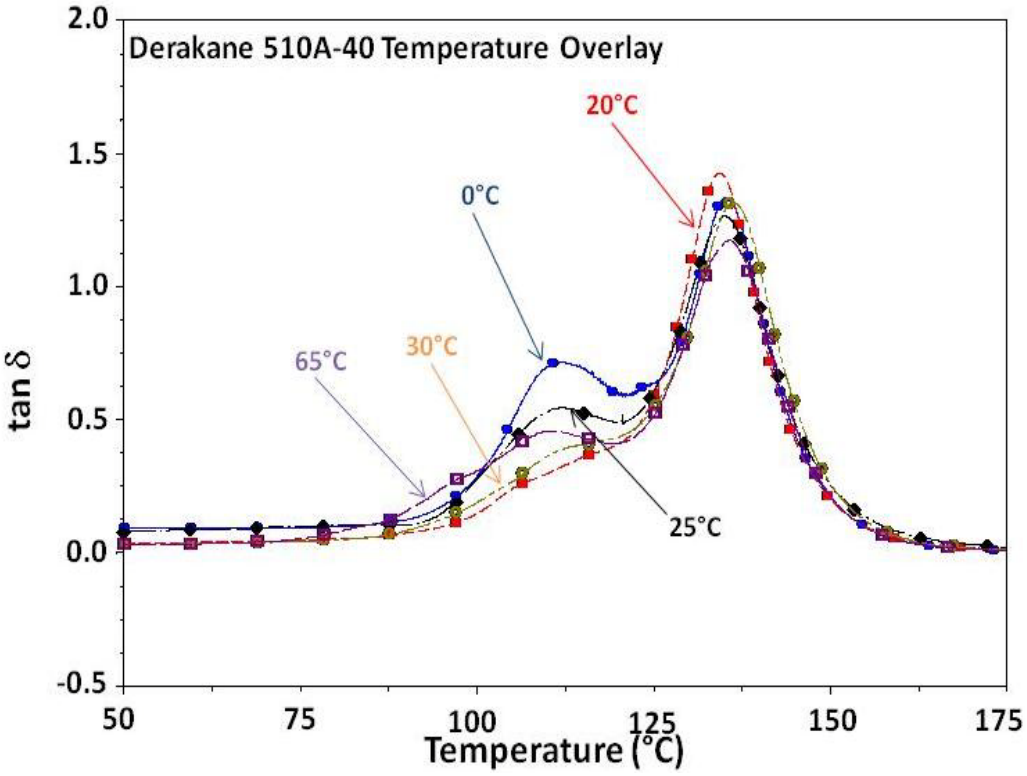

Figure 35. DMA tan δ of VER films cured for 24 hours at the listed temperature followed by an additional post-cure at 125°C for 2 hours.

Table 6

Properties of Post-Cured VERs

Sample	Density (g/mL)	T_g (°C)	FWHH	DMA E'_R @ T_g + 40°C (MPa)	DMA M_c (g/mol)
0 °C PC	1.349	135.2	14.3	7.78 ± 0.55	735 ± 133
20 °C PC	1.402	135.9	15.8	7.83 ± 0.23	759 ± 58
25 °C PC	1.393	134.3	16.9	8.18 ± 0.26	722 ± 60
30 °C PC	1.409	135.6	13.9	7.77 ± 0.38	769 ± 102
65 °C PC	1.386	133.3	15.1	8.08 ± 0.26	727 ± 60

Tensile Testing

Tensile data for samples cured at various temperatures is plotted in Figure 36. The samples cured at 0 °C exhibited significant elongation (up to ~ 65%) due to low levels of conversion. At moderate initial cure temperatures (close to ambient, 20 - 30 °C), elongation was between 6-7%, atypical for brittle glassy networks. Also, a yielding event, more consistent with thermoplastics, was observed and is indicative of insufficient conversion/connectivity for optimal resistance to deformation.

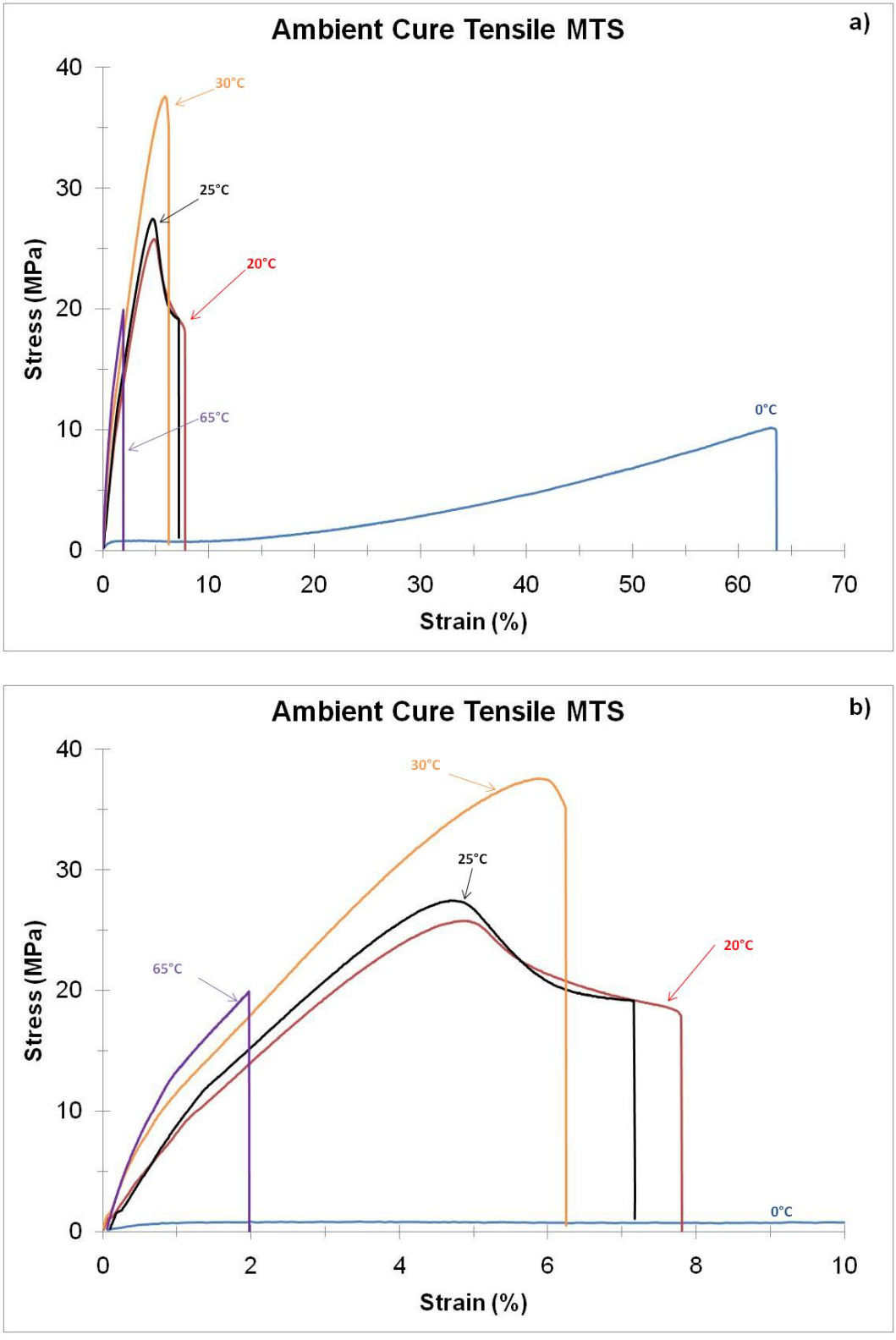

Figure 36. Stress/strain data from tensile specimens cured at the stated temperature for 24 hours, a) depicts complete overlay and b) highlights region up to 10% strain.

Tensile data for post-cured samples (Figure 37) indicate reduced variability in stress/strain response due to the homogenization of network structure. Properties of ambient and post-cured samples are summarized in Table 7. The post-cured samples do not exhibit the yielding observed with the samples cured at ambient, and exhibit brittle failure due to higher levels of conversion and increased connectivity.

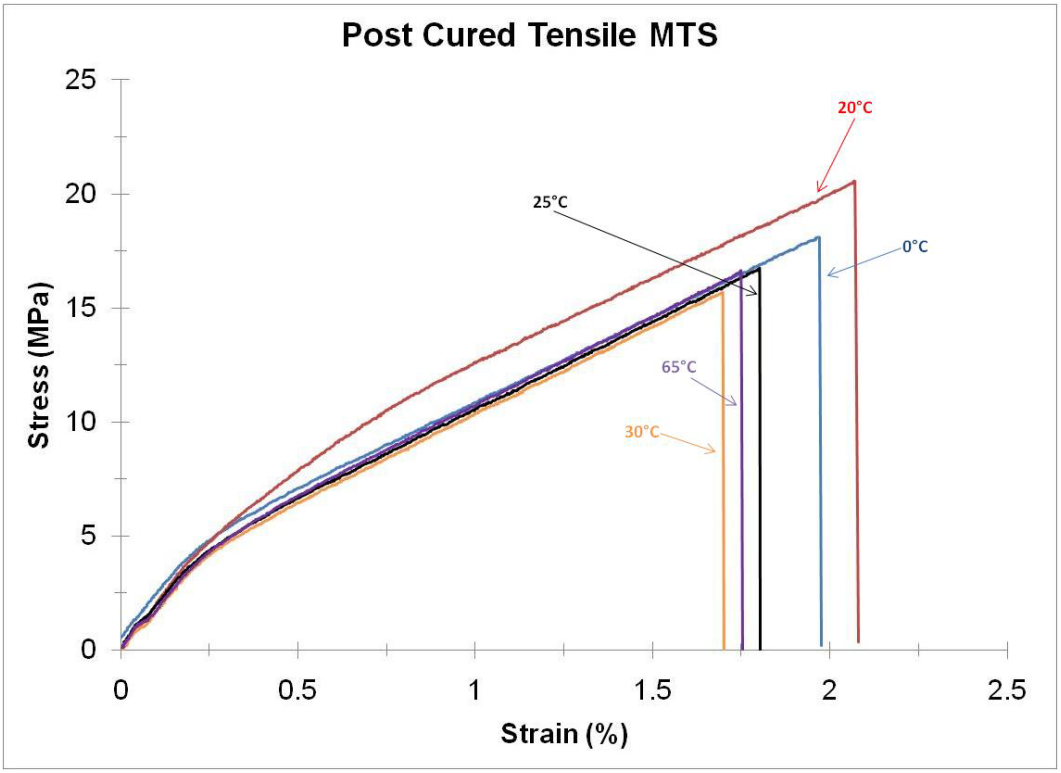

Figure 37. Stress/strain data of tensile specimen cured at the stated temperature for 24 hours followed by an additional post-cure for two hours at 125 °C.

Table 7

Tensile Stress/Strain Data of VER Specimens

Initial Cure Temperature (°C)	Peak Stress (MPa)	Strain-at-Break (MPa)	Young's Modulus (GPa)
0 °C	8.89 ± 1.2	59.7 ± 6.07	0.02 ± 0.002
20 °C	27.63 ± 2.2	6.84 ± 1.84	0.75 ± 0.04
25 °C	28.39 ± 1.7	5.64 ± 1.27	0.84 ± 0.02
30 °C	36.99 ± 1.7	6.16 ± 0.42	0.82 ± 0.02
65 °C	18.96 ± 1.2	1.94 ± 0.08	1.35 ± 0.17
0 °C PC	19.35 ± 4.6	1.91 ± 0.60	1.34 ± 0.26
20 °C PC	19.98 ± 1.9	2.09 ± 0.25	1.21 ± 0.17
25 °C PC	17.49 ± 1.1	1.85 ± 0.15	1.13 ± 0.09
30 °C PC	16.61 ± 2.5	1.68 ± 0.30	1.26 ± 0.18
65 °C PC	16.91 ± 0.5	1.73 ± 0.09	1.27 ± 0.18

Note. PC designations refer to post-cured samples.

Summary and Conclusions

Network architecture development as defined by conversion and connectivity was investigated as a function of temperature. A single VER was cured at 25°C to evaluate network development. Additional VERs probed changes in temperature using initial cure environments of 0 °C, 20 °C, 25 °C, 30 °C, and 65 °C and compared with post-cured materials.

Reactivity of the styrene and methacrylate moieties are not uniform during network formation. Careful procedures, to affect low temperature cure profiles, resulted in preferential conversion of the methacrylate species until diffusion limited reactivity results from gelation and vitrification. FTIR analysis of a sample cured at 25 °C indicated that at three hours, vitrification occurred with

approximately 55% conversion of the methacrylate (vinyl ester) component. Initial rates for styrene conversion were low, but it continued to advance after three hours, albeit slowly. Upon post-cure, the methacrylate was unable to achieve full conversion at lower temperatures than the developed T_g at that level of conversion (91.6%) due to topological constraints within the gel architecture while styrene achieved full conversion. DSC analysis showed minimal increase in conversion after six hours, with complete conversion occurring upon post-cure. DMA data indicated increased storage modulus and decreased low temperature tan δ maxima as cure proceeded. Despite achieving a T_g of 132.9 °C, in the range expected for this material, the tan δ maxima of the post-cured sample retained a low temperature shoulder (~105 °C) indicative of inadequate conversion/connectivity or secondary morphology as a result of the conditions and reactivity ratios versus conditions. The molecular level morphology and mechanical response is described by microgel theory.

For materials cured at an initial temperatures of 0 °C, 20 °C, 25 °C, 30 °C, and 65 °C, conversion (as measured by DSC) ranged from ~ 70% to > 98%. Post-cure conditions above the vitrification limits maximized conversion, resulting in no detectable additional cure exotherms by DSC. DMA of the samples after 24 hours indicated softening and tan δ transitions associated with low levels of conversion. The onset of softening and low temperature tan δ peak correlate to the initial vitrification temperature, which was ~ 10-15 °C higher than the cure temperature. The higher rubbery modulus values noted with increasing cure temperature indicated differences in molecular level connectivity. This is due to

higher initial conversion and less residual functionality, producing a more connected albeit inhomogeneous network architecture. M_c values supported the trend, with the 65 °C sample exhibiting a ~ 200 g/mol reduction in molecular weight compared to the 0 °C sample. Post-curing increased conversion in all systems and shifted all samples to a similar, almost identical range of rubbery plateau modulus values. The presence of a low temperature shoulder in the tan δ curves of all the samples indicated topological limitations imposed during the cure schedule. The transition temperature ranged from 85-105 °C and is indicative of network plasticization via low molecular weight / poorly connected oligomers/monomers. Additional conversion occurring during the characterization and analysis results in a more uniform network, as is evident from the rubbery modulus values and calculated Mc values.

Ambient cured materials exhibited thermoplastic-like tensile behavior when subjected to mechanical testing. Strain-to-break values increased due to reduced conversion and significant monomer plasticization. Post-curing minimized variation in all values across all cure temperatures. Post-cured samples exhibited glassy polymer behavior albeit with reduced peak stress, strain-at-break and Young's modulus values.

In addition to thermal conditions, catalyst activity is an important factor in the development of molecular level network architecture. Catalyst activity is often adjusted to control gel points without concern for mechanical properties. The impact of catalyst activity on initial network formation and ultimate mechanical properties has not been thoroughly evaluated. The next chapter is

focused on the use of *in situ* ligand exchange to reduce catalytic activity, elongate gel times, and increase processing capabilities of VERs.

References

1. Odian, G. *Principles of Polymerization, 4th Ed*. John Wiley & Sons, Inc.: New Jersey, 2004.
2. Sperling, L. H. *Introduction to Physical Polymer Science, 4th Ed*John Wiley & Sons, Inc.: New Jersey, 2006.
3. Dusek, K., Plestil, J., Lednicky, F. & Lunak, S. *Polymer* 19 (1978): 393.
4. Ikkai, F. & Shibayama, M. *Journal of Polymer Science Part B Polymer Physics,* **2005**, 43, 617.
5. Kannurpatti, A. R., Anseth, J. W. & Bowman, C. N. *Polymer,* **1997**, 39, 2507.
6. Cook, W. D., Simon, G. P., Burchill, P. J., Lau, M. & Fitch, T. J. *Journal of Applied Polymer Science*, **1997**, 63, 769.
7. Ziafe, S. & Palmese, G. R. *Journal of Polymer Science Part B Polymer Physics,***1999**, 37, 725.
8. Li, H., Burts, E., Bears, K., Ji, Q., Lesko, J.J., Dillard, D., & Riffle, J.S. *Journal of Composite Materials,* **2000**, 34, 1512.
9. Gangliani, M., Carr, S. H. & Torkelson, J. M. *Polymer,* **2002**, 43, 2747.
10. Scott, T. F., Cook, W. D. & Forsythe, J. S. *European Polymer Journal*, **2002**, 38, 705.
11. Scott, T. F., Cook, W. D. & Forsythe, J. S. *Polymer,* **2002**, 43, 5839.
12. Scott, T. F., Cook, W. D. & Forsythe, J. S. *Polymer,* **2003**, 44, 671.
13. Cook, W. D., Forsythe, J. S., Irawati, N., Scott, T. F. & Xia, W. Z. *Journal of Applied Polymer Science*, **2003**, 90, 3753.

14. Cook, W. D., Scott, T. F., Quay-Thevenon, S. & Forsythe, J. S. *Journal of Applied Polymer Science,* **2004**, 93, 1348.

15. Schroeder, W. F., Auad, M. L., Barcia Vico, M. A., Borrajo, J. & Aranguren, M. I. *Polymer,* **2005**, 46, 2306.

16. Li, P., Yu, Y. & Yang, X. *Journal of Applied Polymer Science,* **2008**, 109, 2539.

17. Rosario, A. C., Burts-Cooper, E. & Riffle, J. S. *Polymer,* **2007**, 48, 1203.

18. Rey, L., Galy, J. & Santerau, H. *Macromolecules*, **2000**, 33, 6780.

19. Morais, V., Encinar, M., Prolongo, M. G. & Rubio, R. G. *Polymer*, **2006**, 48, 2349.

CHAPTER V

EFFECT OF 2,4-PENTANEDIONE ON THE NETWORK DEVELOPMENT AND MECHANICAL PROPERTIES OF VINYL ESTER RESINS

Introduction

Apart from processing temperature concerns, a key concern with composite resins is process flexibility. Resin transfer molding (RTM) and vacuum-assisted resin transfer molding (VARTM) are two fabrication techniques that commonly utilize VERs.[1] These molding techniques require low viscosity resins to fill a particular cavity rapidly and completely, while simultaneously being capable of low/ambient cure profiles.

Thermal decomposition of ambient stable peroxides to produce initiating radicals proceeds too slowly for practical composite processing conditions specific to large parts. For this reason, VERs commonly employ redox initiators that involve ambient temperature decomposition of a peroxide using metal ion catalysts such as cobalt salts. Cobalt (II) derivatives of naphthenic acids are commonly used because of their low cost and high solubility. Initially, metal catalysts act as single electron donors to produce peroxy radicals (Figure 38).[2] The oxidation of M^{2+} to M^{3+} is followed by a reduction step which may proceed via one of three ways, producing a second radical and regenerating M^{2+}.

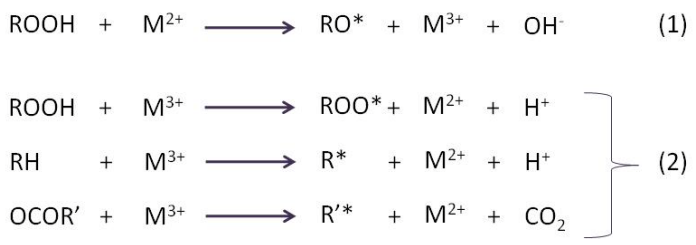

Figure 38. Metal catalyzed redox reaction.[2]

Complications arise when the reaction exotherms increase resin temperature before it can completely fill the mold cavity. At appropriate temperatures, thermal decomposition of uncatalyzed initiators or self-initiation of monomers will increase the reaction rate and viscosity, resulting in an unusable composite part, wasted processing materials, and lost time that dramatically increases cost.

Free radical polymerizations permit rapid growth of the three dimensional polymer network and result in excellent mechanical properties. However, microgels develop early during polymerization, controlling kinetics and introducing heterogeneities in the matrix. The impact of thermal environment on kinetic parameters is well documented.[3-9] A strong correlation between temperature and conversion is observed. With increasing temperature, the size of the microgel domains decreases.[10,11] More importantly, conversion is often limited by conversion-diffusion relationship limitations associated with vitrification, reduced intrinsic reactivity, and phase separation.

To overcome these limitations by practical methods, formulation changes are introduced to drive higher conversion after an elongated/prolonged gelation specifically for part fabrication. The use of multiple initiating species has produced mixed results.[12,13] While temperature is still the primary controlling factor in most instances, other additives can be used to alter reaction rates through pH, catalyst activity, or peroxide selection. Such accelerators often develop greater reaction exotherms and result in complex and competitive cure mechanisms. It is important to note that accelerators do not have the same

impact on mechanical properties as increasing temperature, although both increase the rate of conversion in VERs.[14]

To reduce reaction rates, inhibitors and retarders can be used. In general, inhibitors capture all active radicals, while retarders are typically less effective and simply reduce the number of radical available to initiate reactions. Inhibitors function by competing for the primary radicals and if the inhibitor is highly efficient, complete inhibition of initiation and propagation can be observed.[15] Hydroquinone and benzoquinone are frequently used inhibitors. Rate control is also obtained by altering the catalytic activity of a particular metal through appropriate ligand selection. Carboxylic acids, acetates, aldehydes and polyamines are capable of forming strong complexation/chelation with metal ions, altering catalytic activity and reactivity with peroxides.[2,13] Ligand control permits selectivity and control of redox potential and subsequently catalytic activity and reaction rates in redox initiated free radical polymerizations. Acetylacetone (2,4–pentanedione, Figure 39) has been shown to be effective in delaying gel times.[16] Significant reduction in reaction rates was observed at low loadings, with little impact on final conversion. It is believed that 2,4-pentanedione (2,4-P) instantaneously exchanges with the ligands on the cobalt species, reducing reactivity and altering the reaction rate. As previously examined, temperature plays a significant role in the development of heterogeneous phases early in the polymerization.[3,4, 7-15] The microgel domains play a dominating role in determine the ultimate conversion and performance of VERs by altering the molecular level network architecture and connectivity. However, the mechanisms and use of

extenders such as 2,4-P has not been thoroughly explored in literature, despite their widespread commercial use.

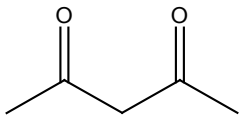

Figure 39. 2,4-pentanedione.

In this study, the mechanical properties of VERs containing an extended commercial cure package were investigated at various loadings of 2,4-P. The development of T_g and modulus as a function of 2,4-P is of considerable interest. By investigating 2,4-P as the primary variable, it is possible to identify conversion and molecular level structure development during the early stages of cure.

Derakane 510A-40 was blended manually with 0.2 phr CoNap for one minute and equilibrated at 25 °C, followed by the addition of the appropriate amount of 2,4-P (0.00, 0.25, 0.50, 0.75 and 1.00 wt%). Subsequently, 1.0 phr MEKP was added and the system was blended manually for one minute. The blends were then transferred to silicon molds (already equilibrated to the desired cure temperature) and cured for 24 hours. An additional set of the same formulation was post-cured for two hours at 125 °C.

Differential Scanning Calorimetry

DSC heating scans of the VER systems cured at various 2,4-P loadings are shown in Figure 40. The initial conversion(s) as measured by DSC were not limited by 2,4-P until its concentration was increased to 1.0 wt%. Upon heating, the ambient cured systems exhibited an exotherm consistent with additional conversion. As the 2,4-P concentration was increased, the catalyst activity was

reduced, resulting in reduced low temperature shoulder (correlating to the redox reaction) and an increase/broadening of the overall exotherm. This is indicative of thermal dissociation of the peroxide.[13-16] The reduced redox exotherm lowers the overall conversion of the ambient temperature reaction and limits the advancement of network formation. As a result, the initial conversion and connectivity is altered while T_g is reduced slightly, as determined from the midpoint of the second heating scans.

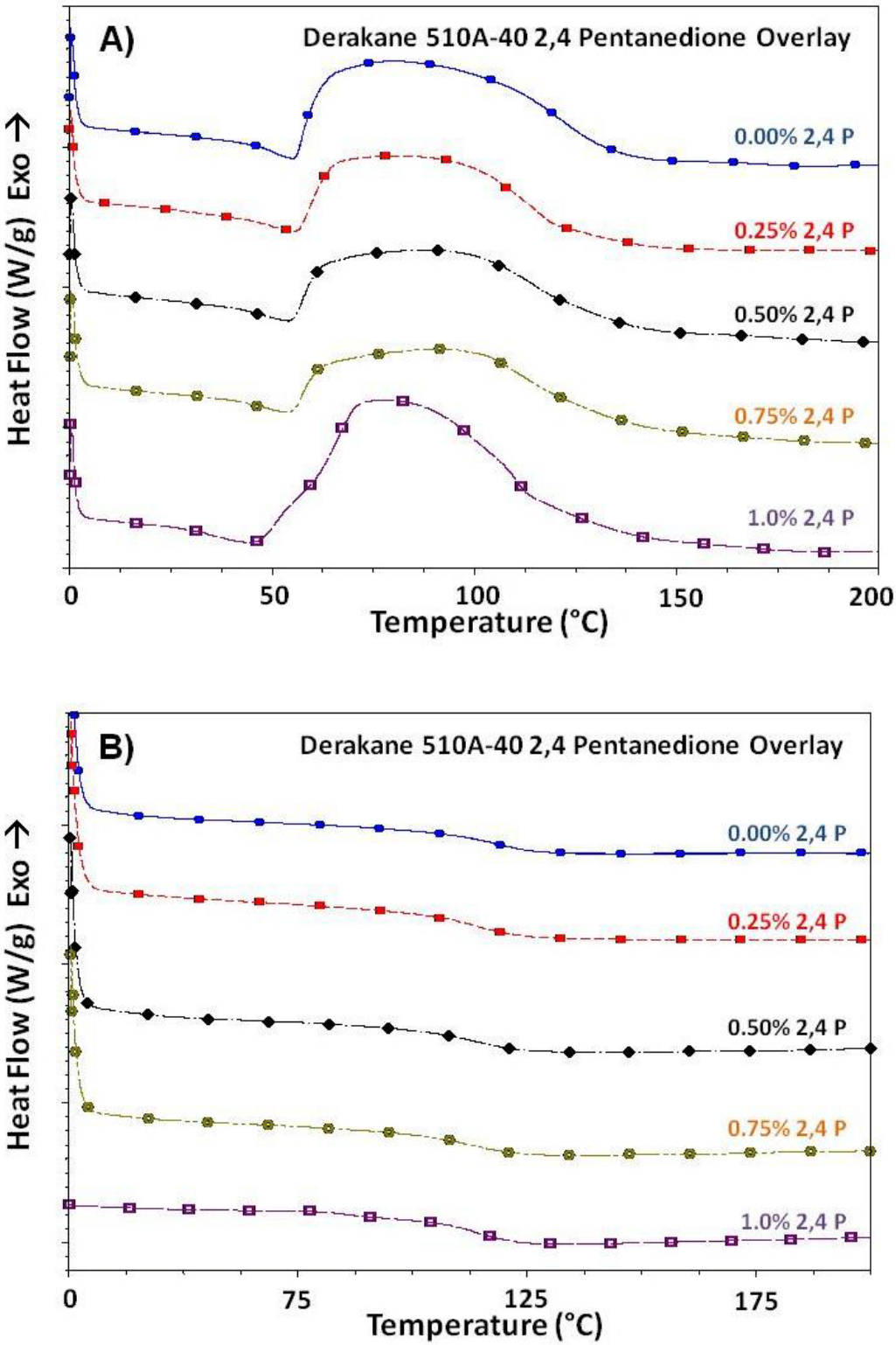

Figure 40. DSC heating scans of ambient VER films cured for 24 hours with 0 - 1 wt% 2,4-P; A) first heating scan and B) second heating scan.

DSC heating scans of the post-cured systems (Figure 41) indicate much higher initial conversion as expected, with no apparent exotherms present. At higher 2,4-P loadings, the T_g onset temperature shifted to lower temperatures with T_g broadening, indicating an increase in network heterogeneity.

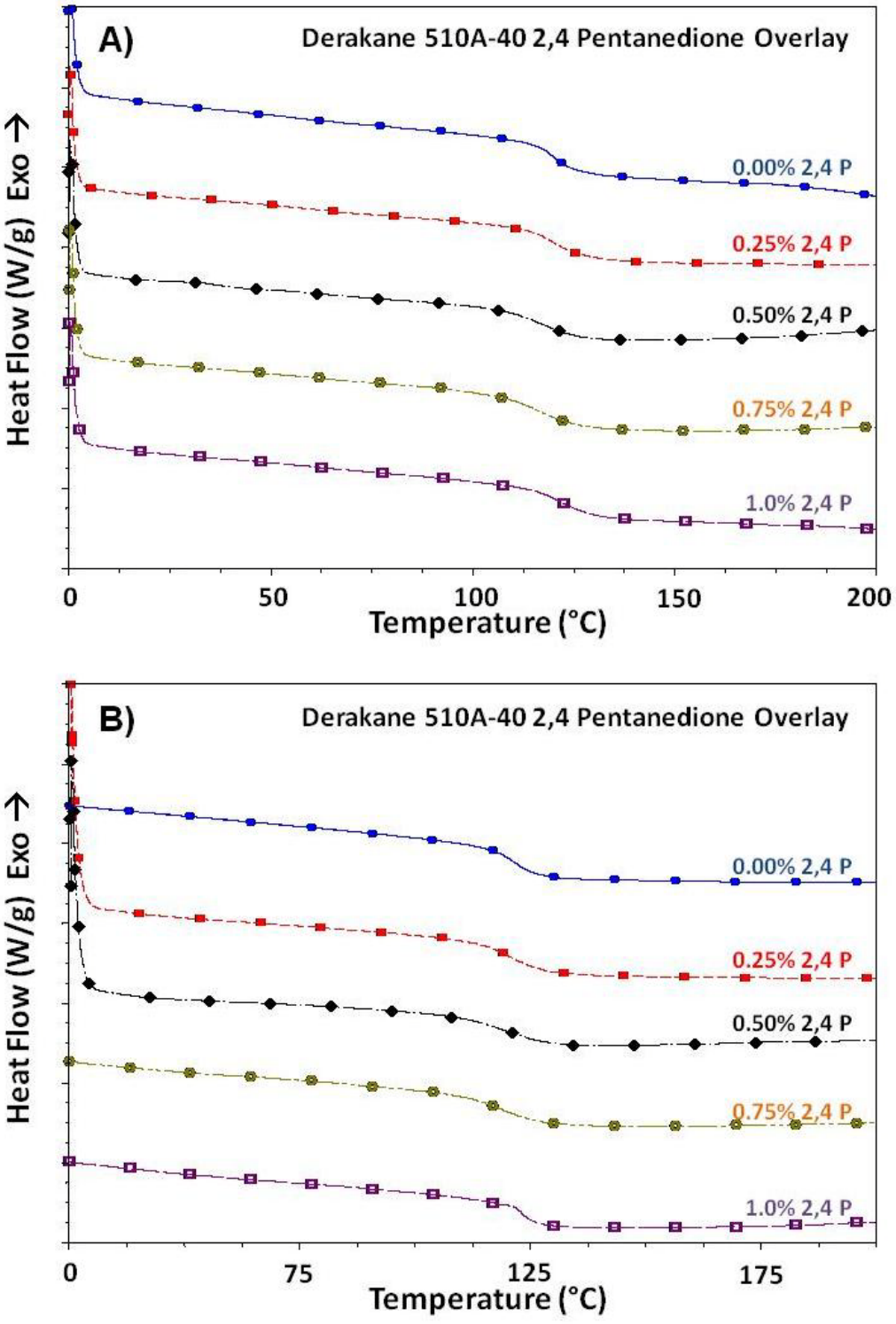

Figure 41. DSC scans of post-cured VER films with 0 - 1 wt% 2,4-P; A) first heating scan and B) second heating scan.

The residual heat evolved during the crosslinking process was determined by measuring the area under the curve and used to calculate the degree of cure (Table 8). Conversion as calculated from the exotherm area is consistent across all samples except the 1.0 wt% 2,4-P. As previously stated, this is a complication of the analysis, as the thermal decomposition of the peroxide becomes the dominant mechanism during the heating scan. Therefore, the initial conversions are likely to be much lower than evaluated from this method.

Table 8

DSC Thermal Analysis of VERs Containing 2,4-P

2,4-P (%)	Exotherm Area (J/g)	Conversion (%)	T_g 2nd Heat (°C)
0.00	59.05	83.5	118.7
0.25	47.97	86.7	114.1
0.50	50.61	85.9	113.2
0.75	49.96	87.9	112.8
1.00	80.66	77.6	113.5

Lower T_g was observed in all cases as compared to the neat resin. This results from a change in the primary initiation mechanism and a shift in network construction, altering vitrification and connectivity.

Dynamic Mechanical Analysis

The VER films exhibited an onset of softening indicating low initial conversion and connectivity (Figure 42). As 2,4-P loading is increased, the onset

of softening occurs at lower temperatures. This correlates well with the mechanistic changes observed in the DSC scans as the DMA is relatively more sensitive to changes in molecular level architecture. The neat resin has a softening onset temperature of 49.20 °C while the sample formulated with 1.0 wt% 2,4-P exhibited a lower softening onset temperature of 38.12 °C.

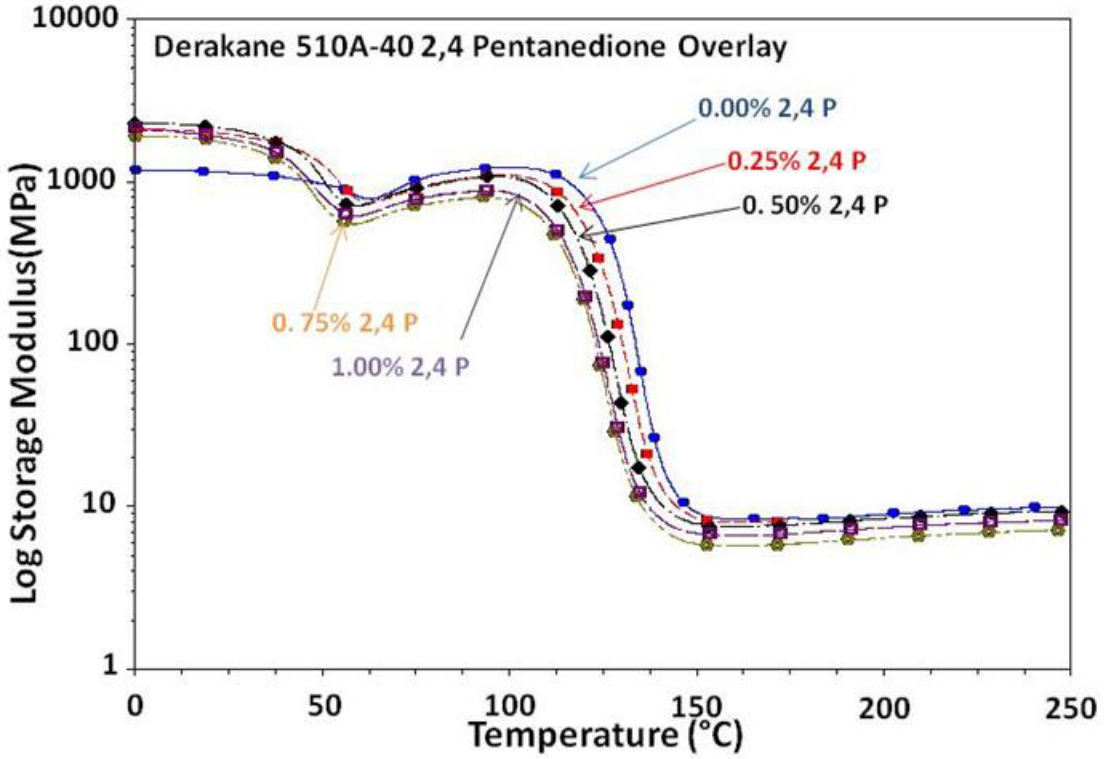

Figure 42. DMA storage modulus of VER films cured at ambient temperature with 0 - 1 wt% 2,4-P.

Additional cure during the dynamic thermal scan enhances the ultimate crosslink density and network connectivity of the VER films. However, upon incorporation of 2,4-P, significant variation is observed in the rubbery modulus of the ambient cured samples (Figure 43). These variations are due to initial limitations in peroxide dissociation, producing fewer radicals and reducing molecular level connectivity that is evident by changes in the calculated M_c

values (Table 9).

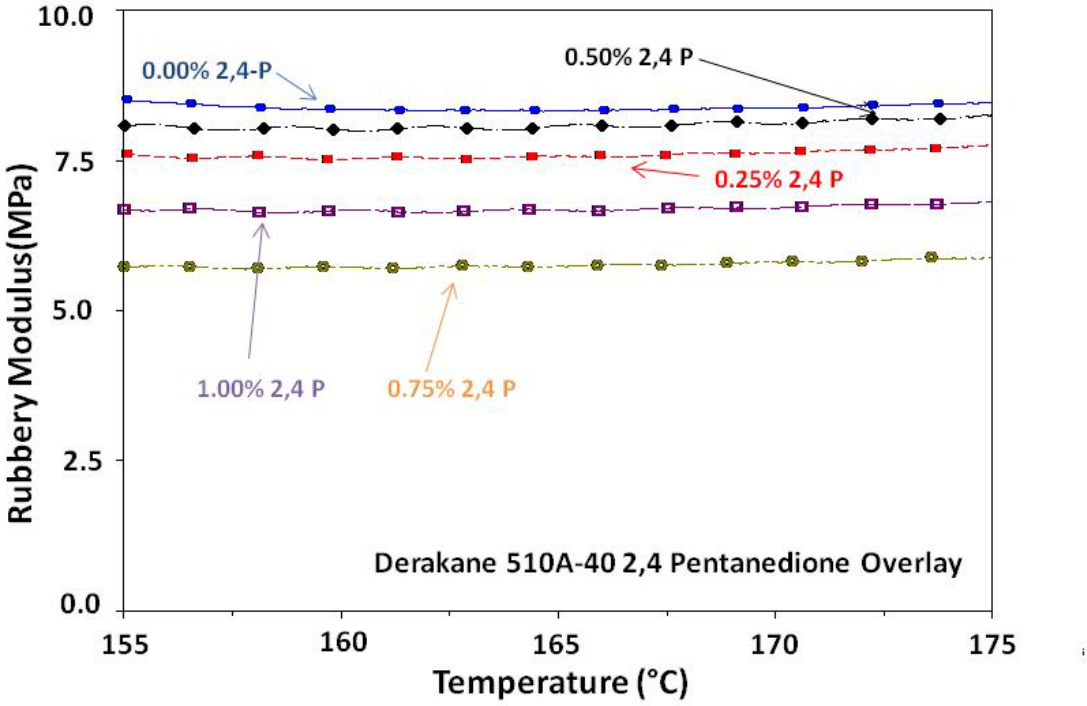

Figure 43. DMA rubbery modulus region of VER films cured at ambient temperature with 0 - 1 wt% 2,4-P.

The changes in softening onset temperatures discussed earlier are more evident in the tan δ curves (Figure 44). Increased 2,4-P loading lowers the T_g onset temperature and enhances the intensity of the low temperature tan δ transition, which is indicative of a change in molecular architecture and connectivity. This results in a reduction in ultimate T_g and M_c observed under the test conditions. As the amount of 2,4-P was increased, catalyst activity decreased resulting in poor conversion/connectivity as observed by larger M_c values and reduced T_gs. The sample containing 1.00 wt% 2,4-P experienced ~ 10 °C reduction in T_g and an increase in M_c of ~ 300 g/mol, while also having significant increase in variability as compared to the neat system.

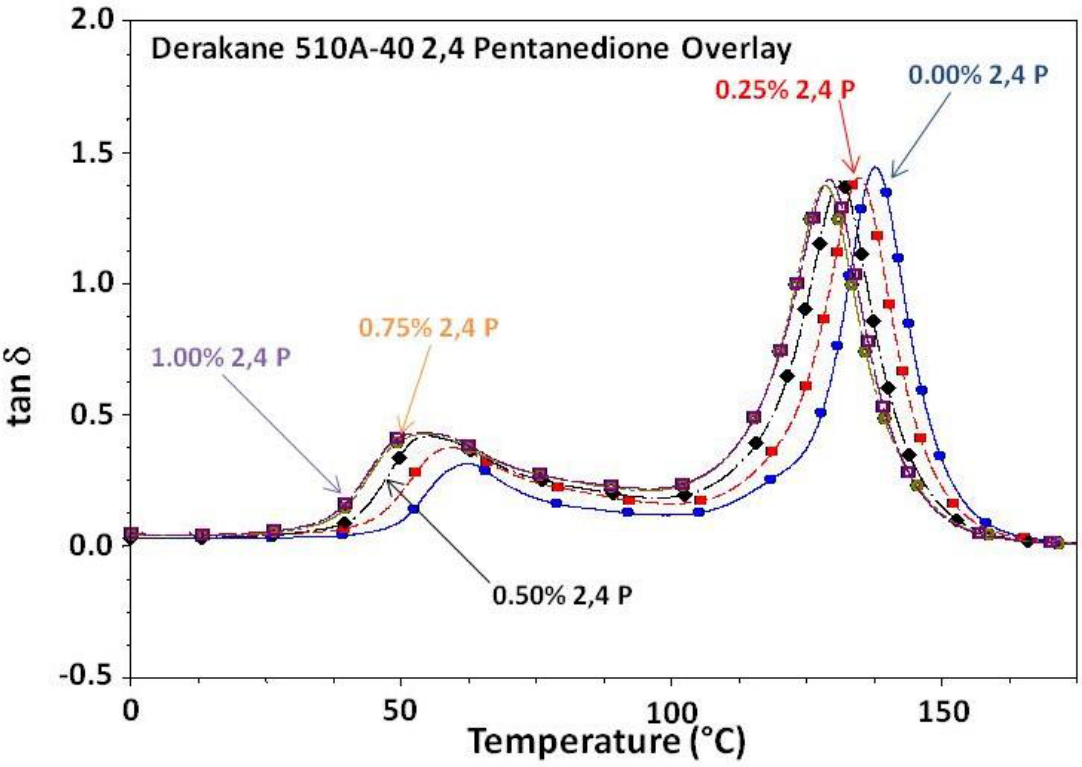

Figure 44. DMA tan δ of VER films cured at ambient temperature with 0 - 1 wt% 2,4-P.

Table 9

Properties of VER Films with Various Amounts of 2,4-P

2,4-P (%)	Density (g/mL)	T_1 (°C)	T_g (°C)	FWHH	DMA E'_R @ 175°C (MPa)	DMA M_c @ 175°C (g/mol)
0.00	1.391	49.20	137.6	14.9	8.72 ± 0.73	676 ± 57
0.25	1.393	45.02	134.7	16.0	7.84 ± 0.59	755 ± 57
0.50	1.376	40.61	131.2	16.6	6.75 ± 0.86	873 ± 112
0.75	1.365	37.62	128.4	18.5	5.91 ± 0.54	984 ± 90
1.00	1.363	38.12	129.2	17.2	5.89 ± 1.65	1037 ± 302

As observed earlier, the softening onset observed as a reduction in storage modulus correlates to incomplete conversion/connectivity within the

network (Figure 45). Post-curing minimized variability in conversion to a degree but the network architecture and connectivity ultimately suffer at higher 2,4-P loadings. Reduction in initiation efficiency by exchanging 2,4-P results in reduced conversion/connectivity of the initial network that was not possible to eliminate via thermal conditioning as was the case in the previous chapter using temperature as a method driving heterogeneity (i.e., network connectivity and mechanical property differences).

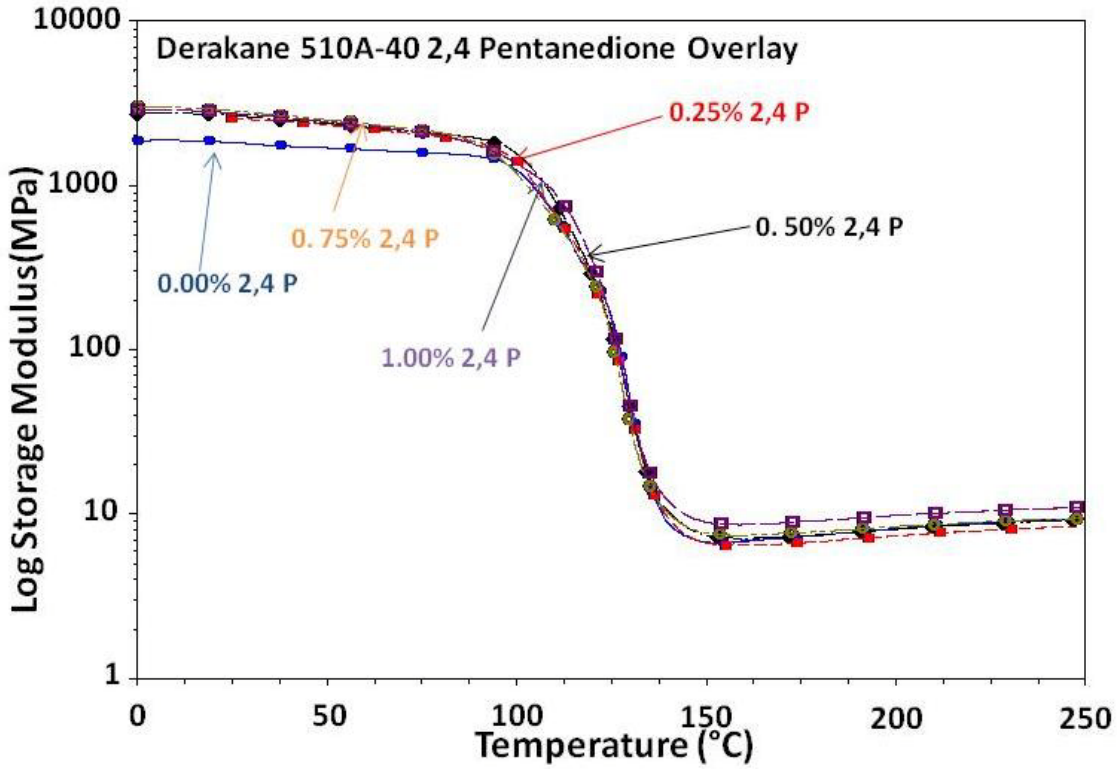

Figure 45. DMA storage modulus of post-cured VER films with 0 - 1 wt% 2,4-P.

The rubbery plateau modulus of the 0.75 and 1.00 wt% 2,4-P samples exhibited the lowest and highest values, respectively (Figure 46). This was not anticipated but is likely a result of increased variability during early stages of cure. The reduced catalytic activity at ambient cure conditions would permit a considerable amount of peroxide to remain. Upon post-cure, the thermal

dissociation of peroxide alters rates and concentrations of radicals, directly impacting network architecture.

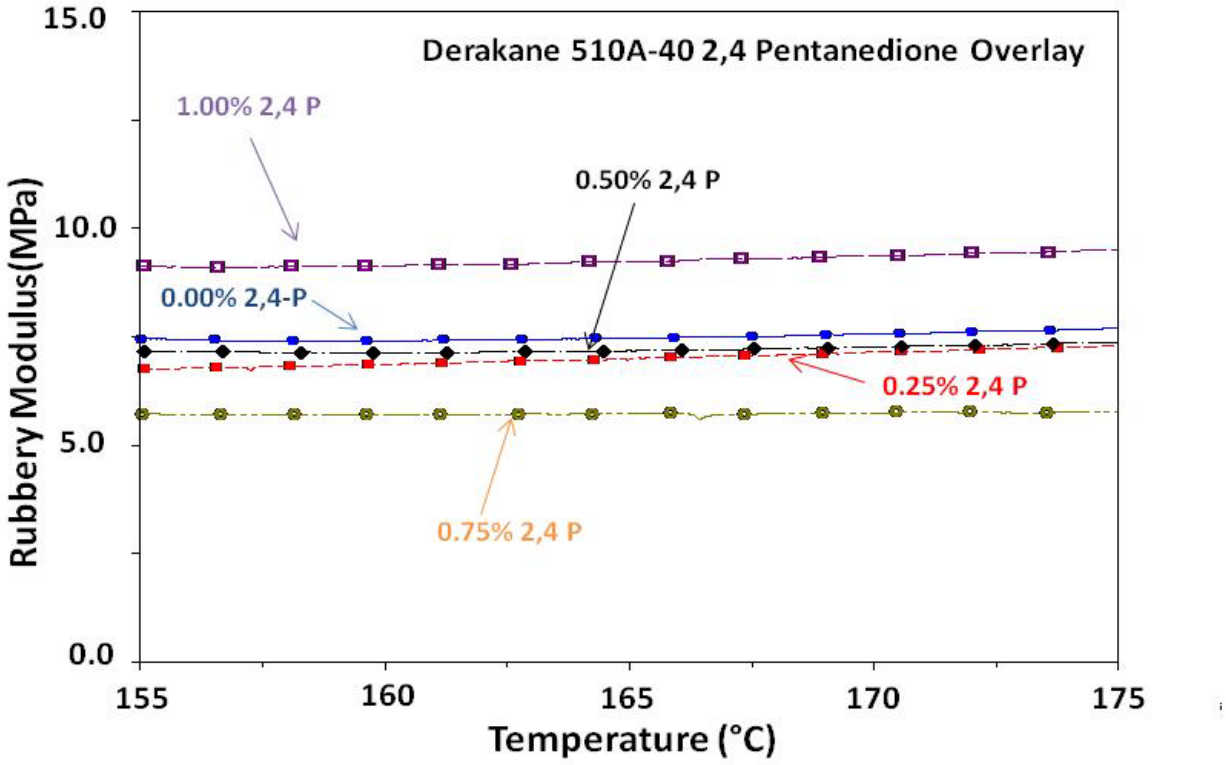

Figure 46. DMA rubbery modulus of post-cured VER films with 0 - 1 wt% 2,4-P.

Low temperature shoulders exist despite the elevated temperature post-cure conditions for all samples involved (Figure 47). Onset temperature for the low temperate tan δ shoulder are decreased with high levels of 2,4-P (0.75 and 1.00 wt%). The tan δ maxima of all samples is also slightly reduced with higher loadings of 2,4-P. Sample variability and calculated M_c values also increase upon 2,4-P loading, however, the variability is not as significant as observed with the ambient cured samples.

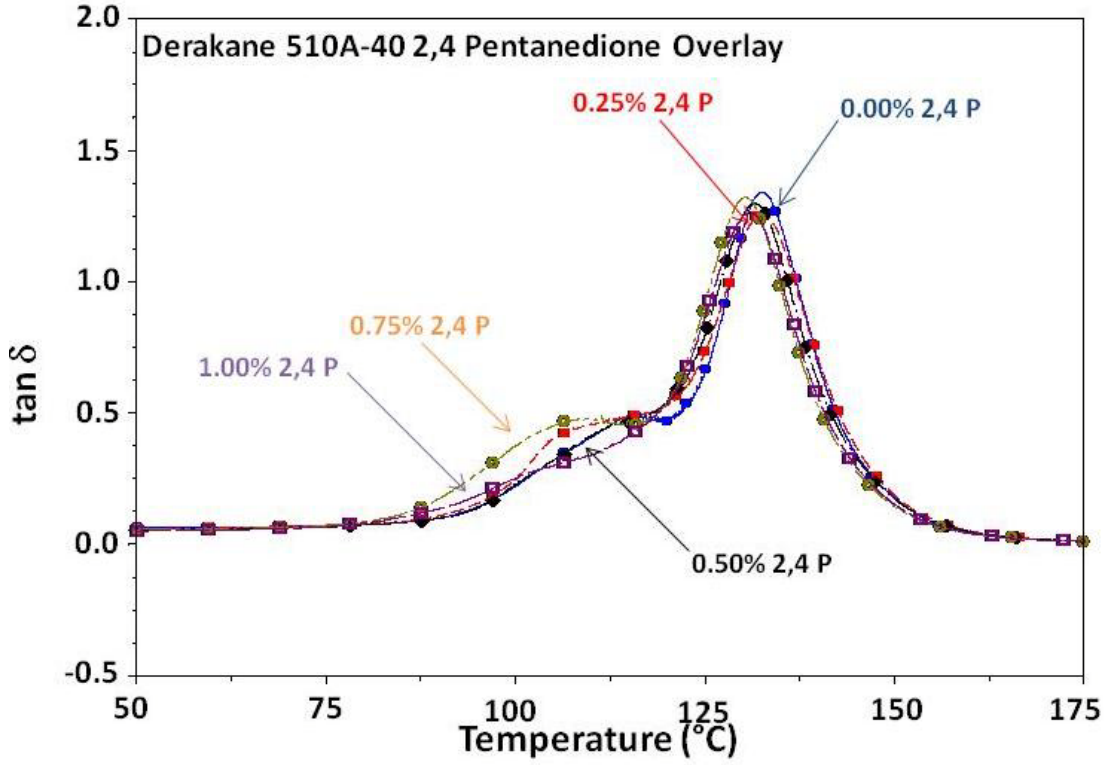

Figure 47. DMA tan δ of post-cured VER films with 0 - 1 wt% 2,4-P.

Table 10

Properties of Post-Cured VER Films with Various Amounts of 2,4-P

2,4-P (%)	Density (g/mL)	T_g (°C)	FWHH	DMA E'_R @ 175°C (MPa)	DMA M_c @ 175°C (g/mol)
0.00	1.395	132.6	14.7	7.06 ± 0.93	847 ± 112
0.25	1.394	132.7	18.1	7.86 ± 1.26	765 ± 124
0.50	1.390	131.6	16.6	6.76 ± 0.58	875 ± 76
0.75	1.385	130.5	16.3	5.76 ± 1.94	1106 ± 395
1.00	1.387	130.9	16.9	8.04 ± 2.09	766 ± 206

Tensile Testing

The tensile data for samples cured at various temperatures is plotted in Figure 48. Ambient samples exhibited poor mechanical response and large deviations from the mean due to poor conversion/connectivity. The sample containing 1.0 wt% of 2,4-P could not be evaluated due to poor sample quality. The neat ambient sample exhibited low modulus and strain-at-break values. Large deviation in mechanical properties of ambient cured samples containing 2,4-P is attributed to a lack of connectivity and conversion (Table 11). Peak stress and strain-at-break values were reduced significantly. The strain-at-break experienced by these samples is significant, as poor connectivity prevents adequate stress transfer and resulted in diminished performance under stress strain testing.

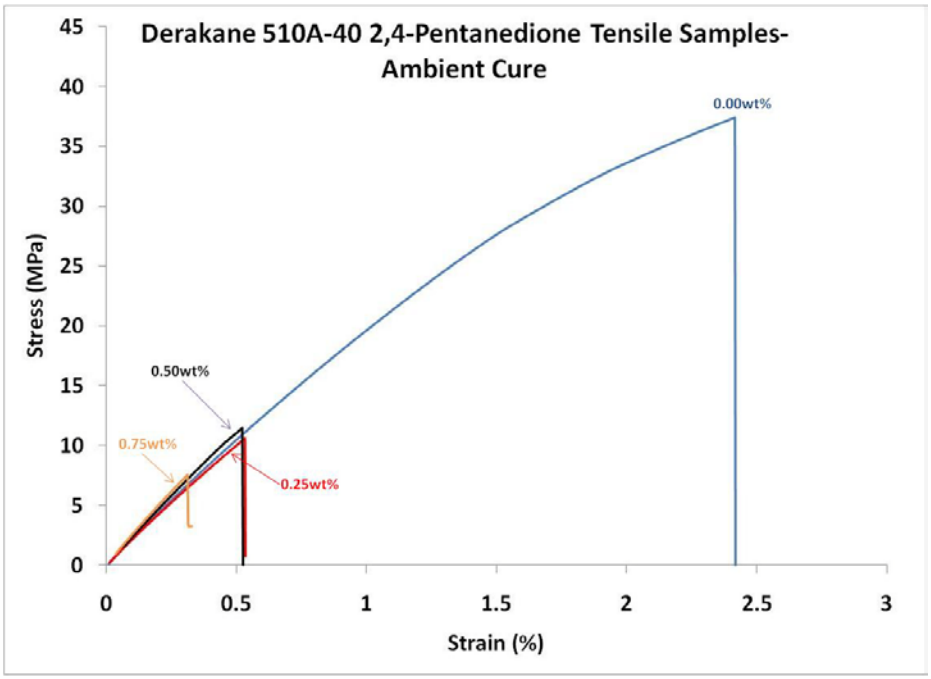

Figure 48. Tensile stress/strain response of ambient cured VER specimens with various amounts of 2,4-P.

Tensile data for post-cured samples are shown in Figure 49. Post-cured systems containing 2,4-P exhibited better stress/strain response than the ambient cured samples. Mechanical properties were still reduced with the addition of 2,4-P. DMA results attested to reduced variability and inhomogeneity in molecular architecture upon post-cure, but high 2,4-P loadings resulted in insufficient mechanical properties due to poor conversion/connectivity. The data support that elongated processing times are possible with 2,4-P, however the resulting matrices are not the same and do not seem to perform similarly during mechanical performance testing.

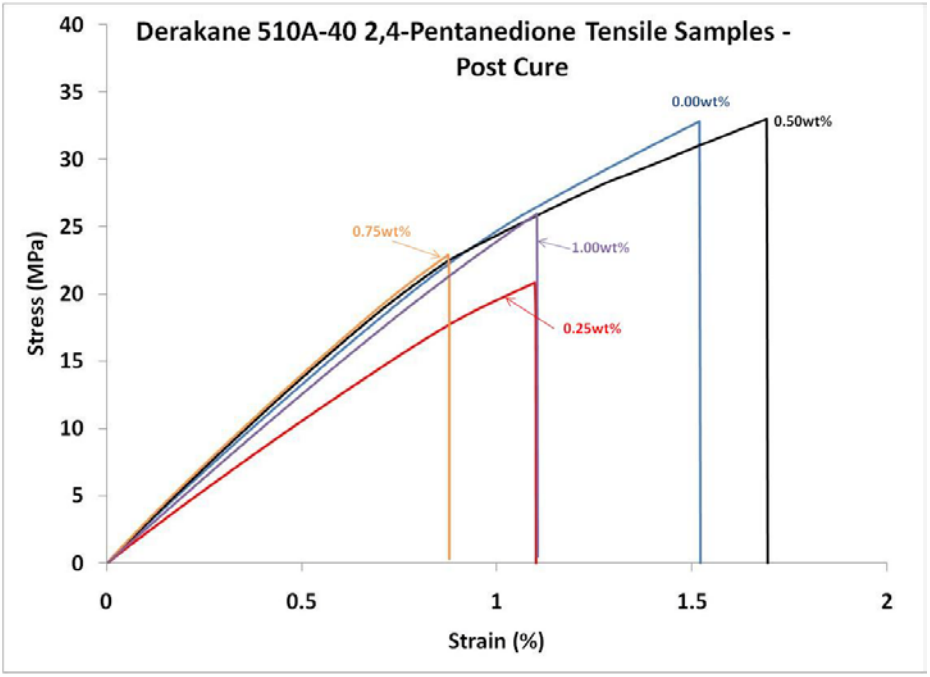

Figure 49. Tensile stress/strain response of post-cured VER specimens cured with 0 - 1 wt% 2,4-P.

Table 11

Tensile Properties of Ambient and Post-Cured VERs with 0-1wt% 2,4-P

2,4-P (%)	Peak Stress (MPa)	Strain-at-Break (MPa)	Young's Modulus (GPa)
0.00	31.6 ± 7.2	1.90 ±0.78	2.25 ± 0.18
0.25	11.4 ± 1.5	0.52 ±0.05	2.40 ± 0.18
0.50	11.4 ± 1.3	0.46 ±0.05	2.71 ± 0.30
0.75	9.7 ± 1.5	0.49 ±0.2	2.58 ± 0.20
1.00	- - -	- - -	- - -
0.00 PC	34.7±4.3	1.64±0.29	2.68±0.09
0.25 PC	20.1±2.6	1.09±0.12	2.16±0.06
0.50 PC	25.0±9.9	1.32±0.53	2.92±0.12
0.75 PC	24.6±7.7	1.02±0.44	2.93±0.14
1.00 PC	24.6±5.9	0.92±0.23	2.84±0.19

Note. PC designations refer to post-cured samples. Ambient samples with 1.00 wt% 2,4 P were of insufficient mechanical integrity to be evaluated

Summary and Conclusions

VER network architecture was manipulated through changes in catalyst activity. An *in situ* ligand exchange replaced naphthenic acids with 2,4-P and reduced catalyst activity. Formulations containing 0-1 wt% 2,4-P cured at ambient conditions yielded viable films with no visible differences or defects. Ambient cured films containing 1.0% 2,4-P did not develop sufficient strength for tensile testing due to inadequate conversion. Post-curing improved the film quality.

DSC results indicate initial conversions were relatively constant among all

sample formulations, with only the 1.00 wt% 2,4-P having a noticeable reduction in conversion (77.6%). However, the exotherm changed upon addition of 2,4-P, indicating a reduction in catalyst activity and a requirement for thermal decomposition of the peroxide during the analysis. This result was supported by the reduction in T_g (~ 5 °C) with 2,4-P loading as observed from the midpoint during the second heating scan.

DMA results indicated that higher loadings of 2,4-P reduced the softening onset and correlated well with the DSC evaluation. Reduced catalyst reactivity was more pronounced in the DMA, as it is more sensitive to molecular level architecture than the DSC. The low temperature tan δ transition onset temperature was reduced by ~ 10 °C by increasing 2,4-P loading to 1.00 wt%. Rubbery modulus was also reduced and M_c subsequently increased with increasing 2,4-P loading. Vitrification limits were reached at lower conversions and temperatures due to reduced exotherms and rates produced by the 2,4-P associated catalysts. Post-curing was able to overcome the initial limits of ambient cure and homogenize molecular level architecture to some degree at lower concentrations of 2,4-P. However, despite the thermal treatment, initial network development dominated ultimate mechanical performance as was evident by the changes seen in tan δ, rubbery modulus and tensile properties. Significant increases in property variation was observed with increasing 2,4-P loading. Tensile properties were reduced upon addition of 2,4-P. Inadequate conversion, connectivity and inhomogeneous network architecture were exaggerated in extended samples and resulted in poor tensile properties.

Another aspect of VER versatility results from the broad range of molecular precursors available. Specific properties are achieved by adjusting monomer chemical structure in VERs. Several variations in chemical architecture are available for enhancing desired parameters such as modulus, toughness, thermal stability, chemical resistance. The next chapter focuses on understanding the effect of changes in chemical architecture of the monomer on network development and mechanical properties of various VERs.

References

1. Mallick, P.K. *Fiber Reinforced Composites, 3rd Ed*. Taylor&Francis Group: Florida, 2008.
2. Waters, W.A. *Journal of the American Oil Chemists' Society,* **1971**, 38, 427.
3. Ikkai, F. & Shibayama, M. *Journal of Polymer Science Part B Polymer Physics*, **2005**, 617.
4. Kannurpatti, A. R., Anseth, J. W. & Bowman, C. N. *Polymer,***1997**, 39, 2507.
5. Scott, T. F., Cook, W. D. & Forsythe, J. S. *Polymer*, **2002**, 43, 5839.
6. Scott, T. F., Cook, W. D. & Forsythe, J. S. *Polymer*, **2003**, 44, 671.
7. Scott, T. F., Cook, W. D. & Forsythe, J. S. *European Polymer Journal*, **2002**, 38, 705.
8. Cook, W. D., Simon, G. P., Burchill, P. J., Lau, M. & Fitch, T. J. *Journal of Applied Polymer Science,* **1997**, 63, 769.
9. Scott, T. F., Cook, W. D. & Forsythe, J. S. *European Polymer Journal,* **2008**, 44, 3200.
10. Rey, L., Galy, J. & Santerau, H. *Macromolecules,* **2000**, 33, 6780.
11. Ziaee, S. & Palmese, G. R. *Journal of Polymer Science Part B Polymer Physics,* **1999**, 37, 725.
12. Li, P., Yu, Y., & Yang, X. *Journal of Applied Polymer Science,* **2008**, 109, 2539.
13. Li, L., Cao, X. & Lee, L.J. *Polymer,* 2004, **45**, 6601.

14. Gangliani, M., Carr, S. H. & Torkelson, J. M. *Polymer,* **2002**, 43, 2747.

15. Ramis, X. & Salla, J.M. *Polymer,* **1995**, 36, 3511.

16. Li, L. & Lee, L.J. *Polymer Composites,* **2002**, 23, 971.

CHAPTER VI

INVESTIGATION OF MONOMER STRUCTURE EFFECTS ON NETWORK DEVELOPMENT AND MECHANICAL PROPERTIES IN VERS

Introduction

Improving the modulus and toughness of polymer matrix materials is a critical first step in improving composite performance. Composite matrix VERs, and highly crosslinked thermosets in general, are convenient for ambient cure but notorious for their brittleness and low fracture toughness. Deformation mechanisms in polymers are controlled by the brittle-to-ductile transition. Glassy polymers with a high crosslink density and/or T_g are often brittle and prone to facile fracture. Although temperature plays a role, toughness is ultimately decided by the ability of a glassy matrix to resist fracture while being capable of yield. Crazing and shear yielding are two primary mechanisms associated with the brittle-to-ductile transition.[1] Classic crazing occurs at 90° to the applied stress and typically permits elongations of 1-2% prior to failure. These are the traditional hard but brittle matrix materials. Shear yielding is a result of molecular motions at 45° to the applied stress and permits elongations > 20 %. Shear yielding is preferred because it enables the material to absorb energy without irreparable damage at low elongations and results in a ductile deformation mechanism.

Elastomer modification is often employed to enhance fracture toughness. For instance, fracture toughness was shown to increase by an order of magnitude over that of neat epoxy resins with the addition of carboxyl terminated

butadiene nitrile rubber (CTBN).[2-5] The rubber particles enhanced shear yielding while simultaneously dissipating bulk strain energy. Crosslink density and T_g do not exert a significant influence on rubber toughening, provided the matrix is sufficiently capable of yielding.[6-8] Reduction in crosslink density often results in a synergistic increase in toughness with the addition of rubber particles.[3,5-7] Kinloch and Hunston also noted that toughness was not related to rubber loading, thus identifying the necessity for the matrix to yield preferentially.[9] Rubber toughening provide greater means for energy dissipation and predisposes the polymer matrix to shear yielding. As Bagheri and Pearson concluded, cavitation of rubber particles does not primarily increase toughness in highly crosslinked systems. Rather, their purpose is to alleviate plane strain conditions and permit plastic deformation (shear yielding) of the matrix.[10]

Several requirements exist for the rubber toughening agent to be effective. Critical aspects of the rubber include size, phase, interaction with the matrix, and T_g. Effective particle size is determined by the intended mechanism of energy dissipation. In general, the particle should be at least as large as the propagating crack tip radius, with a minimum size of 40 nm to induce cavitation.[9] More recently, self-assembling block copolymers have resulted in increased toughness via cavitation with particles as small as 15 nm.[11-15] Crack growth rates relate directly to the T_g of the rubbery phase.[9] Simplistically, fracture resistance is generally improved when the rubber particle has a T_g ~ 60 °C below the application temperature. However, many low T_g materials used in rubber toughening applications have limited thermal stability. To address the thermal

instability of butadiene based elastomer toughening agents, Ratna evaluated liquid rubber modified epoxies based on carboxyl terminated poly(2-ethylhexylacrylate).[16,17] The acrylate functionality had little effect on toughness relative to the CTBN based systems, but it played a significant role in the thermoset network development and cure times. CTBN-based options continue to be one of the most utilized toughness enhancement technologies despite issues with dispersion, mechanical property reduction, and thermal stability.

To understand the impact of chemical structure on molecular level architecture and mechanical behavior, multiple conventional VER systems were investigated and compared for changes in morphology, thermomechanical properties, and fracture toughness. A classic VER system was compared to a fire resistant brominated species as well as an elastomer modified species.

Three different vinyl ester resins were evaluated in this study to determine the effect of VER chemical structure on mechanical properties. Derakane® 411-350, Derakane 510A-40 and Derakane 8084 were diluted with styrene to 45% by weight to isolate the impact of vinyl ester structure on performance. Individual VERs were blended with 0.2 wt% CoNap before adding 1.0 wt% MEKP and mixing again thoroughly until homogeneous. The formulations were then cured for 24 hours under ambient conditions and post-cured for two hours at 125 °C. An additional one hour thermal conditioning at 150 °C followed by a slow cool was done to ensure complete conversion and normalize the samples against any thermal fluctuations experienced during cure.

Gel Permeation Chromatography

Molecular weight analysis showed a distinct difference in the molecular weight and PDI of each commercial VER (Table 12). The Derakane 411-350 and Derakane 510A-40 systems had similar M_n values, with Derakane 510A-40 being slightly higher due to the bromination of the DGEBA backbone. Derakane 8084 displayed a high molecular weight component (~ 16,000 g/mol) that correlates to the functional rubber toughening additive. This additive is approximately 10 wt% of the total resin with the remaining 90% of the dimethacrylate species having nearly half the molecular weight of the other to commercial resins. Predicted M_c values as derived from the kinetic theory of rubber elasticity are shown in Table 1. Similar values for Derakane 411-350, 510A-40 and 8084 were calculated to be ~ 600 g/mol, ~ 700 g/mol and 1,150 g/mol, respectively. Without the contribution of the high molecular weight component, the predicted M_c for the Derakane 8084 system is ~ 370 g/mol. Further analysis of predicted M_c values will be discussed with the experimentally derived M_c values from DMA.

Table 12

GPC Results of Commercial VERs

VER	Peak M_n (g/mol)	PDI	wt%	Predicted M_c (g/mol)
Derakane 411-350	1166	3.28	100	598
Derakane 510A-40	1356	2.24	100	695
Derakane 8084	15,960	1.79	~10	1150
	720	1.38	~90	

Differential Scanning Calorimetry

DSC analysis was used to track conversion during cure. Samples extracted at 2, 6, 12 and 24 hours of ambient cure exhibited exotherms during the analysis, indicative of further conversion during analysis. Conversion proceeded once temperature exceeded the vitrification point (Figures 50-52). Upon post-curing, each sample achieved full conversion, as was evident by the absence of an exotherm during the initial thermal scan.

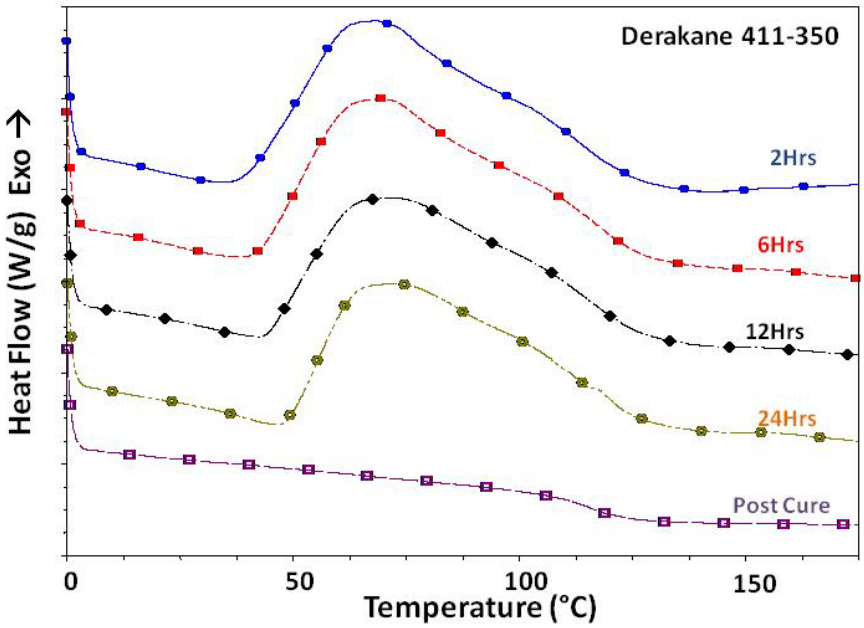

Figure 50. Conversion tracking of Derakane 411-350.

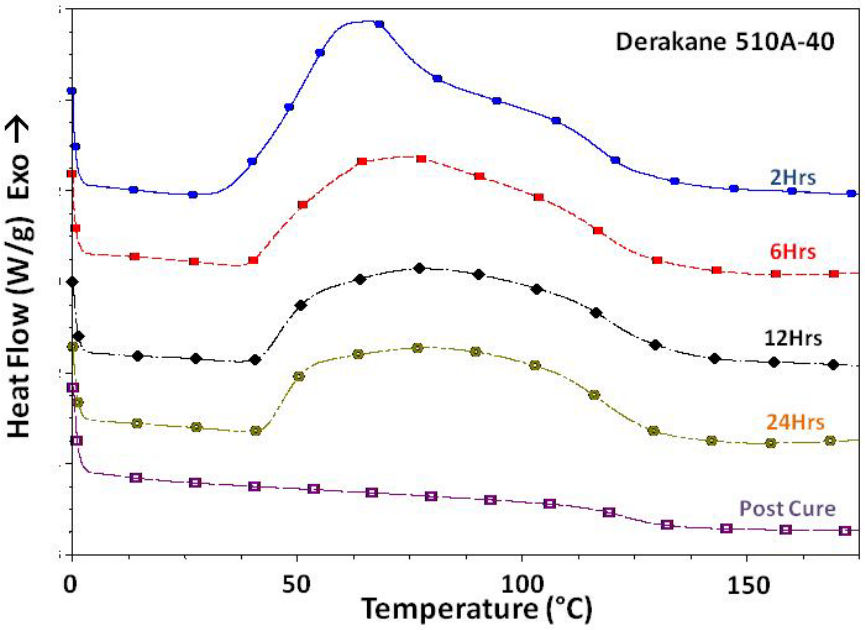

Figure 51. Conversion tracking of Derakane 510A-40.

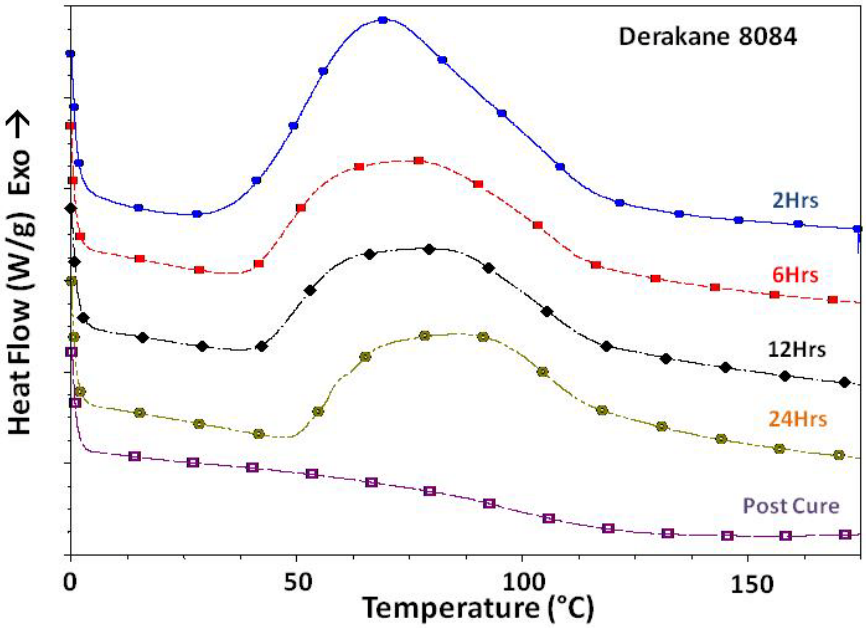

Figure 52. Conversion tracking of Derakane 8084.

Comparison of the post-cured samples is shown in Figure 53. Transitions evaluated from the second heating scan show slightly earlier onset of T_g in Derakane 411-35 with a midpoint T_g of 123.09 °C compared to Derakane 510A-

40 that has a similar midpoint T_g of 123.62 °C. The elastomerically modified Derakane 8084 has a significantly broader transition region and a much earlier onset point than either of the other two systems, with a midpoint T_g of 99.18 °C.

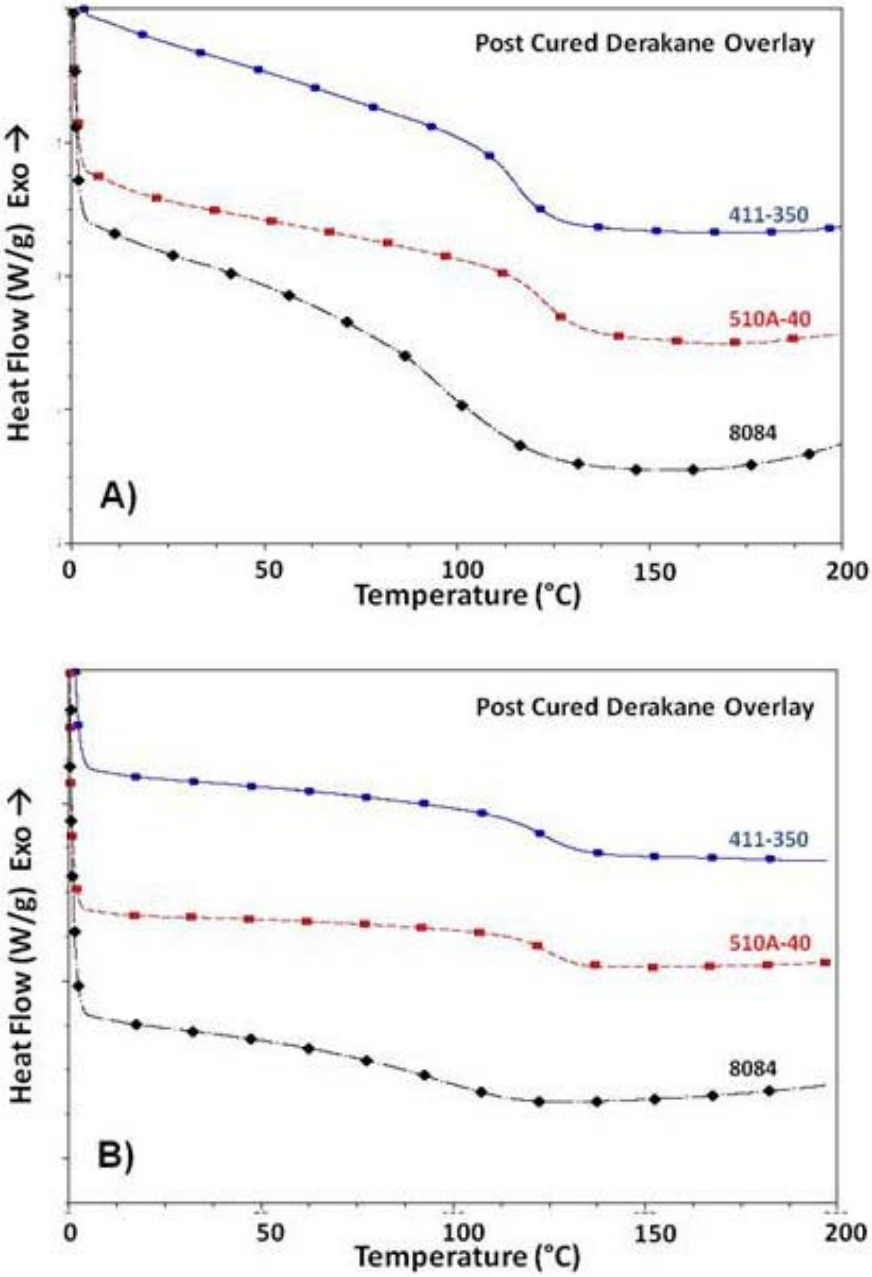

Figure 53. DSC Comparison of post-cured resins; A) first heating scan and B) second heating scan.

Dynamic Mechanical Analysis

The dynamic mechanical responses of these materials exhibited variations corresponding to changes in chemical structure. Glassy modulus values trend accordingly with Derakane 411-350 and Derakane 510A-40 having a higher stiffness than Derakane 8084 (Figure 54). The rubbery plateau region was inverted with Derakane 8084 exhibiting the highest stiffness (Figure 55). This trend was not anticipated as incorporation of an elastomeric component is expected to lower the crosslink density and reduce the rubbery modulus. Additionally, the rubber modulus of Derakane 510A-40 was lower than that of Derakane 411-350 due to incorporation of bulky bromine groups in the backbone.

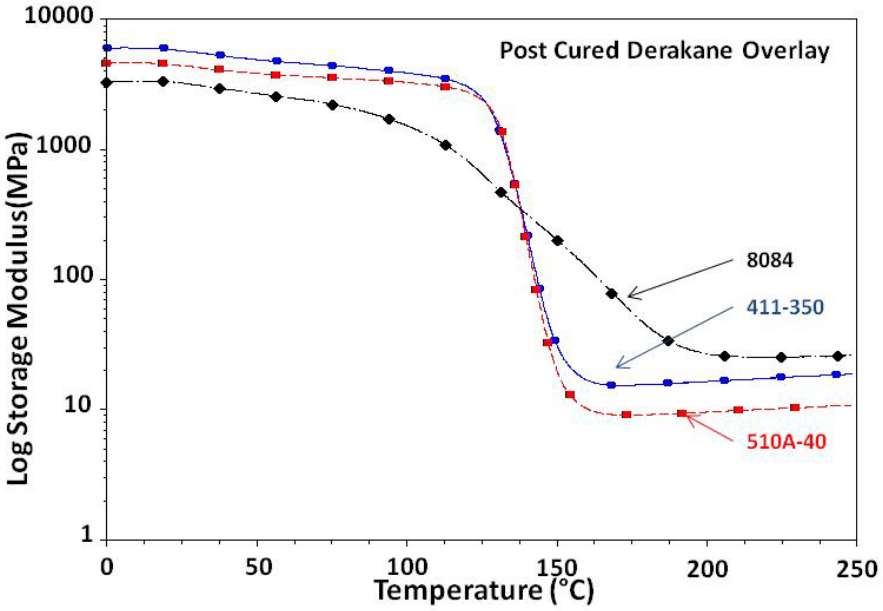

Figure 54. Storage modulus plot of the three Derakane resins. Derakane 411-350 and Derakane 510A-40 exhibit higher glassy modulus than Derakane 8084. Derakane 8084 has an early onset of softening, broader glass transition but overall higher modulus value in the rubbery plateau region.

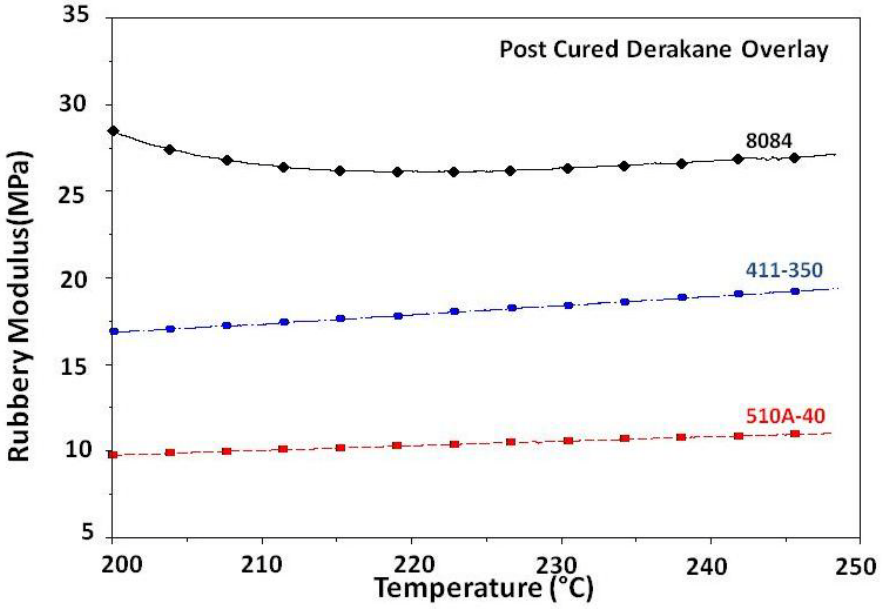

Figure 55. DMA rubbery modulus region of the three Derakane resins. Derakane 8084 exhibits the highest rubbery modulus despite being a rubber toughened resin with a high molecular weight elastomeric component. Derakane 411-350 and 510A-40 differ only by bromination in the latter species, accounting for the reduction in rubbery modulus.

Glass transition temperatures evaluated from the primary tan δ peaks trend well with DSC measurements (Figure 56). Derakane 411-350 and Derakane 510A-40 had similar transition temperatures, although Derakane 510A-40 had a higher transition peak height. Derakane 8084 exhibited multiple transitions that were not evident in the DSC, and highlights DMA's enhanced sensitivity to microstructure.

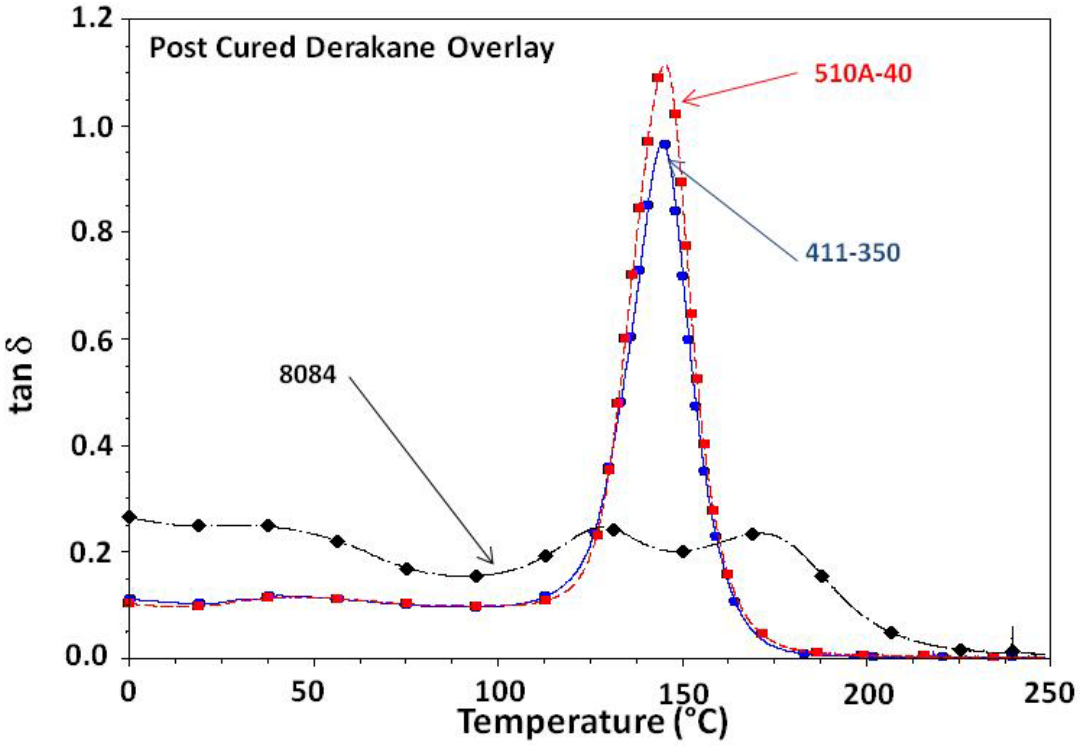

Figure 56. Derakane 411-350 and Derakane 510A-40 exhibit similar T_gs (taken from the tan δ maxima). Derakane 8084 response is much broader with multiple transitions due to increased heterogeneity and phase separation of the elastomeric component.

Derakane 8084 exhibits characteristics of a bimodal network. Bimodal networks have been reported in the literature with low maxima in the tan δ and little impact on the T_g or storage modulus.[18-20] These features are indicative of a heterogeneous network architecture. As expected, the FWHH of Derakane 411-350 and Derakane 510A-40 systems were very similar, i.e., 20.91 and 22.93, respectively (Table 13). It is difficult to discern an exact FWHH for Derakane 8084 as it exhibits multiple low intensity transitions due to the chemical structure of the monomeric components. The difference in M_c between Derakane 411-350 and Derakane 510A-40 is a direct result of bromination in the latter species.

Table 13

Properties Derived from Dynamic Mechanical Analysis

VER	Density (g/mL)	T_g (°C)	FWHH	DMA E'_R @ T_g + 100°C (MPa)	Predicted M_c (g/mol)	DMA M_c (g/mol)
Derakane 411-350	1.184	144.7	20.91	18.19 ± 0.74	598	365 ± 15
Derakane 510A-40	1.289	145.4	22.93	10.83 ± 0.96	695	671 ± 60
Derakane 8084	1.117	125.5	- - -	26.16 ± 2.78	1150	241 ± 26

A comparison with the predicted M_c values shows good agreement for the Derakane 411-350 and Derakane 510A-40 systems, with the latter being more comparable due to a lower PDI. Derakane 8084 M_c is closer to the 370 g/mol M_c value estimated using only the M_n of 720 g/mol, while the contribution of the higher molecular weight component does not impact the network stiffness. This can be attributed to primary load bearing through the shortest chains in the network structure.

Mechanical Testing

Compression testing results are shown in Figure 57. Derakane 510A-40 and Derakane 411-350 exhibit similar moduli values while Derakane 8084 exhibits a lower modulus due to the elastomeric toughening agent (Table 14). Derakane 411-350 has a higher yield stress and strain than Derakane 510A-40. Derakane 8084 yields much earlier than the other two resins. These results display a preference to yield in the following order; Derakane 8084 > Derakane 510A-40 > Derakane 411-350.

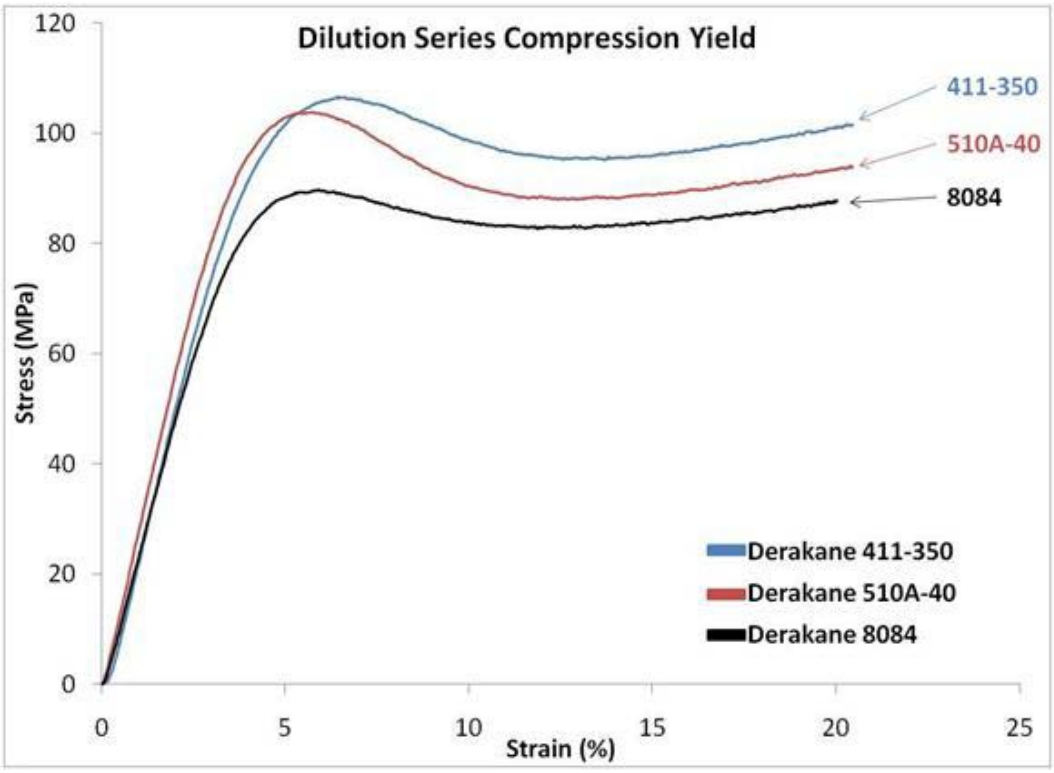

Figure 57. Compression testing of Derakane 411-350 and Derakane 510A-40 indicated a very similar response while the latter has a slightly higher modulus. Derakane 8084 exhibits a much earlier yield point due to the presence of the elastomeric component.

Table 14

Uniaxial Compression Data of VERs

VER	Yield Stress (MPa)	Yield Strain (%)	Young's Modulus (GPa)
Derakane 411-350	106.6 ± 1.4	6.47 ± 0.18	2.67 ± 0.19
Derakane 510A-40	103.6 ± 1.9	5.76 ± 0.24	2.73 ± 0.18
Derakane 8084	90.5 ± 2.0	6.86 ± 0.07	2.36 ± 0.09

Fracture toughness values are listed in Table 15. Derakane 8084 has the highest fracture resistance due to the lower energy required to yield. K_{IC} values describe the critical stress per area required to promote crack growth. Derakane 510A-40 has a K_{IC} value of 0.96 MPa$\sqrt{m}$, higher than that of the non-brominated

Derakane 411-350 (0.67 MPa√m). The introduction of the elastomeric component increases the K_{IC} value of Derakane 8084 to 1.12 MPa√m. These trends are echoed in the strain energy release rate, G_{IC}, which is the maximum strain value a material may experience prior to the spontaneous growth of a crack. Accordingly, Derakane 411-350 was the most brittle matrix with a value of 178.4 J/m^2, followed by Derakane 510A-40 (391.9 J/m^2) and Derakane 8084 (725.1 J/m^2).

Table 15

Fracture Properties of Derakane Resins

VER	K_{IC} (MPa√m)	G_{IC} (J/m^2)
Derakane 411-350	0.67 ± 0.03	178.4 ± 16.5
Derakane 510A-40	0.96 ± 0.06	391.9 ± 38.5
Derakane 8084	1.13 ± 0.06	725.1 ± 166.8

Fracture Surface Analysis

Optical and scanning electron micrographs (Figures 58 and 59, respectively) exhibit smooth fracture surfaces for the Derakane 411-350 and 510A-40 systems. However, incompatibility of the elastomeric phase alters the morphology of Derakane 8084. Derakane 8084 has a lamellar surface morphology, while the Derakane 411-350 and Derakane 510A-40 systems exhibit no surface features, characteristic of a brittle glassy failure mechanism. Surface characteristics correlate directly with the fracture properties of the neat resins.

Figure 58. Optical microscopy of Derakane series fracture surfaces at 300X magnification. Derakane 411-350 and Derakane 510A-40 display characteristic surfaces for brittle glassy systems. Derakane 8084 exhibits a lamellar surface morphology due to the incompatibility of the vinyl ester component and the elastomeric component.

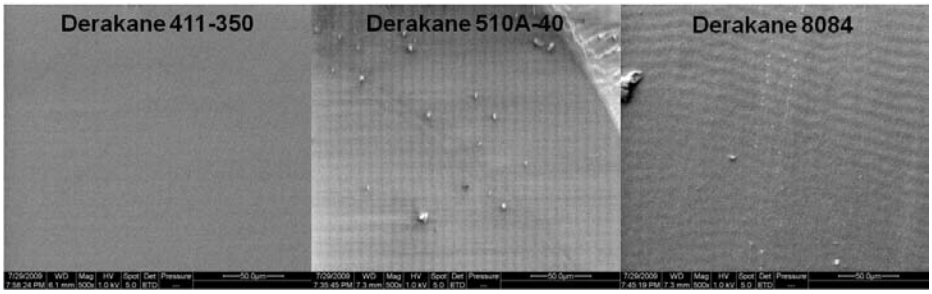

Figure 59. Scanning electron microscopy of Derakane series fracture surfaces. SEM analysis of fracture surfaces exhibits essentially featureless fracture surfaces for Derakane 411-350 and Derakane 510A-40 as expected for brittle glassy systems. Derakane 8084 exhibits a lamellar morphology due to phase separation between the elastomeric component and the vinyl ester resin.

Summary and Conclusions

Derakane 411-350 was evaluated as a baseline against a brominated version, Derakane 510A-40 and an elastomer modified version Derakane 8084. The brominated Derakane 510A-40 exhibits enhanced thermal stability. The Derakane 8084 species possess a different molecular level morphology due to the elastomeric additive.

GPC results indicated minimal differences between Derakane 411-350 and Derakane 510A-40. However, the Derakane 8084 exhibited a bimodal distribution of low and high molecular weight chains, 720 g/mol and 15,960 g/mol respectively. The high molecular weight component comprised approximately 10% by weight of the total composition. This resulted in an increase in calculated M_c from 370 g/mol for a resin comprised solely of the low molecular weight component to 1150 g/mol of the bimodal mixture. The calculated M_c for Derakane 411-350 and Derakane 510A-40 were similar, 598 g/mol and 695 g/mol respectively, as anticipated with the only difference attributed to bromination of the latter.

DSC was used to evaluate conversion and T_g of each system. Conversion proceeded slowly with the onset of vitrification and complete conversions were achieved only upon post-cure. As discussed previously, the redox reaction and thermal decomposition of peroxide was evident by the exotherm peak shape in the first heating scan. Derakane 411-350 and Derakane 510A-40 had similar midpoint T_gs of ~ 123 °C when evaluated via DSC, while Derakane 8084 exhibited a broad T_g (midpoint of 99.18 °C) curve owing to the heterogeneous network architecture induced by the addition of an elastomeric component.

DMA thermal transitions echoed the trends observed in the DSC. T_gs determined from the tan δ maxima for Derakane 411-350 and 510A-40 were similar at 144.7 °C and 145.4 °C respectively. Derakane 8084 exhibited multiple broad and low intensity tan δ transitions, indicative of the bimodal monomer composition identified in the GPC analysis. Glassy modulus values trended as expected. However, Derakane 8084 exhibited the highest rubbery modulus and the lowest molecular weight between crosslinks. This result was not anticipated for an elastomer modified species. Increased rubbery modulus, multiple tan δ transitions and elevated apparent T_gs are attributed to the heterogeneous nature and complex network architecture associated with the bimodal monomer composition of the resin. Predicted M_c values were lower than experimentally derived values for all systems. The Derakane 411-350 and Derakane 510A-40 systems were in general agreement with predicted values. Derakane 8084 exhibited a response more representative of a network architecture that was not influenced by the high molecular weight component than of the value predicted

based on total composition. Analysis suggests long range connectivity is dominated by the shortest chains within the network architecture, resulting in the elevated stiffness response and subsequent M_c calculations.

Uniaxial compression testing was used to evaluate yield characteristics. Derakane 8084 exhibited lower yield stress (90.5 MPa) and yield strain (6.86%) values due to the elastomeric component. Derakane 510A-40 was characterized by a slightly lower yield strain than Derakane 411-350, with other properties being similar. This was attributed to the increased free volume caused by the much larger bromine substituent.

Fracture toughness values correlated directly with network architecture. Increased free volume attributed to the bulky bromine substituents on the Derakane 510A-40 resulted in yielding prior to the architecture of Derakane 411-350, and resulted in higher fracture resistance (K_{IC} and G_{IC}). Derakane 8084 exhibited the highest toughness due to the yield characteristics resulting from the elastomeric toughening.

Surface morphologies exhibited features indicative of the fracture response for these materials. Derakane 411-350 and Derakane 510A-40 exhibited featureless surfaces that are characteristic of brittle glassy materials. The surface morphology of Derakane 8084 reflected the presence of the elastomeric component and exhibited increased fracture resistance.

In addition to elastomer modification, nanoparticles are another option for the enhancement of matrix properties. Nanoparticles offer increased surface area over macroparticles, providing increased interaction with the matrix. The

increased interactions theoretically maximize performance potential at low loading levels. The following chapter will examine the impact of polyhedral oligomeric silsesquioxanes (POSS) on the properties of VERs.

References

1. Sperling, L. H. *Introduction to Physical Polymer Science, 4th Ed*. John Wiley & Sons, Inc.: New Jersey, 2006.
2. Yee, A.F., Pearson, R.A. *Journal of Materials Science*, **1986**, 21, 2462.
3. Yee, A.F., Pearson, R.A. *Journal of Materials Science*, **1986**, 21, 2475
4. Yee, A.F., Pearson, R.A. *Journal of Materials Science*, **1989**, 24, 2571.
5. Pearson, R.A., Yee, A.F. *Journal of Materials Science*, **1991**, 26, 3828.
6. Levita, G., De Petris, S., Marchetti, A., Lazzeri, A. *Journal of Materials Science*, **1991**, 26, 2348.
7. Iljima, T., Naoto, Y., Tomoi, M. *European Polymer Journal,* **1992**, 28, 573.
8. Mafi, E.R., Ebrahimi, M., Moghbeli, M.R. *Journal of Polymer Engineering,* **2009**, 29, 293.
9. Kinloch, A.J., Hunston, D.L. *Journal of Materials Science Letters,* **1987**, 6, 131.
10. Bagheri, R., Pearson, R.A. *Polymer,* **2000**, 41, 269.
11. Ruiz-Perez, L., Royston, G.J., Fairclough, P.A., Ryan, A.J. *Polymer*, **2008**, 49, 4475.
12. Sun, L., Gibson, R.F., Gordaninejad, F., Suhr, J. *Composites Science and Technology,* **2009**, 69, 2392.
13. Dean, J.M., Verghese, N.E., Pham, H.Q., Bates, F.S. *Macromolecules*, **2003**, 36, 9267.

14. Thompson, Z.J., Hillmyer, M.A., Liu, J., Sue, H.-J., Dettloff, M., Bates, F.S. *Macromolecules,* **2009**, 42, 2333.

15. Liu, J., Sue, H-J., Thompson, Z.J., Bates, F.S., Detloff, M., Jacob, G., Verghese, N., Pham, H. *Macromolecules,* **2008**, 41, 7616.

16. Ratna, D. *Polymer,* **2001**, 42, 4209.

17. Ratna, D., Banthia, A.K. *Polymer International*, **2000**, 49, 281.

18. La Scala, J.J., Logan, M.S., Sands, J.M. & Palmese, G.R. *Composites Science and Technology,* **2008**, 69, 1869.

19. Erman, B. & Mark, J.E. *Macromolecules,* **1998**, 31, 3099.

20. La Scala, J.J., Orlicki, J.A., Winston, C., Robinette, E.J., Sands, J.M. & Palmese, G.R. *Polymer*, **2005**, 46, 2908.

CHAPTER VII

PHYSICAL PROPERTIES OF VINYL ESTER NANOCOMPOSITES USING REACTIVE AND NONREACTIVE POLYHEDRAL OLIGOMERIC SILSESQUIOXANES

Introduction

Understanding the limits and potential for composite materials characteristics and performance are critical to tailor the polymer matrix properties. Polymer matrix properties are generally controlled through monomer structure, chain density, molecular weight, reinforcement type and relationship with matrix along with changes induced by varying levels of conversion and homogeneity (i.e., crosslink density and crosslink density distribution).[1-8] Increasing the molecular weight between crosslinks (M_c) typically reduces the T_g as well as modulus as the distance between use temperature and T_g narrows. In this respect, nanoparticle reinforcements are of significant interest. Common fillers in composites range in particle size from 5-100 μm in diameter and are used up to 50% by weight. The use of fillers with particle size less than 100 nm offers the potential to significantly enhance modulus, thermal stability, gas barrier and mechanical/fracture properties. This is accomplished at low loading levels, especially with nanoparticles that exhibit a high aspect ratio.[9] The uniformity of nanoparticle morphology and dispersion within the matrix also offers good control over performance properties.

POSS exhibit potential for tuning matrix performance.[10-14] POSS compounds are characterized by the general formula $Si_8O_{12}R_8$ and possess a

very well defined cage structure with a broad range of chemical functionalities. Compatibilization of POSS nanoparticles via selective functionalization of the R groups offers near limitless opportunities to develop hybrid long-fiber reinforced composites with nano-reinforced matrices. POSS nanomaterials facilitate matrix development through unique molecular level interaction and architecture. POSS incorporation is known to enhance T_g, surface characteristics, thermal stability, barrier properties and flame retardance.[10-15] While POSS dispersion is enhanced with increased functionality, mechanical properties rely heavily on POSS-POSS interactions.[11] Highly functional POSS has been shown to be very reactive, affecting several thermal and viscoelastic properties.[14] POSS nanoparticles with reactive sites increase the average resin functionality, potentially increasing heterogeneities within the matrix. The heterogeneous regions may lead to free volume cavities that are responsible for stress concentration.[16-18] Since the mechanical and thermal properties of these systems are highly dependent upon the free volume properties, it is necessary to establish structure-property relations with respect to free volume behavior.

Pressure-volume-temperature (PVT) relationship in polymers is a topic of considerable interest, particularly from a process design standpoint. PVT measurements involve quantifying the specific volume of a given polymer as a function of pressure and temperature. Specific volume is sensitive to changes in state, therefore pressure-dependent transition temperatures, and derived properties such as thermal expansivities and compressibilities can be determined from PVT data.[16] In addition to assessing free volume, PVT behavior of polymers

is useful for deriving appropriate equations of state (EOS) and constitutive models for predicting the response of polymeric networks to extreme conditions. EOS analysis provides valuable information about fundamental properties and thermodynamic behavior such as cohesive energy density and internal pressure. Several EOS exist for thermoplastics. By contrast, rigorous analyses of PVT behavior for thermoset polymer networks are rare due to complications from the thermodynamic history and network structure.

In the present study, the network structure of a commercial VER was modified by addition of POSS nanoparticles. A commercial brominated vinyl ester resin was reinforced with two different POSS species, one reactive with the matrix and one non-reactive. Viscoelastic behavior and mechanical properties of the resulting nanocomposites were evaluated against the neat resin to determine the influence of POSS nanoparticles.

Derakane 510A-40 was formulated neat and with the addition of 5 wt% (5.5 vol%) of isobutylPOSS (NPOSS) or 5, 15, or 25 wt% (5.1, 15.3 or 25.5 vol%) methacrylPOSS (RPOSS). The VERs were blended with 0.2 wt% CoNap until the system was visibly homogeneous. Subsequently, 1.0 wt% MEKP was added and the system mixed thoroughly until homogeneous. The formulations were cured for 24 hours under ambient conditions and post-cured for two hours at 125°C and an additional one hour at 150°C to ensure complete conversion.

Conversion Analysis

FTIR conversion profiles were tracked using a heating profile of 12 hours at 25 °C followed by a 2 hour post cure at 125 °C (Figure 60). The initial/early

rate of conversion for the methacrylate species was higher than for that of styrene in all cases, as observed in Chapter IV. The low cure temperature results in preferential homopolymerization of the methacrylate, resulting in delayed conversion of the styrene monomer. The neat resin conversion of methacrylate functionality is limited to ~ 50 % for the duration of ambient cure, as observed in Chapter IV. Upon post-cure, there is a sharp increase in conversion of both species, with styrene approaching full conversion. The dimethacrylate component only achieves 90% conversion, and is consistent with earlier studies.

The POSS containing resins both exhibit similar trends, albeit at different levels of conversion. Initial conversion of the methacrylate species approaches 70% in the 5 wt% NPOSS sample while the 5 wt% RPOSS sample reaches nearly 80% very early in the reaction. These trends are attributed to gel effects and autoacceleration within the heterogeneous system early in the reaction, limiting termination and enhancing conversion rates. Both POSS systems reach full conversion upon post-cure.

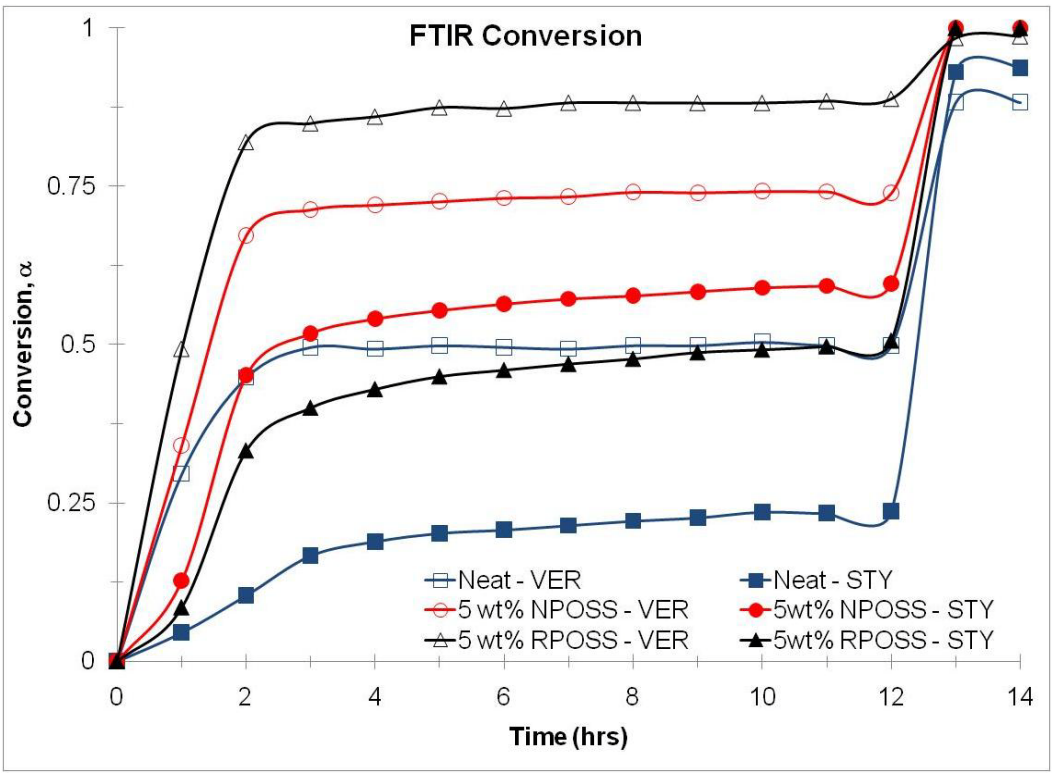

Figure 60. FTIR conversion analysis of POSS containing VERs. Open symbols denote dimethacrylate (vinyl ester component) conversion while closed symbols denote styrene conversion. Samples were cured in the FTIR 12 hours at 25 °C followed by a two hour post-cure at 125 °C.

Differential Scanning Calorimetry

Resin conversion was also tracked using DSC. The initial scans of the post-cured samples did not exhibit exotherms representative of additional cure (Figure 61). Moreover, the second scan T_gs did not advance, indicating that the films had achieved full conversion within detection limits of the DSC and correlate well to FTIR studies.

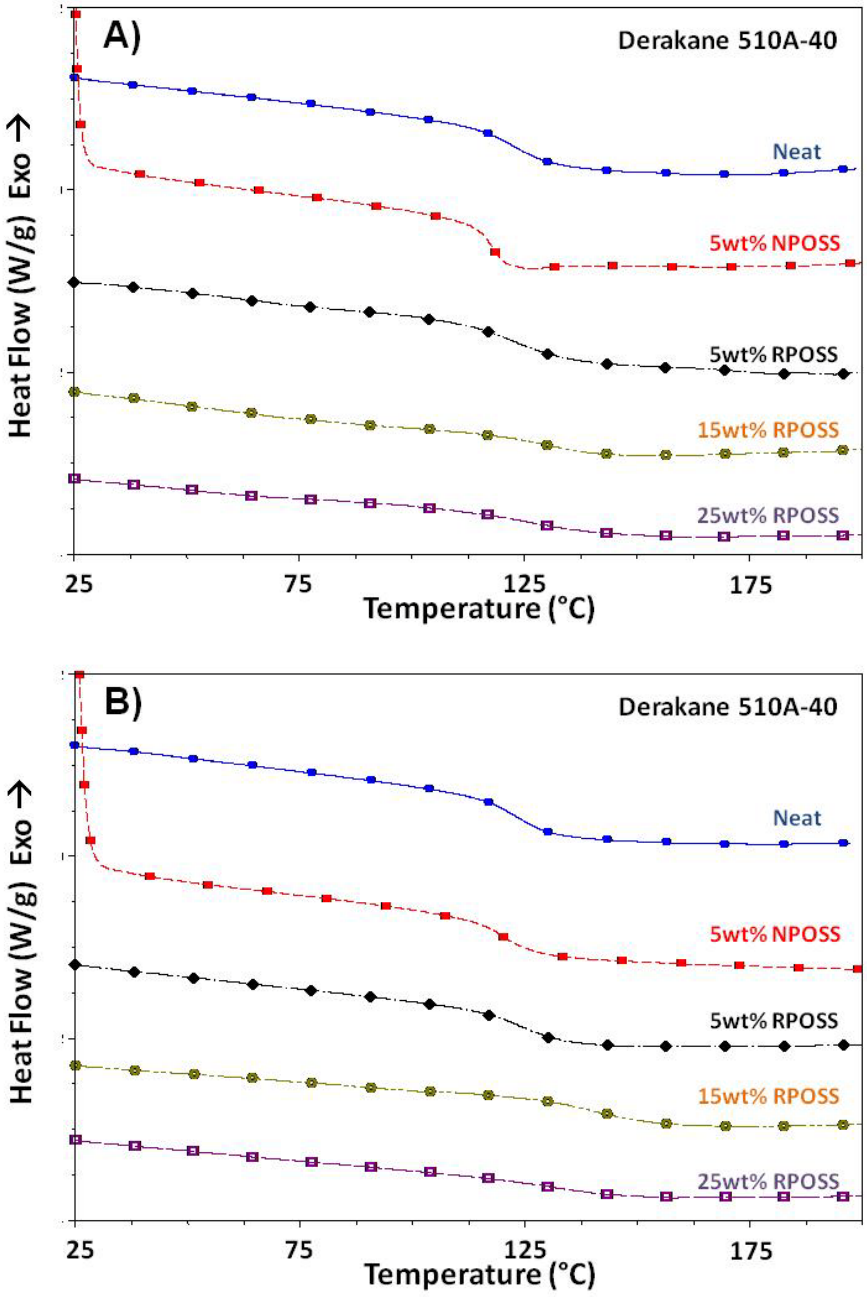

Figure 61. DSC thermograms of post-cured films; A) initial heating scan and B) second heating scan.

The T_gs were evaluated at the midpoint of the second heating scan (Table 16). The 5 wt% NPOSS sample experienced a reduction in T_g (119.98 °C) as expected. Addition of 5 wt% RPOSS did not impact the T_g (122.97 °C) but the sample containing 15 wt% RPOSS displayed the highest T_g at 140.00 °C. The

transition breadth increased and the intensity decreased with additional RPOSS incorporation, where in the case of the sample with 25 wt% RPOSS, a reduction in network connectivity combined with increased heterogeneity reduces T_g.

Table 16

DSC T_gs Evaluated from Midpoint of the Second Heating Scan

Sample	T_g (°C)
Neat Derakane 510A-40	123.65
With 5 wt% NPOSS	119.98
With 5 wt% RPOSS	122.97
With 15 wt% RPOSS	140.00
With 25 wt% RPOSS	131.01

Dynamic Mechanical Analysis

DMA storage moduli of the neat resin and POSS containing resins are shown in Figure 62. Plasticization by 5 wt% NPOSS resulted in reduced glassy modulus and onset of softening at reduced temperature. Incorporation of 5 wt% RPOSS increased the glassy and rubbery moduli values and higher crosslink density due to its high methacrylate functionality (Table 17). At increased loadings, RPOSS significantly impacted the rubbery moduli and broadened the T_g.

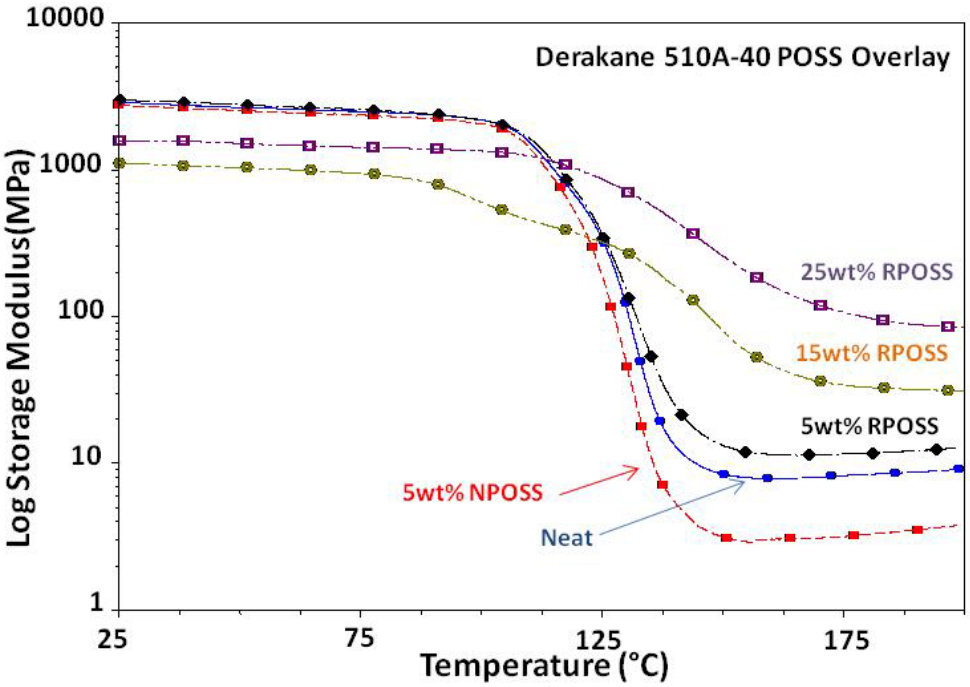

Figure 62. Tensile storage modulus plots of VER with and without POSS.

Changes in T_g are reflected in the maxima of the tan δ plot (Figure 63). The addition of 5 wt% NPOSS reduced the T_g slightly while increasing the maxima of the primary tan δ peak. Upon addition of RPOSS, the height of the tan δ peak was lowered drastically and correlated well with the reduced damping capability of the matrix. The shoulder present in each sample is indicative of inhomogeneous network architecture. Despite elevated cure temperatures, these transitions are indicative of heterogeneous network development, with the greatest impact noted at high loadings of RPOSS. The abrupt reduction in tan δ maxima and multiple low temperature transitions are indicative of multimodal, heterogeneous network architecture induced by the RPOSS species.

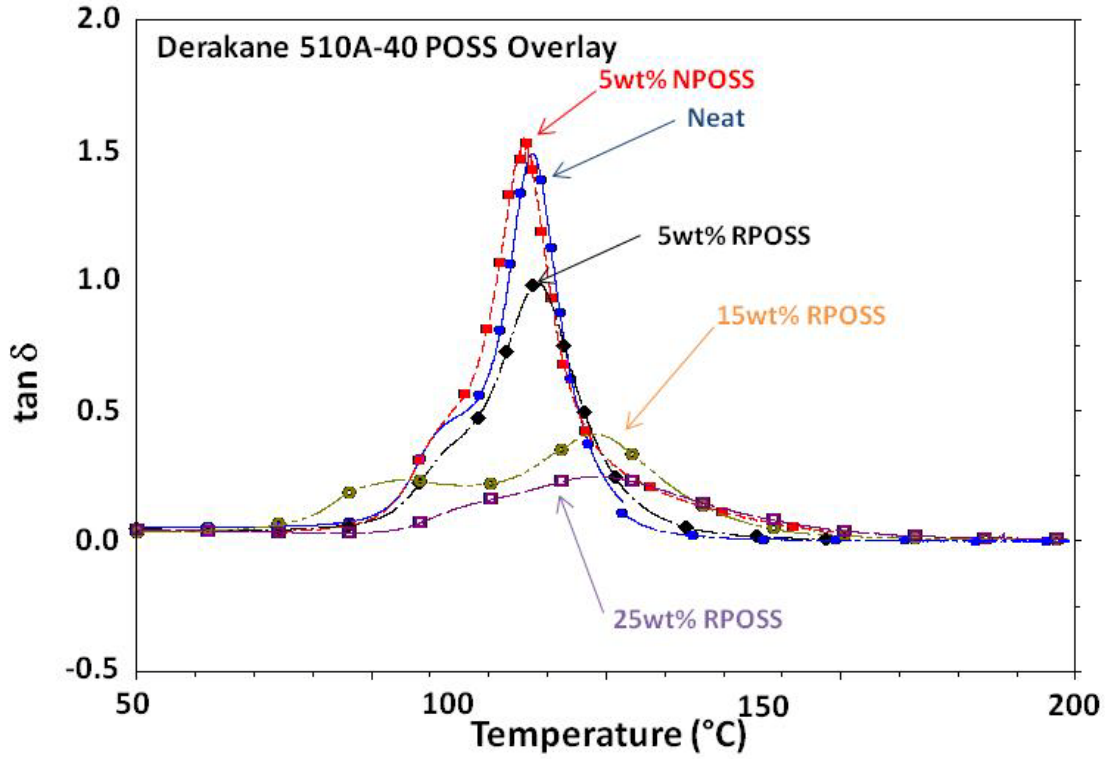

Figure 63. Tan δ peaks of VERs containing POSS.

FWHH increased upon incorporation of POSS particles (Table 17). As noted earlier, a significant increase in rubbery plateau modulus was observed upon RPOSS addition. The M_c of these materials decreased with RPOSS addition as the system functionality increased dramatically. Incorporation of 5 wt% NPOSS altered the network architecture and connectivity as was evident by the increase in M_c.

Table 17

DMA Properties of POSS containing VERs

VER	Density (g/mL)	T_g (°C)	FWHH	DMA E_R' @ T_g + 40°C (MPa)	DMA M_c (g/mol)
Neat D510A-40	1.332	134.29	14.01	8.38 ± 0.12	694 ± 11
With 5 wt% NPOSS	1.305	132.50	17.16	4.71 ± 1.33	1279 ± 376
With 5 wt% RPOSS	1.333	135.55	22.21	11.55 ± 0.65	504 ± 29
With 15 wt% RPOSS	1.316	147.88	38.39	35.7 ± 2.9*	207 ± 17*
With 25 wt% RPOSS	1.319	147.87	59.47	74.7 ± 0.75*	99 ± 2*

Note. Samples containing 15 and 25 wt% RPOSS were evaluated at T_g + 100°C to ensure accurate evaluation of E'_R and M_c

The change in M_c of the NPOSS system is ascribed to increased phase separation. Since RPOSS is soluble in the matrix resin, it provides added functionality that increases both the network continuity and crosslink density.

The β transition is often associated with short range, localized motions and can be attributed to fracture resistance. The β transition for each VER is shown in Figure 64. The neat D510A-40 demonstrates a broad yet identifiable β transition at approximately -73.44 °C. The VER containing 5 wt% NPOSS exhibited a clearly defined β transition at -50.02 °C while the VERs containing RPOSS exhibit a less distinct β transition with a maxima near -70 °C.

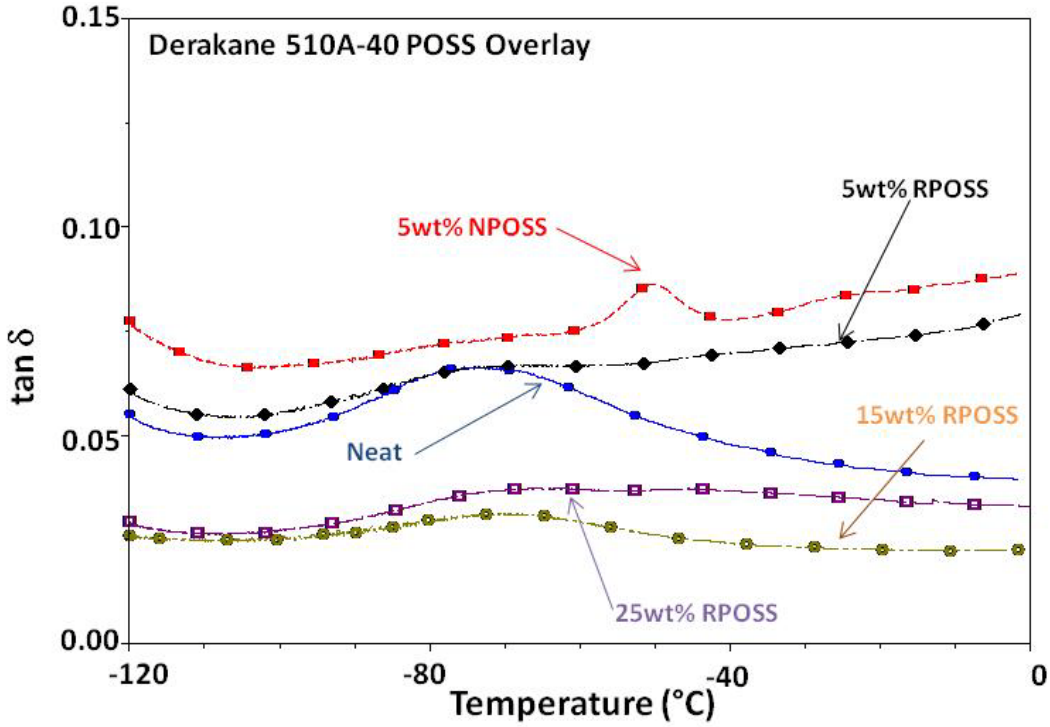

Figure 64. DMA β transitions of POSS containing VERs.

Mechanical Testing

Compression test results are shown in Figure 65. Addition of 5 wt% RPOSS increased the yield stress and strain of Derakane 510A-40 (Table 18). Interestingly, despite the high functionality of RPOSS, there was minimal impact on Young's modulus at all loadings. The samples containing 15 wt% RPOSS and 25 wt% RPOSS displayed higher yield strain and a less distinct yield point. The VER containing 5 wt% NPOSS exhibited definite plasticization effects as evidenced by reduction in both modulus and yield stress.

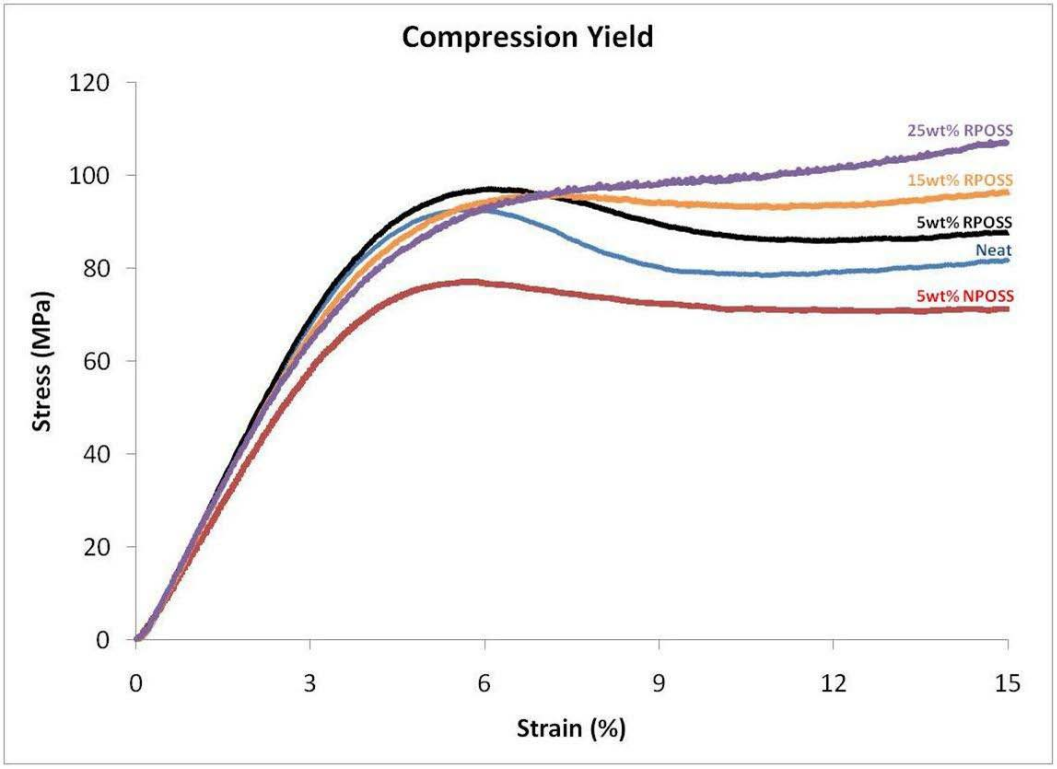

Figure 65. Compression testing of VERs with and without POSS.

Fracture toughness values are indicative of brittle fracture in each system. The stress intensity factor, K_{IC}, describes the critical stress per area required to promote crack growth. Despite increasing free volume, neither POSS species exhibited any ability to enhance fracture resistance. NPOSS incorporation did not affect the K_{IC} value much but the RPOSS species resulted in a more brittle composite (as anticipated from the significantly higher crosslink density). The reduction in fracture toughness was greater at higher loadings of RPOSS. These trends correlate with the magnitude of the β transition determined via DMA, as it often corresponds to energy dissipation.

Table 18

Yield and Fracture Properties of POSS Matrices

Sample	Young's Modulus (GPa)	Yield Stress (MPa)	Yield Strain (%)	K_{IC} (MPa*√m)
Neat D510A-40	2.50 ± 0.02	90.61± 1.3	5.78 ± 0.19	1.11 ± 0.08
With 5 wt% NPOSS	2.13 ± 0.03	76.04 ± 1.0	5.65 ± 0.27	1.07 ± 0.21
With 5 wt% RPOSS	2.51 ± 0.05	93.62 ± 1.2	6.13 ± 0.12	0.63 ± 0.06
With 15 wt% RPOSS	2.46 ± 0.12	94.85 ± 1.0	7.12 ± 0.27	- - -
With 25 wt% RPOSS	2.43 ± 0.11	98.06 ± 1.8	7.97 ± 0.22	- - -

PVT Measurements

The PVT data of neat Derakane 510A-40 and nanocomposites containing 5 wt% NPOSS and 5 wt% RPOSS are shown in Figures 66 - 68. Experimental data were measured as a series of isobars and are shown from 0 MPa to 100 MPa in 20 MPa increments. The T_g can be clearly seen as a change in slope in these figures. The final graph in terms of specific volume (V_{Sp}) versus temperature was further used to calculate material properties in the range between 320 K and 520 K (45 – 245 °C).

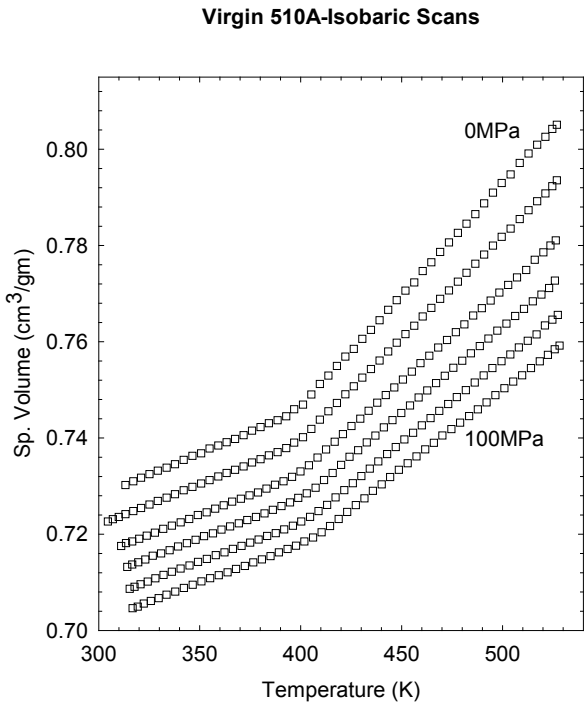

Figure 66. PVT data of the neat D510A-40 obtained by isobaric scans.

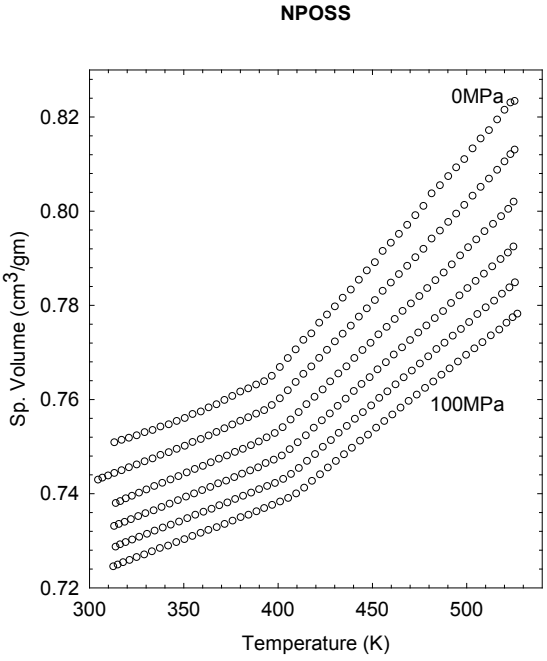

Figure 67. PVT data of Derakane 510A-40 with 5 wt% NPOSS obtained by isobaric scans.

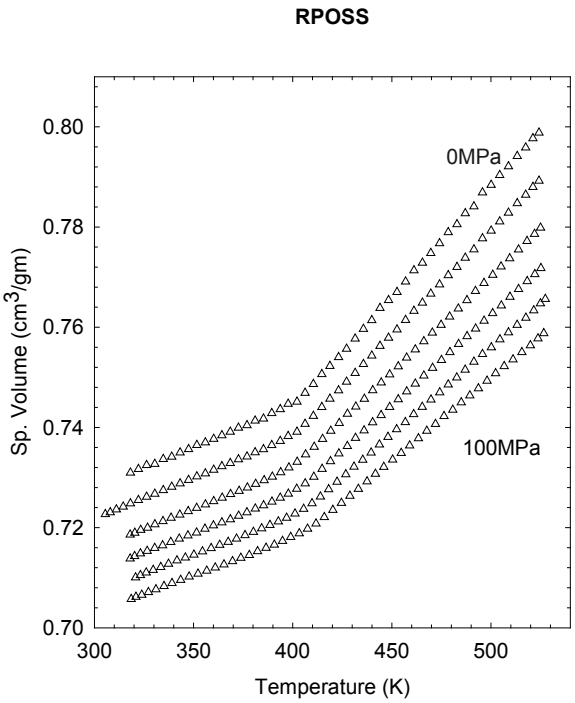

Figure 68. PVT data of Derakane 510A-40 with 5 wt% RPOSS obtained by isobaric scans.

The data from the PVT experiments were used to calculate the temperature-dependent volumetric coefficient of thermal expansion (CTE) and isothermal compressibility. The slope of the V-T curve at constant pressure yields the value of thermal expansivity (α) using the following equation: [16-18]

$$\alpha = \left(\frac{dV}{dT}\right)_P \quad (3)$$

The volumetric CTE was calculated using the following equation:

$$CTE = \frac{1}{V}\left(\frac{dV}{dT}\right)_P \quad (4)$$

PVT data at atmospheric pressure were fitted linearly within the glassy and rubbery temperature range to calculate the thermal expansivity. For neat VER, the slope (volumetric thermal expansivity) in rubbery state was determined

to be $E_r = dV_{Sp}/dT = (4.64 \pm 0.008) \cdot 10^{-4}$ $cm^3/g.K$ and the coefficient of thermal expansion at T_g was determined to be $\alpha_r = E_r/V = (6.19 \pm 0.008) \cdot 10^{-4}/K$. For the VER containing NPOSS, the corresponding rubbery expansivity value and coefficient of thermal expansion were calculated to be $(5.46 \pm 0.02) \cdot 10^{-4}$ $cm^3/g.K$ and $(5.46 \pm 0.02) \cdot 10^{-4}$ /K, respectively. In the glassy state, the neat VER exhibited a smaller value of expansivity, $E_g = (1.78 \pm 0.008) \cdot 10^{-4} cm^3/g.K$. The thermal expansivity and coefficient of thermal expansion values for all three composites in both glassy and rubbery state are tabulated in Table 19. It can be seen that the CTE values of the composites in the rubbery state are approximately three times the respective values obtained in the glassy state.

Table 19

Thermal Expansivity and Coefficient of Thermal Expansion of POSS Vinyl Ester Composites System Calculated from PVT

	E_g $(cm^3/g.K) \cdot 10^{-4}$	E_r $(cm^3/g.K) \cdot 10^{-4}$	$CTE_g/K \cdot 10^{-4}$	$CTE_r/K \cdot 10^{-4}$
Neat D510A-40	1.78 ± 0.008	4.64 ± 0.008	2.31 ± 0.01	6.19 ± 0.008
5 wt% NPOSS	1.63 ± 0.030	5.46 ± 0.020	2.18 ± 0.03	7.09 ± 0.010
5 wt% RPOSS	1.64 ± 0.010	4.44 ± 0.010	2.19 ± 0.01	5.93 ± 0.010

Bulk modulus of glassy polymers is a key mechanical property of thermosetting polymers. Its determination for a wide range of temperature is essential to estimate the polymer performance in end use. It is inversely related to isothermal compressibility (β) which is calculated as follows:

$$Isothermal\ Compressibility\ \beta = \left(\frac{dV}{dP}\right)_T \quad (5)$$

Bulk modulus (K) is calculated from the following equation.[16-18]

$$K = -V\left(\frac{dP}{dV}\right)_T \quad (6)$$

The bulk modulus values obtained for Derakane 510A-40 with 5 wt% RPOSS was higher than comparative values for neat resin as well as Derakane 510A-40 with 5 wt% NPOSS for all temperature ranges (Figure 69). The trend in bulk modulus values observed for DMA and compression modulus correlate well with these findings.

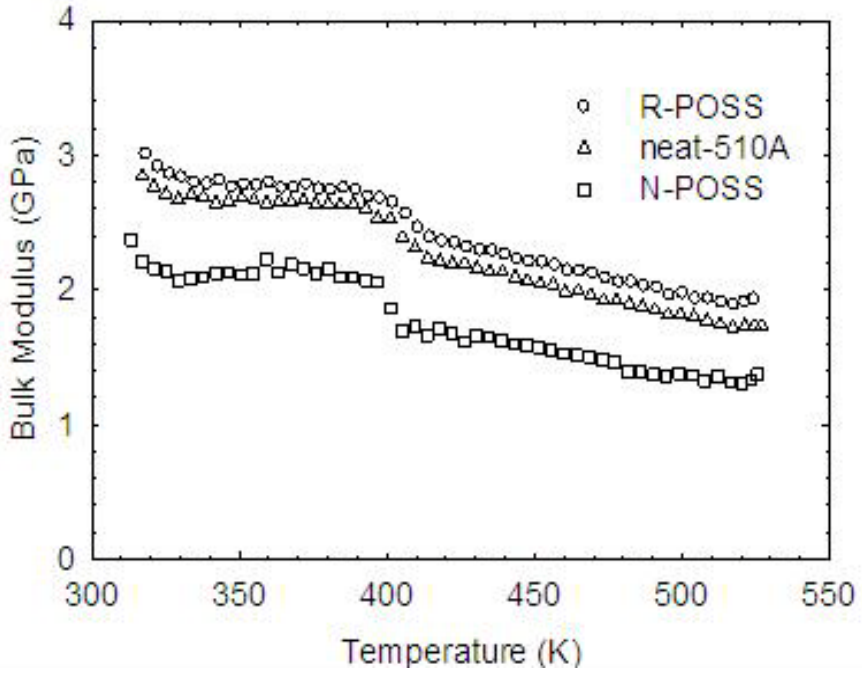

Figure 69. Variation of bulk modulus calculated using PVT data of neat Derakane 510A-40 and the POSS nanocomposites obtained by isobaric scans from 20 to 100 MPa.

Composite Panel Analysis

All composite coupons were fabricated via VARTM employing both unidirectional carbon fiber mats (UC) and chopped strand e-glass fiber mats

(CSM). The composite coupons consisted of resins reinforced with a fiber package of UC/CSM/UC/CSM/UC. All coupons were cured via the same protocol used for the neat resin.

The storage moduli of ambient cured samples as evaluated by three point bend DMA are shown in Figure 70. Increases to both glassy and rubbery modulus were observed with the addition of POSS nanoparticles. The softening at ~ 35 °C correlates to the initial vitrification limit as observed in Chapter 4. Glassy modulus values for the POSS reinforced samples are similar, and increased more than 20% over the neat resin. The rubbery modulus region (evaluated at 175 °C) exhibits increased stiffness with POSS addition with the 5 wt% RPOSS (8.45 GPa), nearly double that of the neat resin (4.25 GPa). Despite showing the opposite trend in the neat resin, the 5 wt% NPOSS species also exhibits an increase in stiffness above T_g (5.87 GPa). The results indicate an improvement to the interfacial region resulting in improved reinforcement from the fibers.

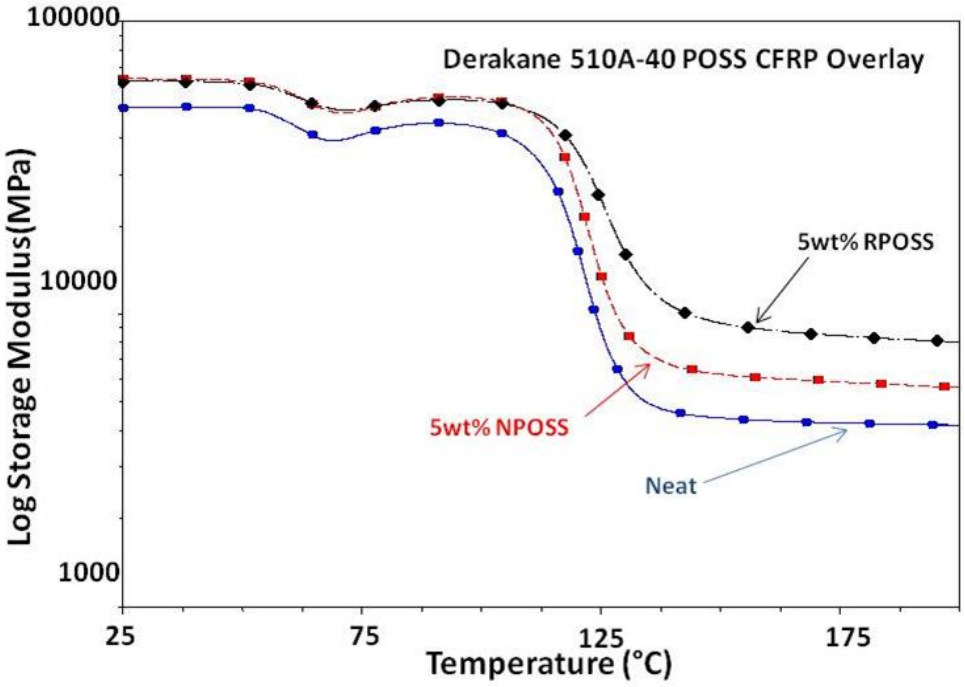

Figure 70. Ambient cure flexural storage modulus of VARTM coupons of the neat Derakane 510A-40, with 5 wt% NPOSS and with 5 wt% RPOSS.

The low temperature shoulder correlating to vitrification limited conversion is evident in the tan δ plot of the fiber reinforced samples and correlates well to the neat resin studies in previous chapters. The low temperate transition is equivalent regardless of POSS addition. The tan δ maxima occurs at 123.2 °C for the neat resin, with the 5 wt% NPOSS and 5 wt% RPOSS being slightly higher at 123.9 °C and 126.5 °C, respectively.

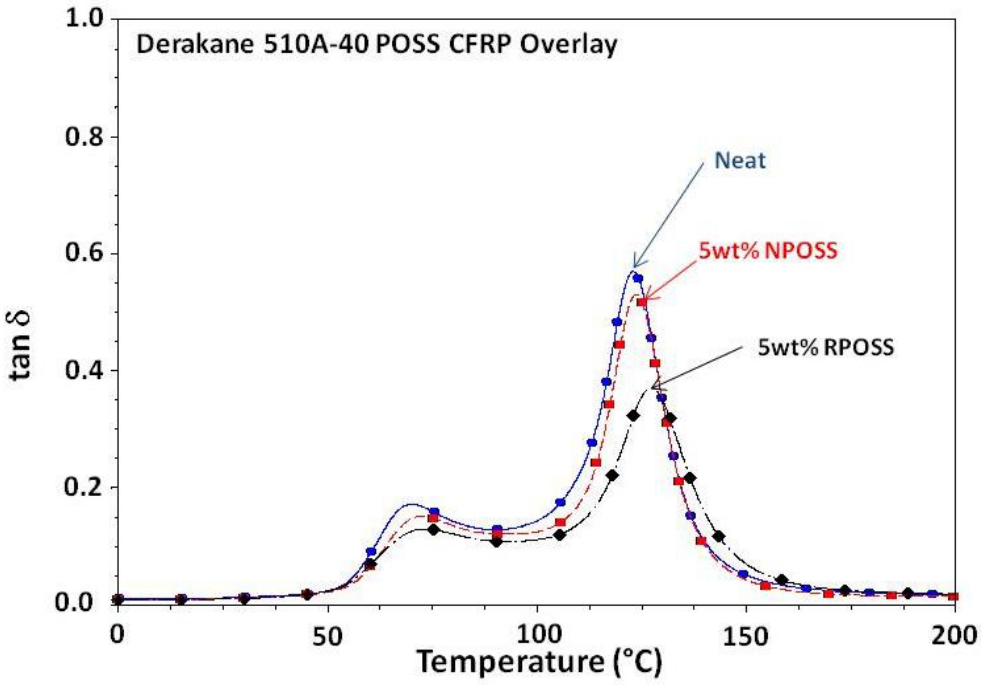

Figure 71. Ambient cure flexural tan δ of VARTM coupons of the neat Derakane 510A-40, with 5 wt% NPOSS and with 5 wt% RPOSS.

Post-curing of the composite panels exhibited the same completion of cure and homogenization of network architecture exhibited in Chapter IV. The same trends exist that were observed in the ambient samples. Glassy modulus is increased upon POSS addition, however, the increase is only 10% over the neat resin in this case (Figure 72). Rubbery modulus for the post-cured neat resin was 4.10 GPa, while the 5 wt% NPOSS and 5 wt% RPOSS were 5.92 GPa and 7.60 GPa, respectively.

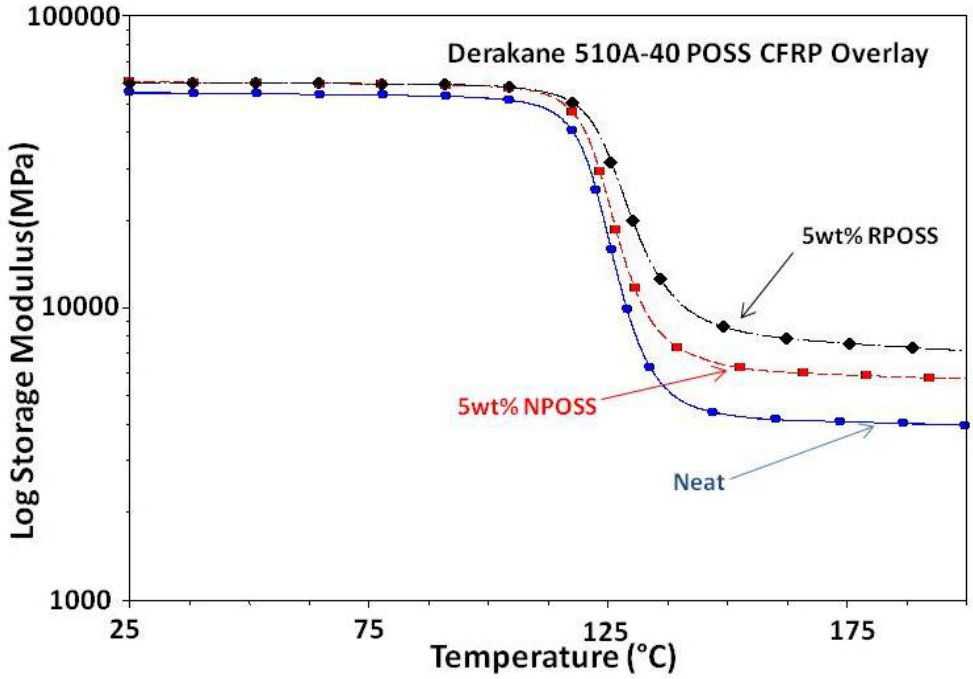

Figure 72. Post-cured flexural storage modulus of VARTM coupons of the neat Derakane 510A-40, with 5 wt% NPOSS and with 5 wt% RPOSS.

No low temperature transitions are evident in the tan δ plot shown in Figure 73. The tan δ maximum for the neat resin occurs at 127.2 °C. The 5 wt% NPOSS and 5 wt% RPOSS are both slightly higher, at 127.5 °C and 130.3 °C respectively. The breadth of the transition at 5 wt% RPOSS is indicative of a more heterogeneous network.

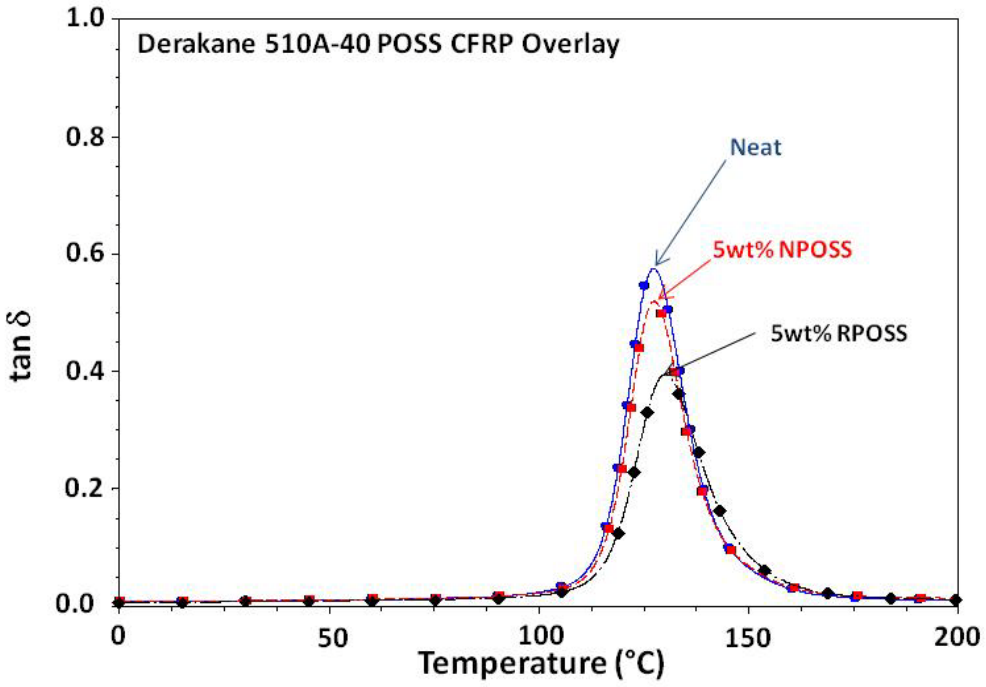

Figure 73. Post-cured flexural tan δ of VARTM coupons of the neat Derakane 510A-40, with 5 wt% NPOSS and with 5 wt% RPOSS.

Summary and Conclusions

Reactive and non-reactive POSS nanoparticles were incorporated into a brominated vinyl ester resin to induce changes in molecular level architecture and chemical composition. The resulting nanocomposite matrices were evaluated for viscoelastic behavior, mechanical properties and free volume. VERs maintained their low viscosity characteristics upon addition of POSS particles and the resulting resins were still suitable for infusion techniques.

Conversion was analyzed via FTIR and indicated significant changes upon POSS addition. Conversion of both dimethacrylate and styrene increased with the addition of POSS, likely due to elevated gel effects. Conversion of the methacrylate species for the neat resin was ~ 50%, while the 5 wt% NPOSS increased to ~ 70% and the 5 wt% RPOSS was ~ 85% after 3 hours. Styrene

was initially slower to incorporate into the network and continued to react during the duration of ambient cure. Both POSS systems achieved complete conversion upon post-cure while the neat resin exhibited very near complete conversion of dimethacrylate and styrene at 88% and 94%, respectively.

DSC was used to investigate changes in thermal transitions. No additional cure exotherms were observed during the initial heating scan and correlated well with FTIR results. T_gs did not vary significantly at low POSS loadings and elevated levels of RPOSS were explored. Addition of 5 wt% NPOSS lowered the T_g to 120 °C, while increasing the RPOSS loading to 15 and 25 wt% increased the T_g to 140 °C and 131 °C, respectively. The transitions also broadened significantly for higher RPOSS loading. Similar effects were observed via DMA. The T_g of the neat resin was not impacted significantly at 5 wt% NPOSS or RPOSS. However, the 15 and 25 wt% RPOSS samples exhibited a decrease in tan δ maxima with a higher peak temperature (~ 145 °C) and a significant broadening. The result is indicative of an increase in network heterogeneity. The greatest impact was observed in the rubbery modulus region where the neat resin has a modulus value of 8.4 MPa. NPOSS exhibited plasticization of the neat resin reducing rubbery modulus values by ~ 50% while incorporation of 5 wt% RPOSS increased rubbery modulus by ~ 50%. Due to the broadening of the glass transition, the rubbery modulus region did not plateau for the 15 and 25 wt% RPOSS samples until after 225 °C, with significantly higher values of 36 and 75 MPa respectively.

Mechanical testing exhibited no change in Young's modulus with the

addition of RPOSS, as all values were between 2.4 and 2.5 MPa. However, RPOSS nanocomposites exhibited increases in yield strain and yield stress over the neat resin. Samples containing 5 wt% NPOSS exhibited a reduction in Young's modulus (2.1 MPa) due to plasticization and connectivity effects. Fracture resistance was dramatically reduced to 0.63 MPa*√m with the incorporation of 5 wt% RPOSS. Samples containing 15 and 25 wt% RPOSS were too brittle to be tested. No significant impact was observed in fracture behavior between the neat resin and the sample with 5 wt% NPOSS, each having values of ~1.0 MPa*√m.

Mechanical properties were echoed in the PVT data. Samples containing 5 wt% RPOSS exhibited a slight increase in bulk modulus over the neat resin, while the samples containing 5 wt% NPOSS samples reduced bulk modulus. The reduction in thermal expansivity at low loading levels is valuable in many applications.

VARTM fabrication techniques were implemented to investigate the impact of fiber on resin conversion and properties. DMA results indicated a similar vitrification limit as observed in previous chapters. Increased glassy and rubbery modulus values were noted for the POSS containing systems. This was not the trend observed in the neat resin, where the 5 wt% NPOSS reduced modulus. Therefore, an increase in modulus for fiber reinforcement is attributed to an improved interface between the resin and fiber, increasing stiffness over the neat resin. The T_g was not dramatically impacted at these loading levels, as was observed in the neat resin studies.

In addition to VERs, epoxy resins are widely used for many high performance composite applications due to the large chemical library of starting materials. In the next chapter, a series of epoxy resins will be investigated for differences in the development of network architecture.

References

1. Mafi, E., Ebrahimi, M., Moghbeli, M. *Journal of Polymer Engineering* , **2009**, 29, 293.
2. Haris, A., Adachi, T., Araki, W. *Journal of Material Science,* **2008**, 43, 3289.
3. Haris, A., Adachi, T., Araki, W. *Materials Science and Engineering A*, **2008**, 496, 337.
4. La Scala, J., Orlicki, J., Winston, C., Robinette, E., Sands, J., Palmese, G. *Polymer*, **2005**, 46, 2908.
5. Zubeldia, A., Larranaga, M., Remiro, P., Mondragon, I. *Journal of Polymer Science Part B: Polymer Physics,* **2004**, 42, 3920.
6. Crawford, E., Lesser, A. J. *Journal of Polymer Science Part B Polymer Physics*, **1998**, 36, 1371.
7. Erman, B., Mark, J. *Macromolecules,* **1998**, 31, 3099.
8. Bos, H., Nusselder, J. *Polymer,* **1994**, 35, 2793.
9. Ruiz-Perez, L., Royston, G., Fairclough, R., Ryan, A. *Polymer,* **2008**, 49, 4475.
10. Lee, A., Lichtenhan, J. *Macromolecules*, **1998**, 31, 4970.
11. Strachota, A., Kroutilova, I., Kovarova, J., Matejka, L. *Macromolecules,* **2004**, 37, 9457.
12. Glodek, T., Boyd, S., McAninch, I., LaScala, J. *Composites Science and Technology,* **2008**, 68, 2994.

13. Ragosta, G., Musto, P., Abbate, M., Scarinzi, G. *Polymer*, **2009**, 50, 5518.

14. Bizet, S., Galy, J., Gerard, J-F. *Macromolecules,* **2006**, 39, 2574.

15. Glodek, T., Boyd, S., McAninch, I., LaScala, J. *Composites Science and Technology,* **2008**, 68, 2994.

16. Rey, L., Galy, J., Sauterau, H., Simon, G., Cook, W. *Polymer International,* **2004**, 53, 557.

17. Ramos, J.A. *Polymers for Advanced Technologies,* **2009**, 20, 35.

18. Kilburn, D. *Journal of Polymer Science Part B Polymer Physics,* **2003**, 41, 3089.

CHAPTER VIII

DEVELOPMENT OF NETWORK MORPHOLOGY AND MECHANICAL PROPERTIES IN 3,3'-DIAMINODIPHENYLSULFONE CURED EPOXY RESINS

Introduction

Thermosetting epoxy-amine systems are preferred for composite materials that require high stiffness, temperature stability, and chemical resistance. Improved performance is achieved by tailoring mechanical and thermal behaviors via appropriate monomer selection. Network development and heterogeneity play a crucial role in determining epoxy resin properties.[1-4] Excellent mechanical properties with high resistance to solvents and corrosion, excellent fiber wetting, and low shrinkage upon curing are possible due to a seemingly limitless combination of starting materials.[2]

Epoxy cure is one of the most common thermosetting reactions. Near infrared (NIR) spectroscopy has been shown to be an effective technique in tracking cure.[5-9] NIR is sensitive to the presence of primary and secondary amines as well as the oxirane ring even at high levels of conversion. The impact of etherification on epoxy system property development has also been documented.[6-9]

The T_g of a cured epoxy resin is heavily dependent upon the resulting network architecture, and is driven by crosslink density, monomer architecture and intermolecular interactions. Structure-property relationships to conversion have been reported.[10-21] However, the effect of many parameters such as T_g, M_c, yield, and fracture toughness on glassy state properties is not well documented.

Although mechanical properties have been reported for epoxy resins with a range of architectures, very little information is available that correlates conversion, network structure, and mechanical properties of epoxy resins cured with 3,3'-diaminodiphenylsulfone (3,3'-DDS).

The present study investigated the network structure of a series of epoxy resins cured with 3,3'-DDS. The resulting formulations were evaluated for changes in network architecture and their impact on mechanical properties. Resin conversion was tracked using NIR, DSC and DMA to evaluate limitations in the cure process. Viscoelastic behavior and mechanical properties of the fully cured formulations were evaluated against the same epoxy resin cured with 4,4'-DDS to determine the influence of *meta*- and *para*-substitution.

Epoxies were mixed with stoichiometric amounts of 3,3'-DDS in an oil bath at 100 °C until the blend turned transparent and then the temperature was raised to 125 °C to initiate the study. For NIR spectroscopic analysis, the resin mixture was sandwiched between two glass slides with a PTFE spacer to achieve a standard sample thickness. The remaining resin mixture was transferred to heated silicone molds and cured at 125 °C for 5 hours followed by a post-cure at 200 °C for up to 3.5 hours.

Resin Conversion

NIR spectra of neat 3,3'-DDS, Epon 828, Epon 1001F and Araldite MY0610 are shown in Figure 74. The 3,3'-DDS primary amine bands are located at 4543, 5061, and 6588-6750 cm^{-1} while bands for phenyl and C-H groups were observed at 4640-4665 cm^{-1} and 5958-6027 cm^{-1}, respectively. Epon 828 resin

exhibits characteristic bands for epoxy and phenyl groups at 4530 and 4622-4680 cm^{-1}, respectively. Bands observed at 5886-6069 cm^{-1} were attributed to the presence of $-CH_3$, $-CH_2$, and -CH groups. The spectrum of Epon 1001F was similar to that of Epon 828 except for an additional band at 6987 cm^{-1} due to the increased -OH group concentration.

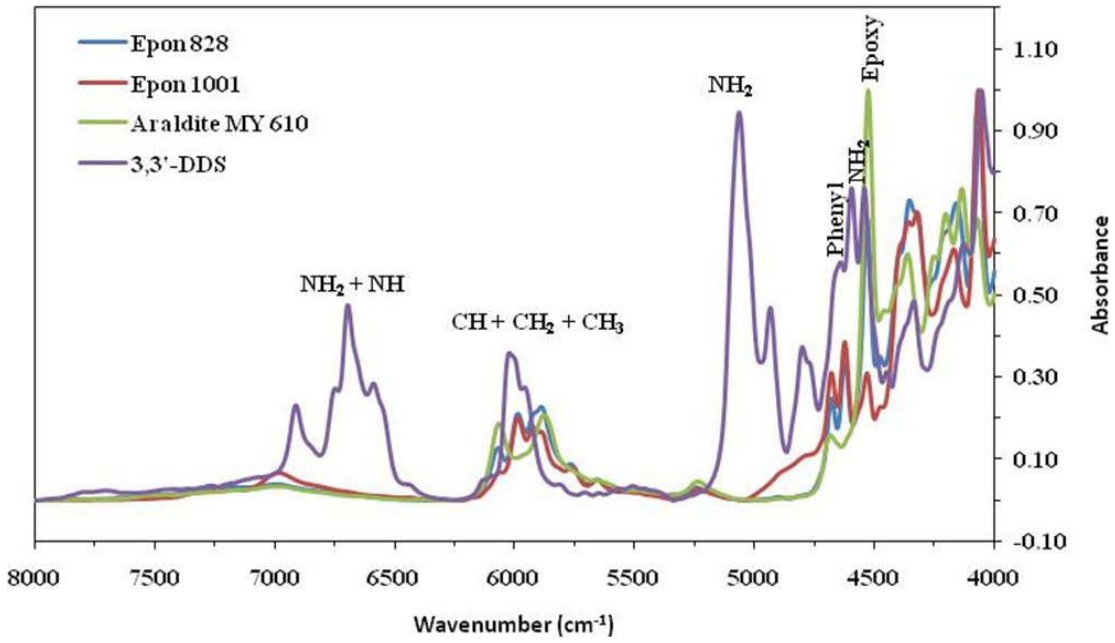

Figure 74. NIR spectra of neat monomers; 3,3'-DDS, Epon 828, Epon 1001F and Araldite MY0610.

Figure 75 is NIR spectra (4400 – 5200 cm^{-1} and 7500 – 6300 cm^{-1}) of Epon 828 cured with stoichiometric ratios of 3,3'-DDS . Each spectrum was normalized using the phenyl band at 4622 cm^{-1}. Decreases in the primary amine band at 5066 cm^{-1}, combined band of epoxy and primary amine groups at 4531 cm^{-1}, and a combined band of primary and secondary amine groups at 6569-6678 cm^{-1} were observed over time while the hydroxyl band at 6991 cm^{-1} increased in intensity as the cure proceeded. Trends were evaluated using the same process with a stoichiometric ratio of 3,3'-DDS to each epoxy monomer.

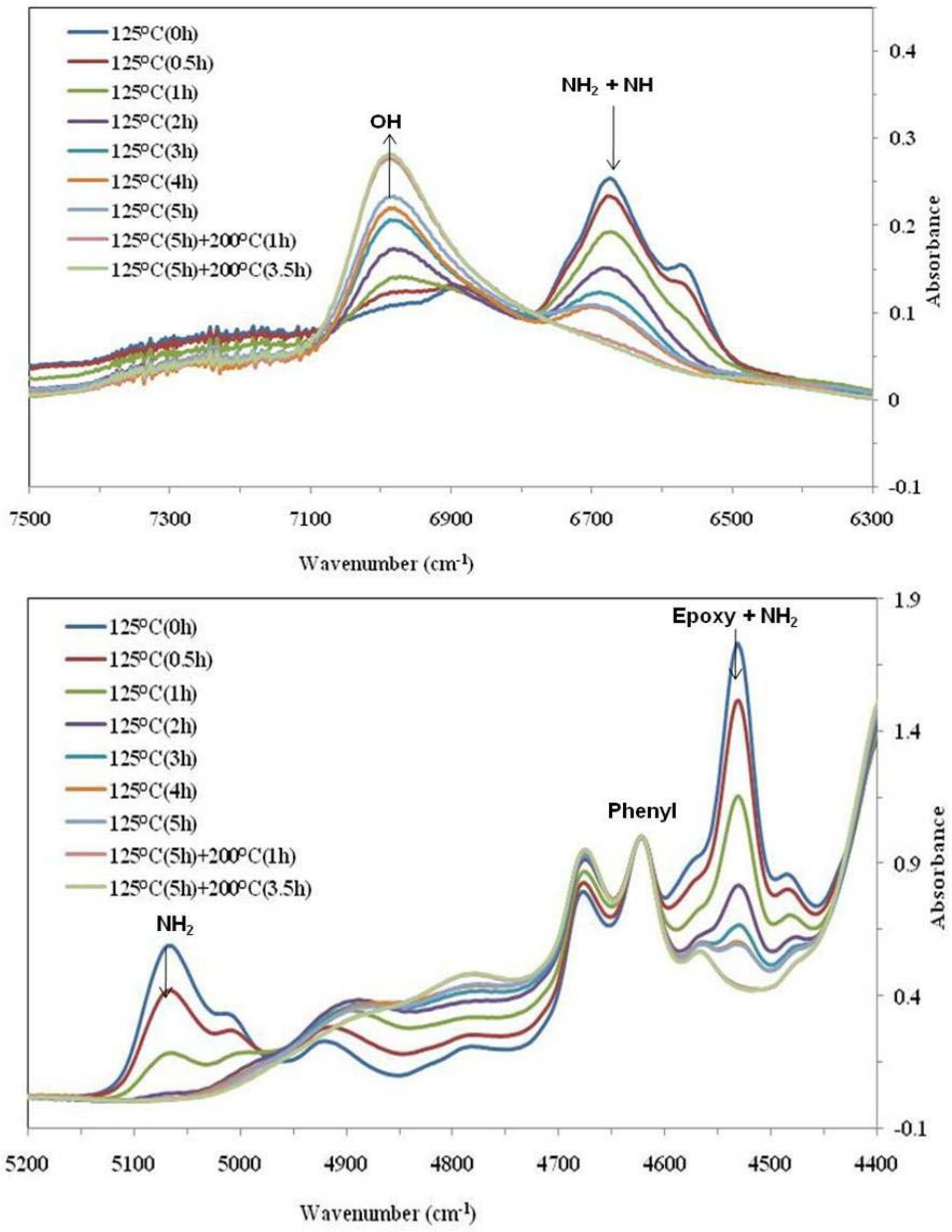

Figure 75. NIR spectra of Epon 828 cured with stoichiometric amounts of 3,3'-DDS.

Conversion data evaluated from the NIR spectra of Figure 75 is shown in Figure 76. Initial monomer concentration is recorded as time -1 h to represent pre-mixing. Epoxy conversion reached 80.82% within three hours at 125 °C before reduced concentration of reactive species limited conversion to 87.08% after five hours at 125 ºC. Post-curing at 200 °C for one hour increased the

conversion to 96.52%. Since curing the samples for an additional two hours at 200 °C only enhanced the conversion to 96.68%, it was determined that a one hour post-cure was sufficient to maximize conversion.

As expected, the primary amine was rapidly consumed early in the reaction and was immediately followed by an increase in secondary amine conversion. Secondary amine formation yielded linear segments and it is not until the concentration of primary amines was exhausted that the secondary amine species began to react and form branches. After three hours of cure, conversion of both epoxy groups and secondary amines slowed down due to the reduced concentration of reactive species. Post-curing at 200 °C overcame mobility restrictions and resulted in complete conversion.

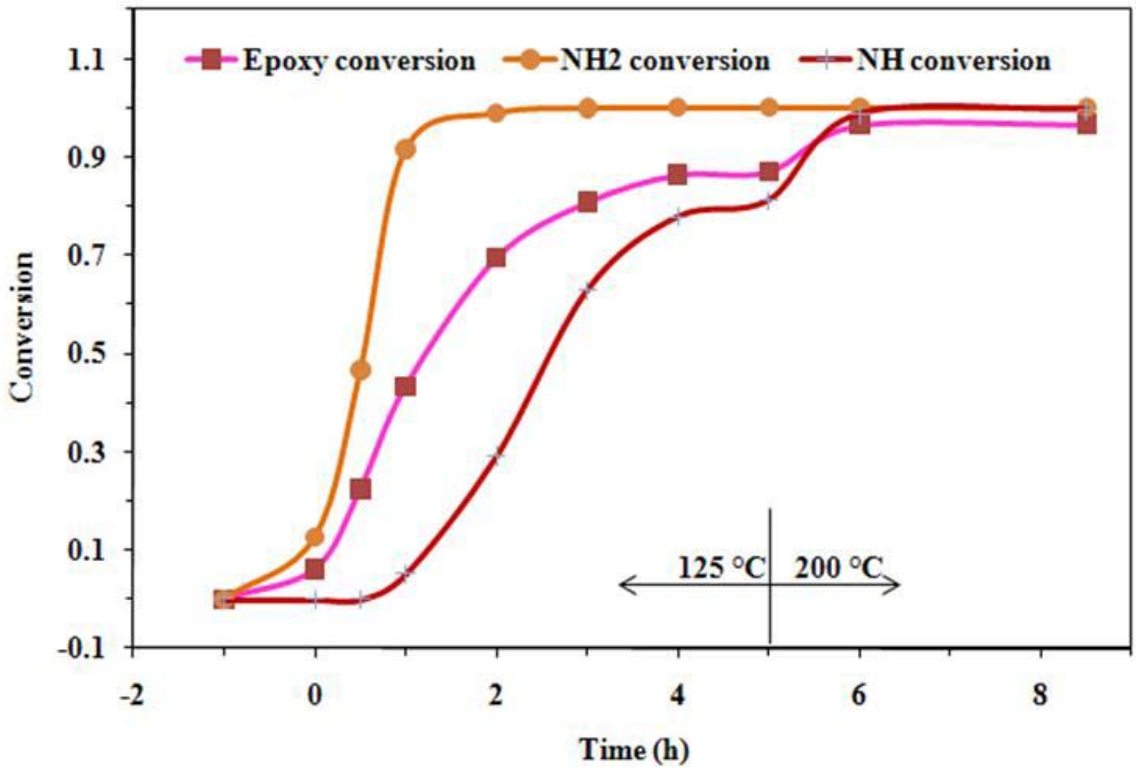

Figure 76. Conversion data for epoxy, primary and secondary amines for stoichiometric ratios of Epon 828 with 3,3'-DDS.

NIR spectra of the Epon 1001F – 3,3'-DDS system is shown in Figure 77. The epoxy equivalent weight of Epon 1001F is ~ 3 times that of Epon 828 and is accompanied by elevated initial viscosity. The difference in behavior between the two epoxy resins is reflected in their conversion profiles. Increased viscosity and reduced functional group concentration restricted the Epon 1001F conversion to only 79.66% after 5 hours at 125 °C. Post-curing at 200 °C for one hour increased the conversion to 81.32%. The reduction in conversion is directly related to the increase in functional equivalent weight. The increase in precursor molecular weight leads to increased viscosity, a reduction in functional group mobility and reduced final conversion. Primary amine conversion proceeded rapidly while the secondary amine conversion was significantly slower. Unlike Epon 828, the secondary amine does not achieve complete conversion.

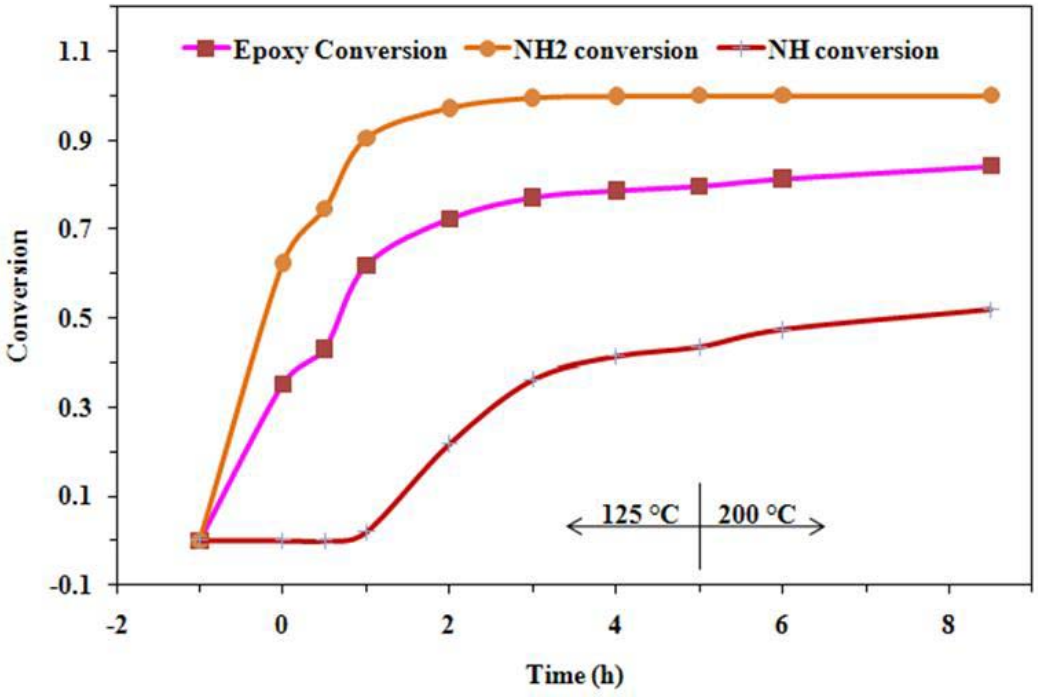

Figure 77. Conversion data for epoxy, primary and secondary amines for stoichiometric ratio of Epon 1001F with 3,3'-DDS.

The NIR evaluated conversion profile for MY0510 – 3,3-DDS is shown in Figure 78. As before the initial monomer concentration is taken to be at time -1 hour. Within two hours, the epoxy conversion surpassed 80%. Increasing the temperature to 200 °C for post-cure raised the epoxy conversion to 99% but an additional hour of cure at 200 °C only increased the conversion to 99.1%. The MY0510 system reached its plateau at 125 °C sooner than the Epon 828 system due to its higher functionality and lower critical conversion for network development.

It is important to note that the monomeric MY0510 contains a tertiary amine diepoxide moiety that functions as a catalyst for several alternative reactions, increases the reactivity of oxirane functionality and reduces the energy requirement for etherification reactions. Secondary amine conversion does not reach 100% despite complete conversion of the epoxy groups. Etherification during the reaction is accredited to the ~ 20% epoxy conversion without a decrease in secondary amine concentration.

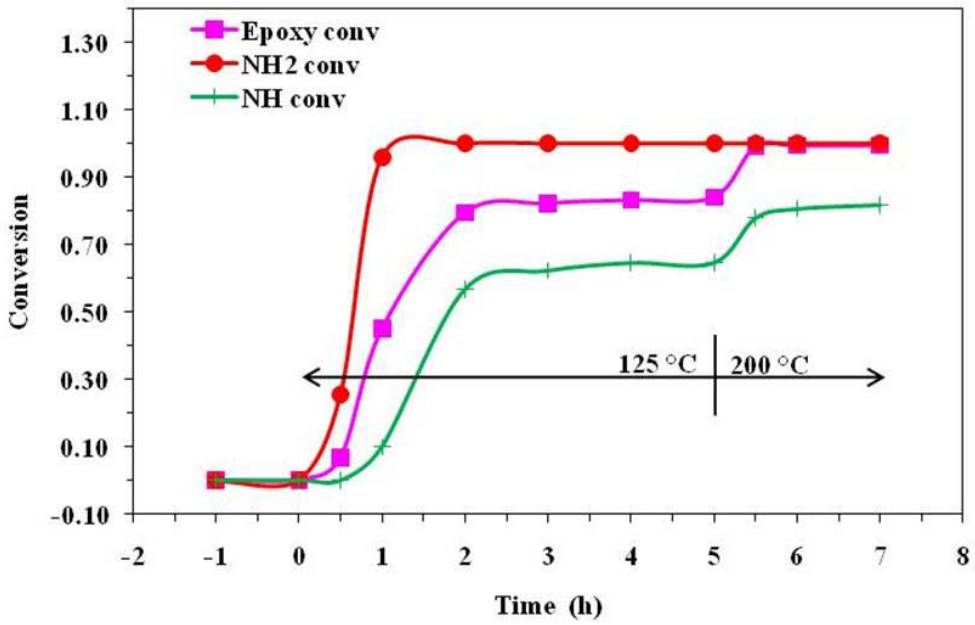

Figure 78. Conversion data for epoxy, primary and secondary amines for stoichiometric ratio of MY0510 with 3,3'-DDS.

Conversion data for MY0610 is shown in Figure 79. Monomeric MY0610 has the same chemical composition and potential to be catalytic as MY0510, but is *meta*-substituted. The increased functionality of this system resulted in rapid formation of branched species. Tertiary amines catalyze the early stages of reaction and rapidly progress conversion. Almost 75% of the epoxy groups were consumed in the first hour. The rate of epoxy conversion was significantly higher with this system than either Epon 828 or Epon 1001F, and translated into rapid development of three-dimensional structure and connectivity.

As noted previously, the epoxy groups were rapidly consumed. Secondary amines began to convert as early as the first hour, but remained at prevalent quantities even after post-cure. As with MY0510, this is a result of tertiary amines being present at high concentration throughout the reaction, which promotes side reactions with secondary hydroxyls to play a much more

prevalent role in converting all available epoxy groups.

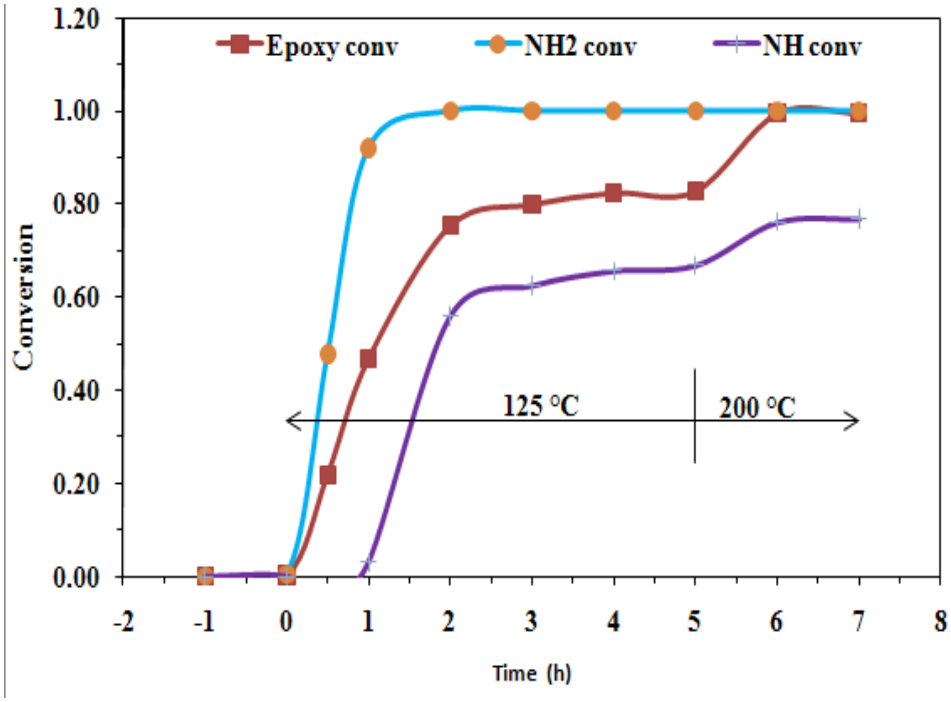

Figure 79. Conversion data for epoxy, primary and secondary amines for stoichiometric ratio of Araldite MY0610 with 3,3'-DDS.

The MY721 – 3,3-DDS conversion profile is shown in Figure 80. The epoxy conversion for the MY721 system reaches ~ 78% percent after two hours but further progress is limited due to reduced mobility. During post-cure at 200 °C, the conversion rises sharply to 98% in the first hour but does not progress much further in the next hour (98.2%).

The loss of primary amine precedes the conversion of secondary amine. As noted with the MY0510 and MY0610 systems, the epoxy and primary amine groups reach full conversion while the secondary and tertiary amine moieties do not. The complete epoxy conversion without corresponding full conversion of secondary amines is attributed to etherification.

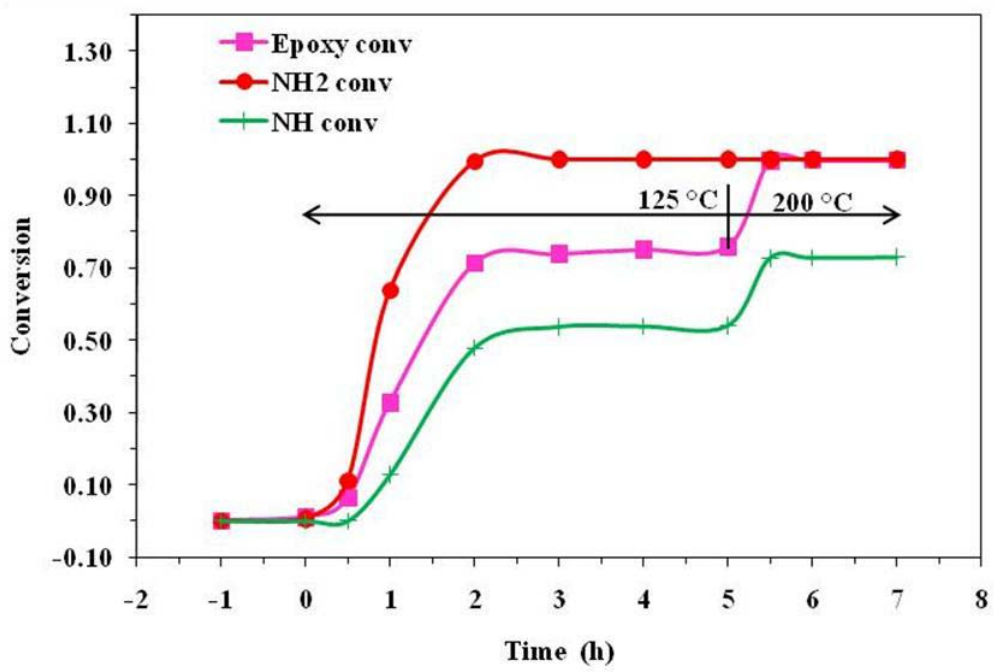

Figure 80. Conversion data for epoxy, primary and secondary amines for stoichiometric ratio of MY721 with 3,3'-DDS.

Of the three resins investigated here, the MY721 resin has the highest functionality and thus the lowest epoxy conversion prior to gelation. Due to the increased functionality, the MY721 system reached a plateau within two hours at 125 °C, compared to the Epon 828 system that took four hours (Figure 81). All systems achieved near complete conversion of the epoxy species with the exception of Epon 1001F.

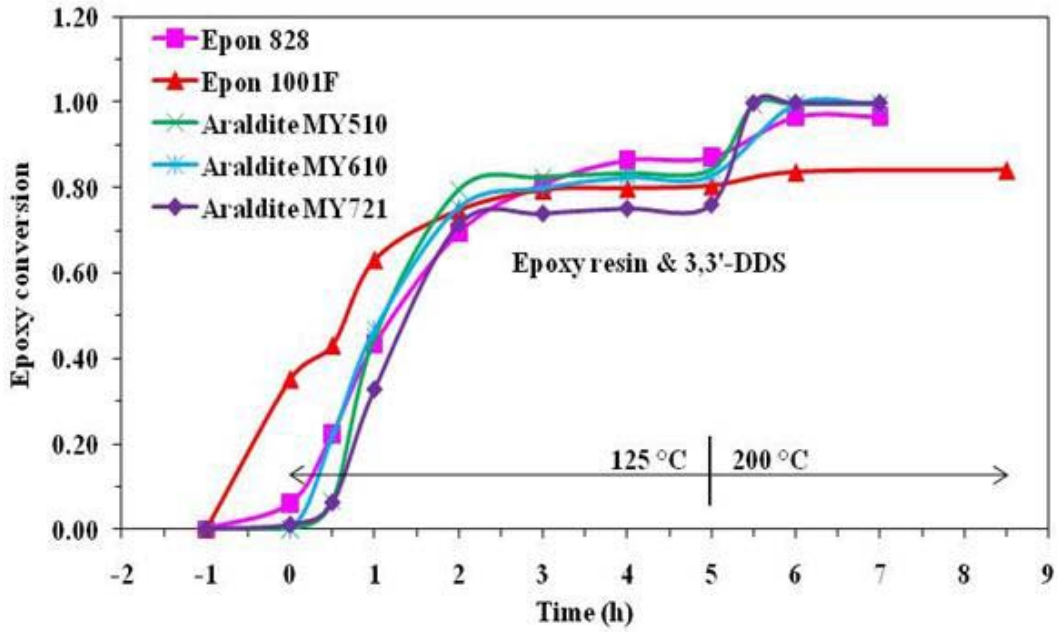

Figure 81. Epoxy conversion of each epoxy monomer with 3,3'-DDS.

Conversion of the primary amine species was rapid and proceeded to completion in all cases (Figure 82). Secondary amine conversion varied between the formulations, with only Epon 828 reaching complete conversion. All the multifunctional epoxy resins registered ~ 80% secondary amine conversion, while Epon 1001F converted roughly half of the available secondary amines (Figure 83).

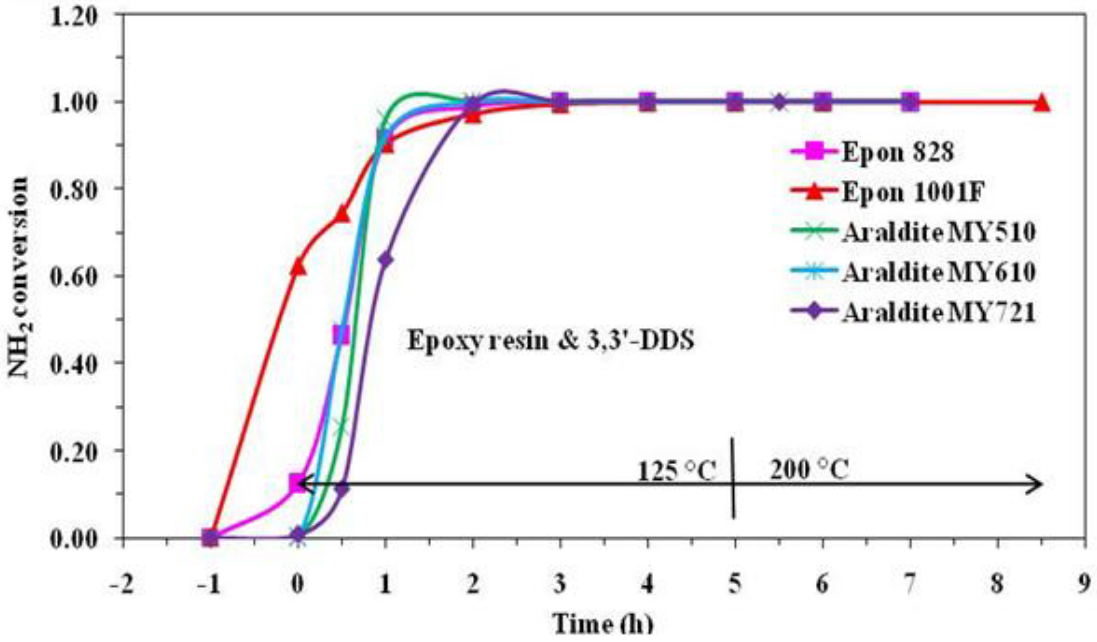

Figure 82. Primary amine conversion of each epoxy monomer with 3,3'-DDS.

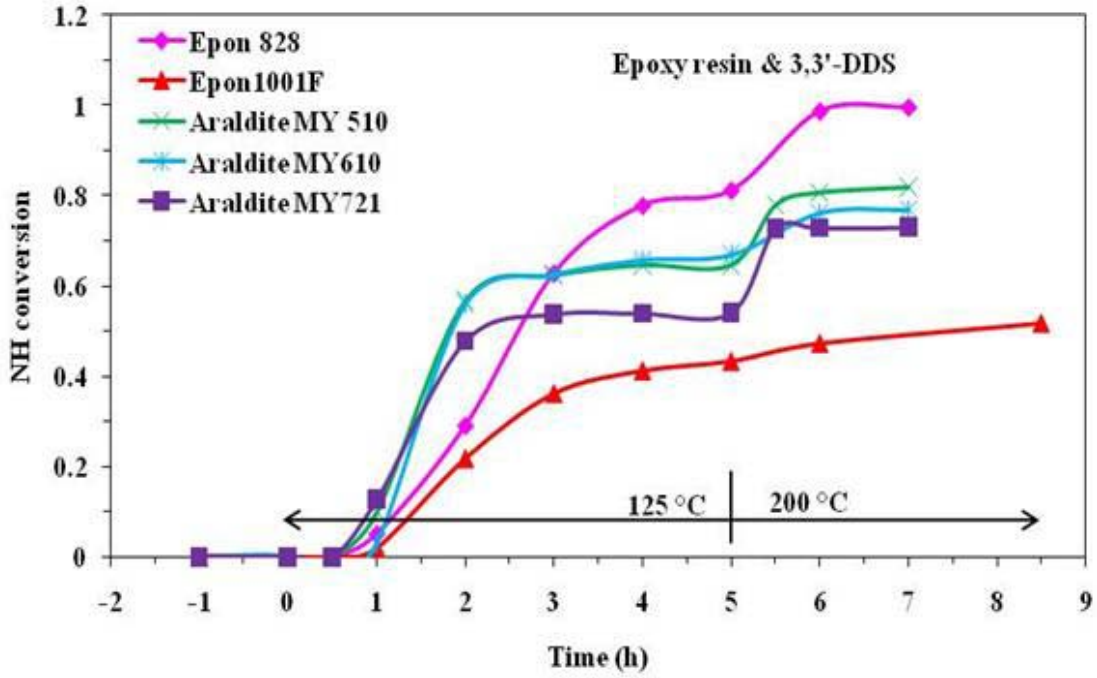

Figure 83. Secondary amine conversion of each epoxy monomer with 3,3'-DDS.

Differential Scanning Calorimetry

DSC studies were employed to track T_g development after each hour of cure. Figure 84 shows DSC thermograms of the Epon 828 system taken from

the first heating scan. The first three hours of cure exhibited a high exotherm related to the primary amine reaction. The first hour of cure yielded a T_g of 115.2 °C which rose to 150.8 °C by the end of the third hour and signifies the onset of vitrification, corresponding to the plateau onset observed in NIR results. Additionally, the T_g region begins to exhibit a transition indicative of physical aging, resulting in enthalpy relaxation during the first heating cycle. This is attributed to vitrification and sample cooling effects that result in increased free volume. Upon post-cure, the T_g reached 155.6 °C.

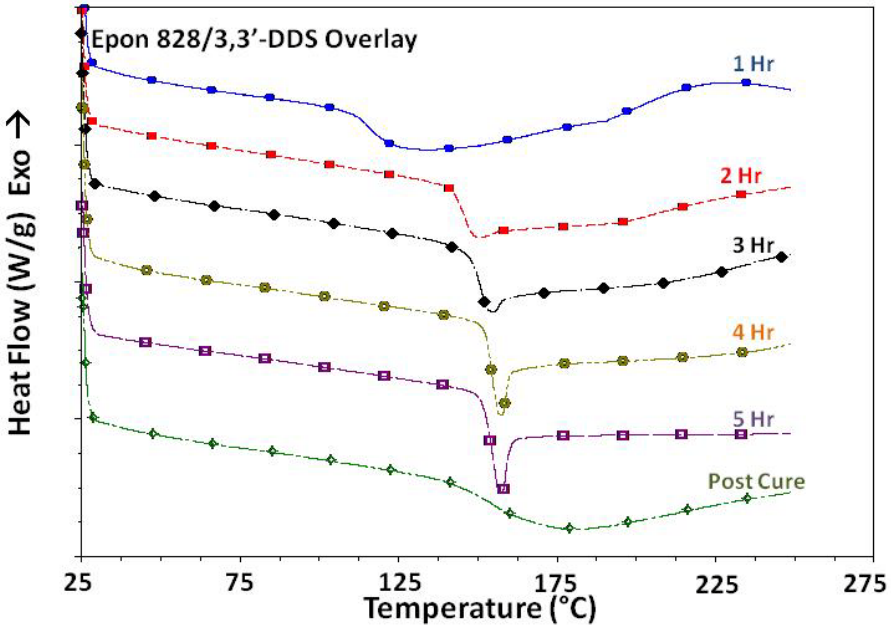

Figure 84. DSC thermograms taken from the first heating scan at various stages of cure for stoichiometric ratio of Epon 828 with 3,3'-DDS.

DSC thermograms taken from the first heating scan for the Epon 1001F system are shown in Figure 85. The T_g at the end of the first hour of cure was much lower at 61.3 °C and only reached 105.6 °C after five hours of cure. This suggests that limited mobility and low concentration of functional groups is the likely cause of a reduction in conversion as opposed to vitrification. The T_g

transition region was not similar to that seen with the Epon 828 series and indicates diffusion limitation as opposed to vitrification. Post-curing yielded a final T_g of 123.2 °C, slightly below the cure temperature.

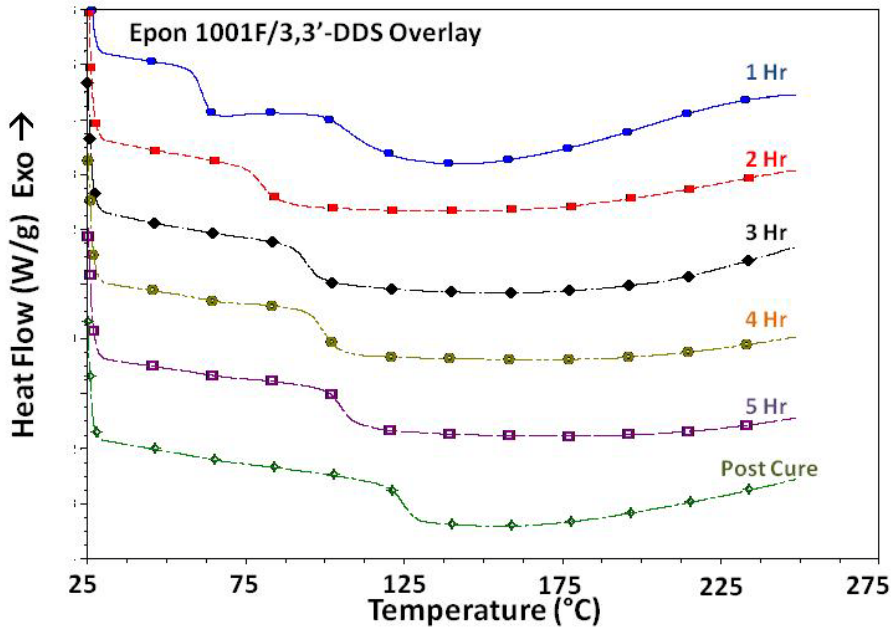

Figure 85. DSC thermograms at various stages of cure for stoichiometric ratio of Epon 1001F with 3,3'-DDS.

Thermograms of MY0510 cured with 3,3'-DDS are shown in Figure 86. The T_g at the end of the first hour of cure was 128.2 °C. These systems rapidly approach vitrification limits and correlate well with the plateau observed in NIR at approximately two hours. The significant exotherm observed in this system is due to the autocatalytic nature of the tertiary amine, triglycidylaminophenol. Upon post-cure, the exotherm is no longer present and a final T_g of 223.3 °C is achieved.

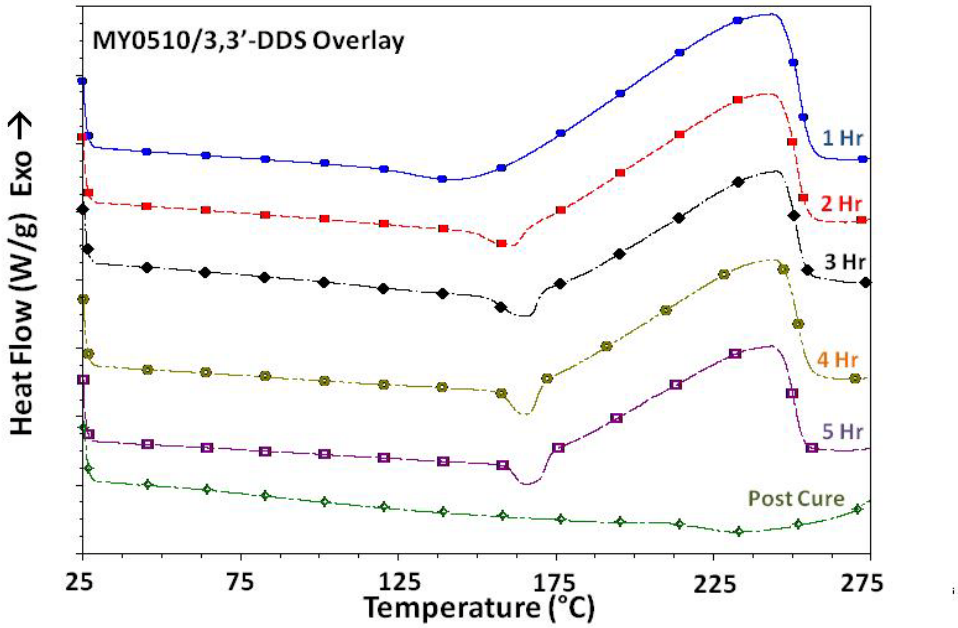

Figure 86. DSC thermograms at various stages of cure for stoichiometric ratios of MY0510 with 3,3'-DDS.

Thermograms of MY0610 cured with 3,3'-DDS are shown in Figure 87. Changing from *para*- to *meta*- substitution results in a much lower initial T_g at the end of the first hour of cure (89.3 °C). After three hours, the system is above the vitrification point and correlates to the reduction in conversion rates observed in the NIR. Similar to MY0510, the significant exotherm observed in this system is related directly to the autocatalytic nature of the tertiary amine, triglycidylaminophenol. Post curing at 200 °C advances conversion and T_g reaches 214.3 °C.

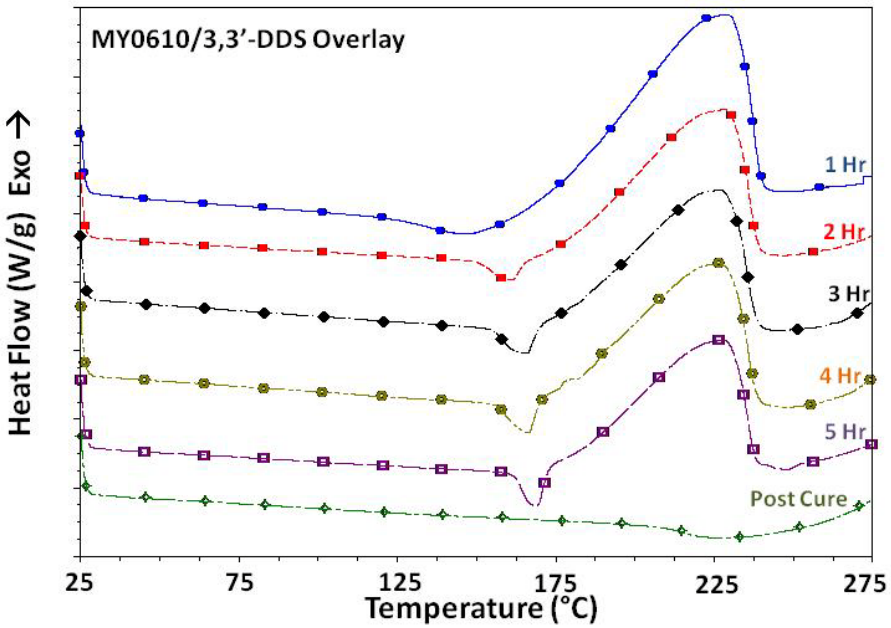

Figure 87. DSC thermograms at various stages of cure for stoichiometric ratio of Araldite MY0610 with 3,3'-DDS.

DSC thermograms of the tetrafunctional MY721 are shown in Figure 88. After only an hour of cure, the T_g reached 139.9 °C and initiated the onset of vitrification. The system also exhibited an exotherm related to the two tertiary amines present in tetraglycidyldiaminodiphenylmethane. An exotherm present in the post-cured sample is indicative of incomplete cure prior to characterization.

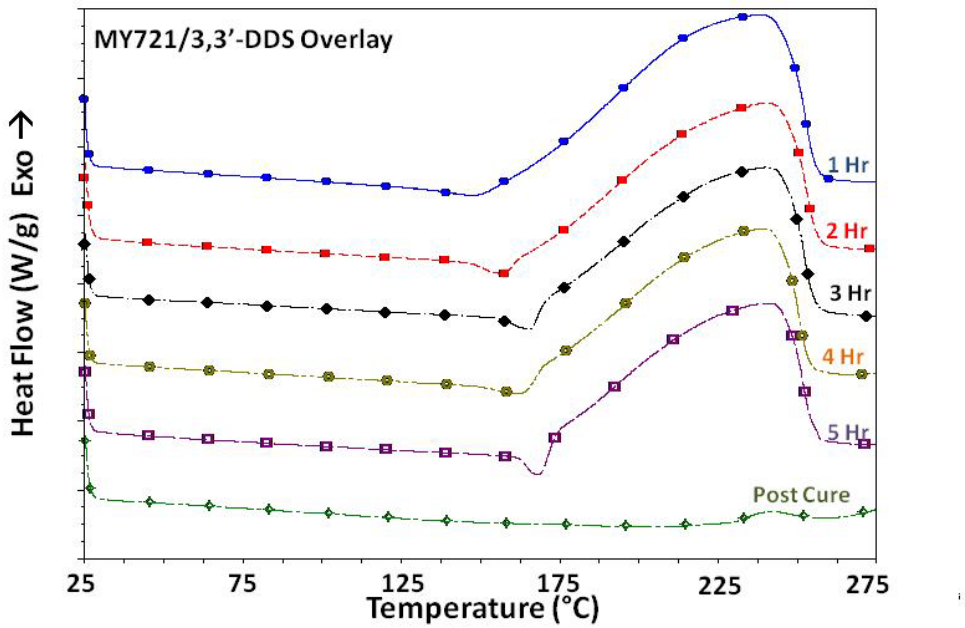

Figure 88. DSC thermograms at various stages of cure for stoichiometric ratio of MY721 with 3,3'-DDS.

Dynamic Mechanical Analysis

DMA was used to investigate modulus and T_g development during cure. Figure 89 shows the storage modulus and tan δ values for the Epon 828 system. Epon 828 samples were not viable for tension analysis until the second hour of cure at 125 °C. An increase in the softening temperature corresponds to the T_g and increased rubbery modulus, and can be directly correlated to increased crosslink density. A significant increase in both the onset of softening and rubbery modulus was observed between the second and third hour of cure as more secondary amine is incorporated into the network. The positive change in slope of the rubbery modulus region in under-cured samples was also indicative of further reaction during the analysis. The tan δ curve indicated a T_g of 128.0 °C after two hours that increased to 179.5 °C after post-curing. A reduction in the

peak height of the tan δ curve also correlates to increased crosslink density.

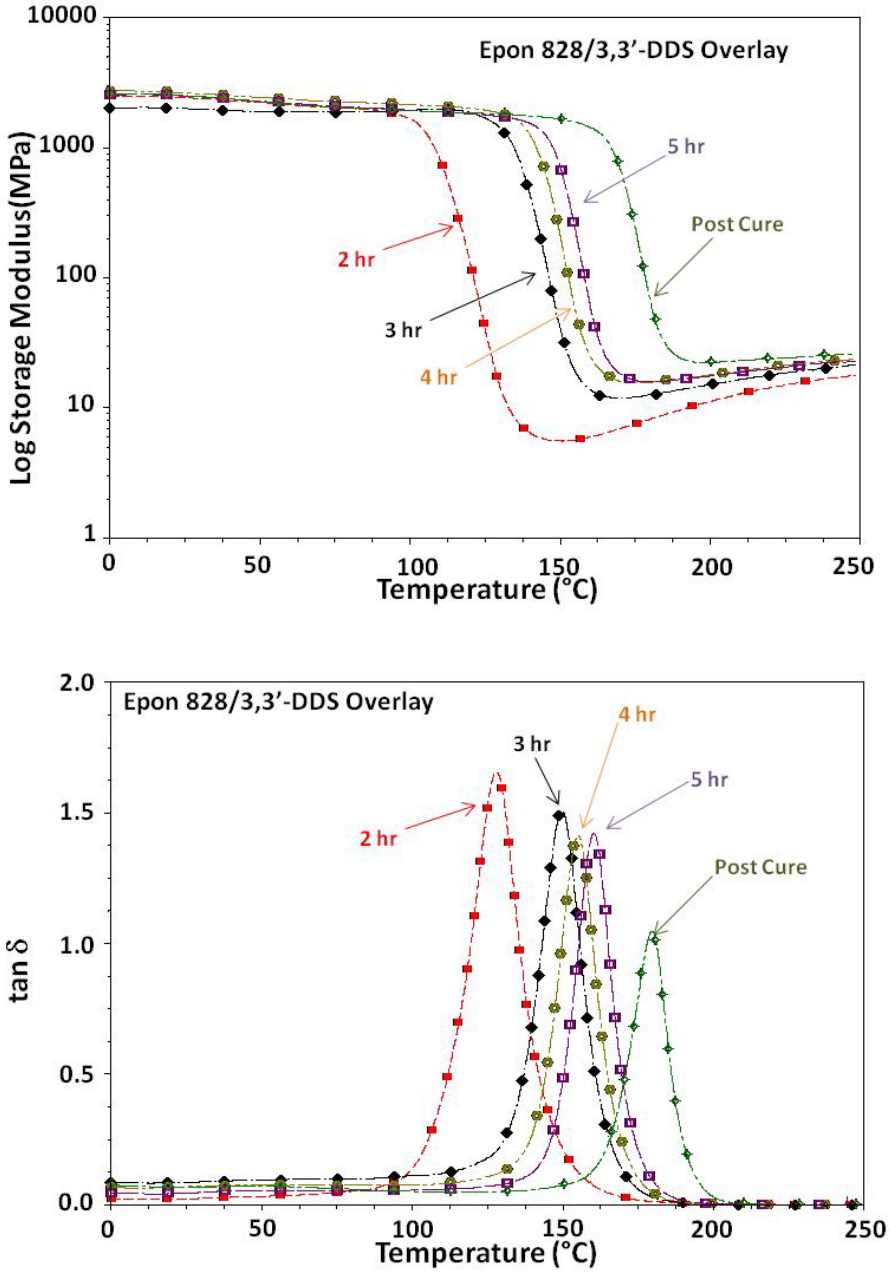

Figure 89. DMA storage modulus and tan δ of various stages of cure for stoichiometric ratio of Epon 828 with 3,3'-DDS.

Figure 90 shows DMA results for the Epon 1001F system. Epon 1001F samples were not viable for tension analysis until after three hours of cure. As with the Epon 828 system, an increase in the onset of softening and the rubbery modulus correlated directly to an increase in conversion and crosslinking. A T_g of 108.9 °C was noted after three hours of cure which increased to 141.8 °C upon post-curing.

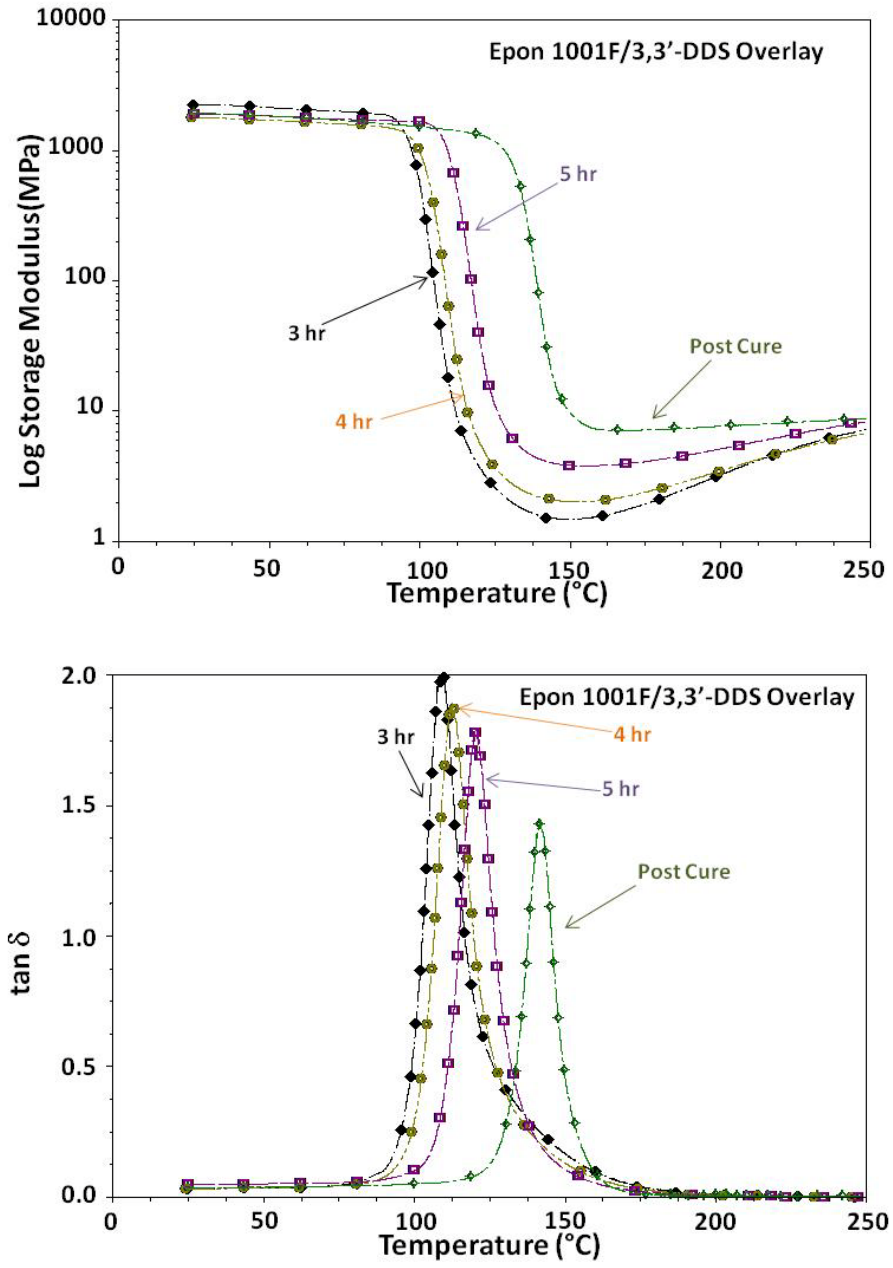

Figure 90. Storage modulus and tan δ curves of various stages of cure for stoichiometric ratio of Epon 1001F with 3,3'-DDS.

DMA results of the MY0510 system are shown in Figure 91. After one hour of cure, the T_g as determined from the tan δ maxima was 178.0 °C, however, the onset of softening occurs at 98.6 °C. As the network forms, the onset temperature of the primary transition increases with cure time, ultimately

reaching an upper vitrification limit at 164.5 °C. The Epon 828 system does not exhibit a low temperature transition because the low epoxide reactivity results in network formation via formation of linear segments prior to building crosslink density and develops its highest T_g at later stages of cure. Consequently, vitrification occurs after three hours of cure at 125 °C. In the case of multifunctional epoxides, network formation and subsequent vitrification occurs rapidly at lower conversion due to the high system functionality and reactivity. The post-cured MY0510 system reaches a final T_g of 239.7 °C.

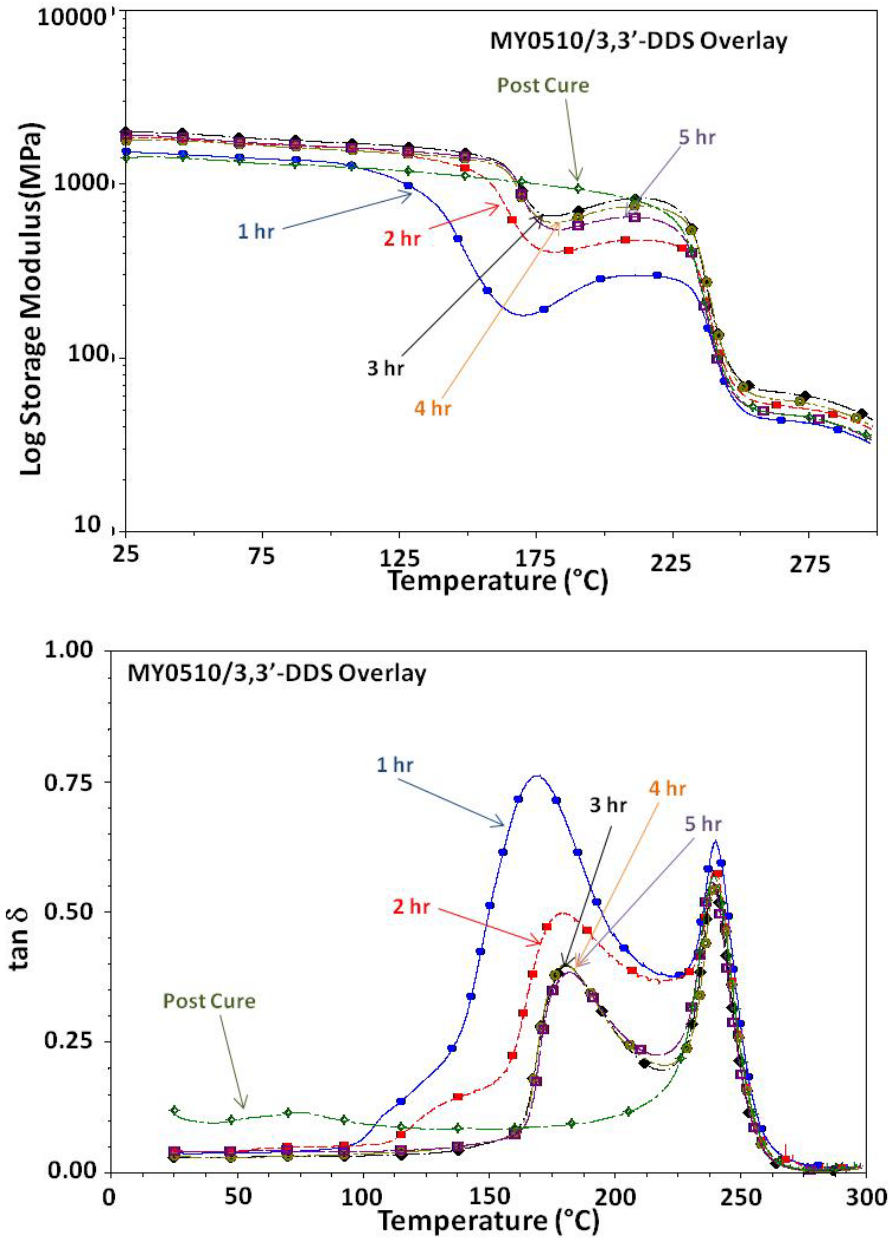

Figure 91. DMA storage modulus and tan δ of various stages of cure for stoichiometric ratio of MY0510 with 3,3'-DDS.

Free films of the MY0610 system were also viable at one hour of cure (Figure 92). The initial system exhibited a softening onset at 106.2 °C with a one hour primary tan δ maxima of 172.5 °C. During the 2nd to 5th hours of cure at 125 °C, the neat resin exhibited rapid increases in conversion as the onset of

softening increased dramatically to 170.6 °C. Further conversion was still observed during the analysis until post-cure. Post-cure at 200°C yielded a final T_g of 236.37 °C. However, a distinct transition was noted between 50-80°C that has been attributed to specific crosslinkers, unreacted monomer/oligomer, heterogeneities, and/or moisture.

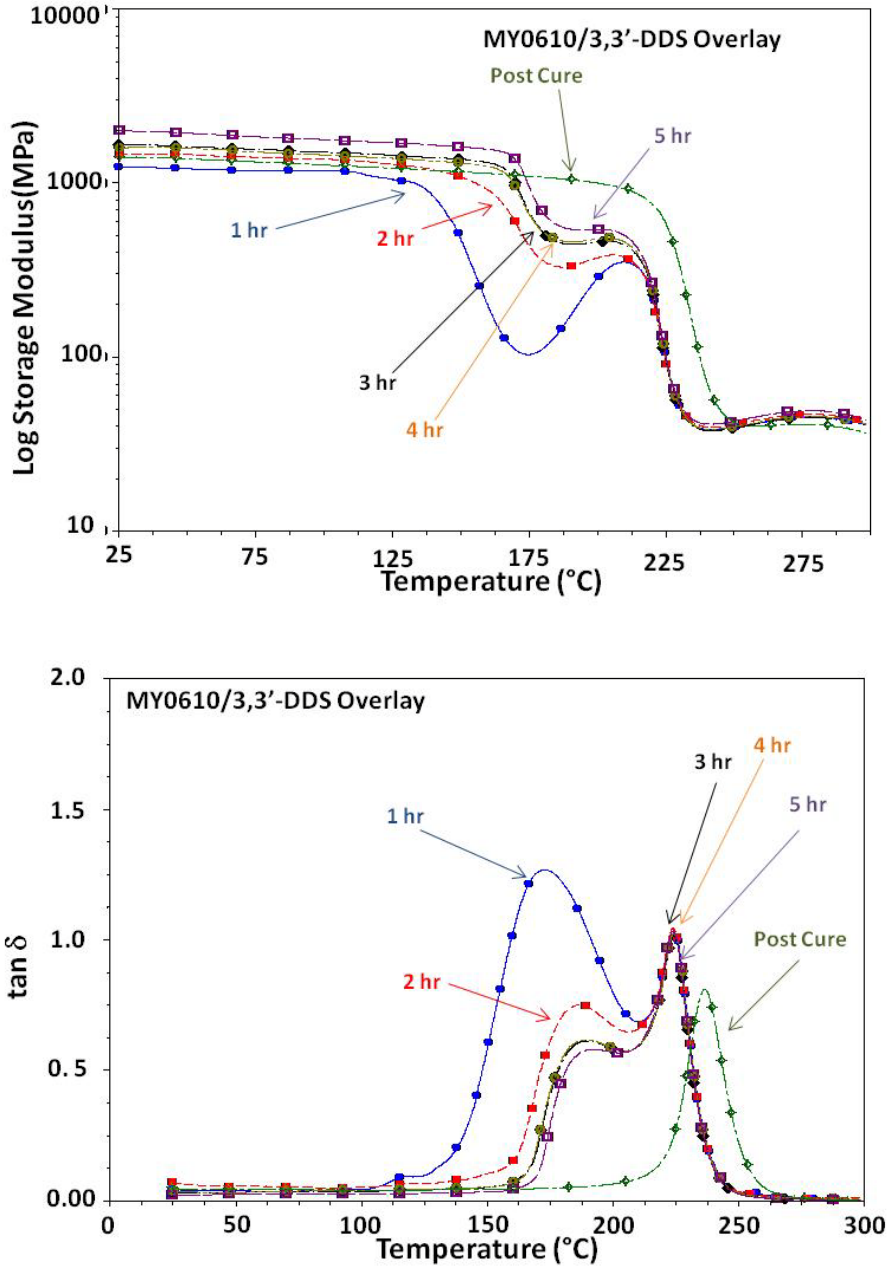

Figure 92. DMA storage modulus and tan δ of various stages of cure for stoichiometric ratio of Araldite MY0610 with 3,3'-DDS.

DMA results for the MY721 system are shown in Figure 93. After one hour, the onset of softening occurs at 130.2 °C in this system, higher than that noted with both MY0510 and MY0610. This is attributed to the increased

functionality and lower conversion requirements for gelation. The MY721 network displays an initial T_g of 164.0 °C and conversion proceeds until an upper vitrification point is reached at 166.1 °C after three hours at 125 °C. Upon post-cure, the final T_g is driven to 252.6 °C and is indicative of a homogeneous network architecture.

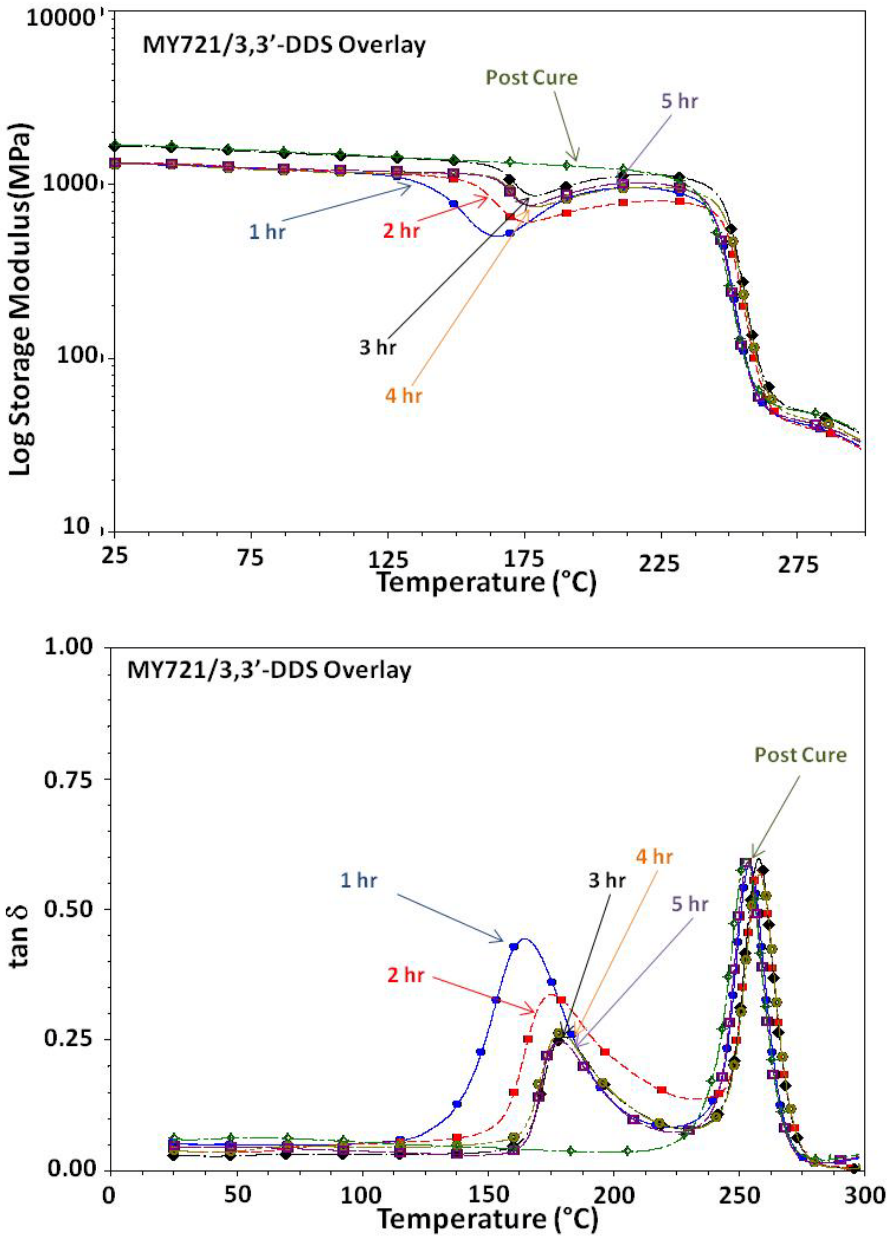

Figure 93. Dynamic mechanical analysis of various stages of cure for stoichiometric ratio of MY721 with 3,3'-DDS.

Figure 94 compares the storage modulus and tan δ plots of the post-cured Epon 828, MY0510, and MY721 systems. The Epon 1001F system has the lowest T_g and rubbery modulus due to its high equivalent weight and low functionality. Epon 828, MY0610, MY0510 and MY721 networks exhibited

progressively higher T_g and rubbery moduli because of their increased functionality and lower equivalent weight. The onset of degradation is observed as a reduction in rubbery modulus above 275 °C.

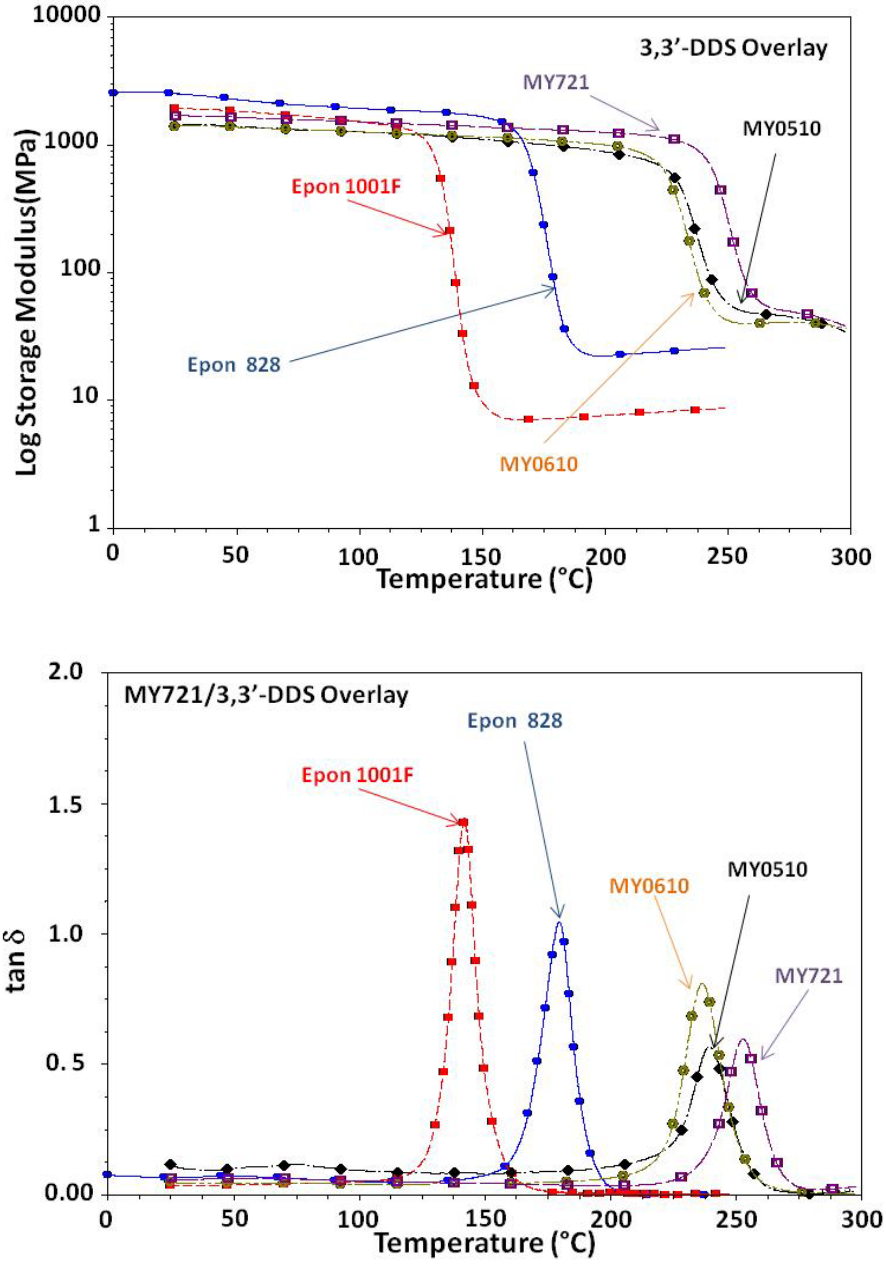

Figure 94. Storage modulus and tan δ plots of stoichiometric ratio of various epoxies with 3,3'-DDS.

Mechanical Testing

Compression testing results are shown in Figure 95. MY0510 and MY0610 systems exhibited the highest modulus value (Table 20). Epon 828 and 1001F systems exhibited reduced moduli compared to the other systems as a result of lower average functionality. Epon 828 system achieved the highest strain at yield of 10.21%. The multifunctional samples did not yield sufficiently to determine an exact yield point.

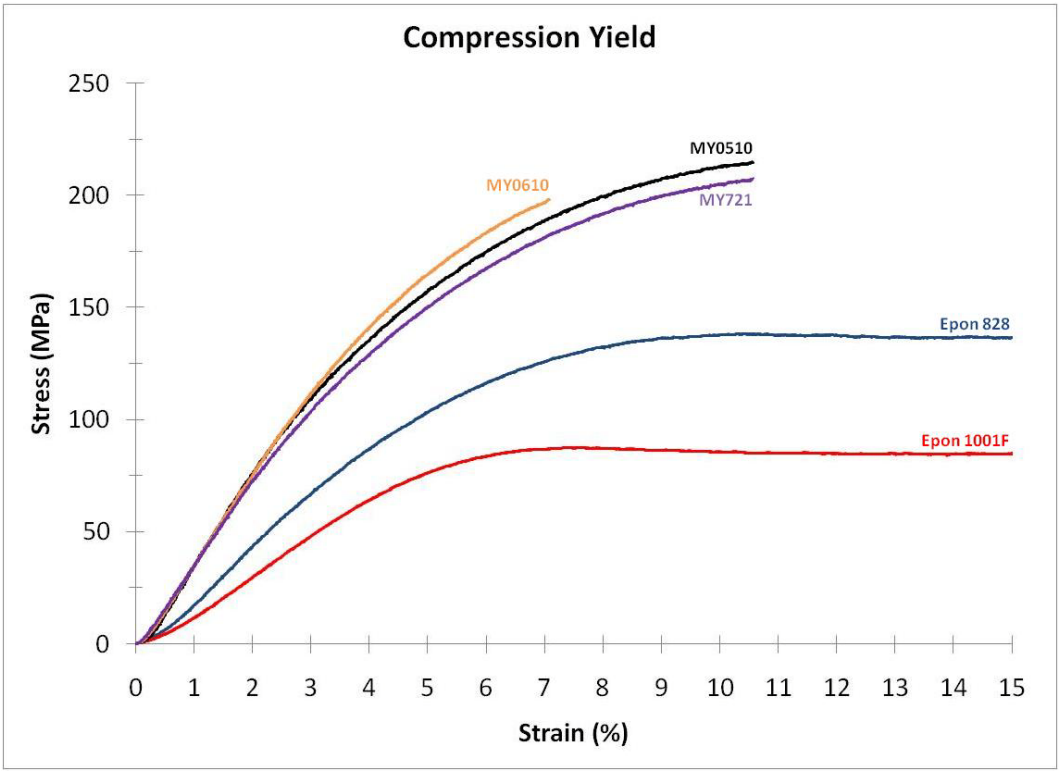

Figure 95. Compressive yield data of post-cured epoxy systems.

MY0510 and MY0610 systems exhibited the highest modulus values, which is attributed to the increased crosslink density resulting from the lower equivalent weights of the starting materials. MY0610 system displays the highest offset yield stress at 115.4 MPa, which is expected from the increased conformational entropy resulting from *meta*-substituted epoxy and amine

components. The multifunctional epoxy systems exhibited brittle behavior and did not display distinct yield points.

Table 20

Compression Testing Data for Various Epoxies Cured with 3,3'-DDS

Epoxy	Young's Modulus (GPa)	Offset Yield Stress (MPa)	Yield Strain (%)
Epon 828	2.52 ± 0.18	77.2 ± 4.9	10.21 ± 0.5
Epon 1001F	2.02 ± 0.14	65.4 ± 0.5	7.48 ± 0.2
MY0510	4.26 ± 0.08	100.4 ± 1.2	--- ± ---
MY0610	4.15 ± 0.13	115.4 ± 2.9	--- ± ---
MY721	3.86 ± 0.02	100.1 ± 0.5	--- ± ---

Note. MY0510, MY0610, and MY721 did not display a distinct yield strain

Comparison with 4,4'-DDS Cured Epoxies

Significant differences were noted between the systems cured with 3,3'-DDS and 4,4'-DDS resulting from the molecular architecture of the monomers. The density of each material is shown in Table 21. In general, the 3,3'-DDS cured systems exhibit higher densities except for Epon 1001F, possibly due to differences in conversion. Due to incomplete conversion in curing Epon 1001F with both 3,3'-DDS and 4,4'-DDS, the respective samples were removed from this comparison. The increase in density of 3,3'-DDS systems over 4,4'-DDS systems results from the increased conformational entropy as it leads to improved packing and lower free volume for 3,3'-DDS cured epoxies. A direct comparison can be made between 3,3'-DDS/MY0610 and 4,4'-DDS/MY0510 systems, as the former is completely *meta*-substituted while the latter is completely *para*-substituted, provided differences in molecular level architecture

while remaining chemically identical. Following the expected trend, 3,3'-DDS/MY0610 has a higher density of 1.331 g/mL relative to 4,4'-DDS/MY0510 (1.318 g/mL).

Table 21

Density of Various Epoxy Resins Cured with DDS

Epoxy	Density (g/mL)	
	3,3'-DDS	4,4'-DDS
Epon 828	1.250	1.233
MY0510	1.325	1.318
MY0610	1.331	1.327
MY721	1.284	1.279

Compressive moduli values for epoxies cured with *meta*- and *para*-substituted DDS are shown in Table 22. Increased packing efficiency and reduced free volume in 3,3'-DDS cured epoxies result in improved modulus as compared to 4,4'-DDS systems. This is a result of increased potential intermolecular interactions and subsequently increased network cohesive energy density. Again, comparing the most architecturally different systems, the 3,3'-DDS/MY0610 system exhibits ~ 20% higher modulus than the chemically similar but structurally different 4,4'-DDS/MY0510 system.

Table 22

Modulus of Various Epoxy Resins Cured with DDS

Epoxy	Modulus (GPa)	
	3,3'-DDS	4,4'-DDS
Epon 828	2.52 ± 0.18	2.84 ± 0.05
MY0510	4.26 ± 0.08	3.42 ± 0.04
MY0610	4.15 ± 0.13	3.44 ± 0.38
MY721	3.86 ± 0.02	3.38 ± 0.03

The trend is also observed in values of offset yield stress (Table 23). Offset yield stress increases in 3,3'-DDS systems due to increased conformational entropy and cohesive energy density. In comparing the 3,3'-DDS/MY0610 and 4,4'-DDS/MY0510 systems, the former exhibits a 62% increase in offset yield stress.

Table 23

Offset Yield Stress of Various Epoxy Resins Cured with DDS

Epoxy	Offset Yield Stress (MPa)	
	3,3'-DDS	4,4'-DDS
Epon 828	77.2± 4.9	68.9 ± 0.93
MY0510	100.4± 1.2	71.4 ± 1.83
MY0610	115.4 ± 2.9	96.9 ± 6.83
MY721	100.1 ± 0.5	81.3 ± 1.04

Increased segmental mobility results in reduced T_g values for 3,3'-DDS cured epoxies compared to those cured with 4,4'-DDS (Table 24). Increased kinks in the backbone architecture of 3,3'-DDS/MY0610 results in a 43.6 °C reduction in T_g relative to 4,4'-DDS/MY0510.

Table 24

T_g of Various Epoxy Resins Cured with DDS

Epoxy	DMA T_g (°C)	
	3,3'-DDS	4,4'-DDS
Epon 828	179.7	222.6
MY0510	239.7	280.3
MY0610	236.7	272.2
MY721	252.6	284.8

Summary and Conclusions

Diglycidyl ether bisphenol-A-based resins (Epon 828 and Epon 1001F), *p*-aminophenol (Araldite MY0510), *m*- aminophenol (Araldite MY0610) and tetraglycidyldiaminodiphenylmethane (Araldite MY721) were cured with stoichiometric proportions of 3,3'-diaminodiphenylsulfone and 4,4'-diaminodiphenylsulfone for specific times at 125 °C followed by a post-cure at 200 °C.

The use of NIR to evaluate functional group conversion indicated that Epon 828 and Epon 1001F initially proceeded through a linear approach to network development before the secondary amines reacted to form a three-dimensional network. Multifunctional epoxies MY0510, MY0610 and MY721

immediately developed highly branched network architecture due to the increased functionality and autocatalytic behavior. Conversion in all systems was controlled initially by functional group concentration and ultimately by the onset of vitrification as T_g surpassed the cure temperature. Multifunctional species achieved a plateau in epoxy conversion after only two hours at 125 °C. The difunctional species continue to react longer at 125 °C, although reduction in functional group concentration plays a larger role. This effect was more pronounced with the higher molecular weight precursor, Epon 1001F, which has an equivalent weight approximately three times that of Epon 828 and five times that of the multifunctional species, resulting in a significantly higher initial viscosity. Ultimately, Epon 1001F is unable to reach full conversion under these conditions due to viscosity, functional group concentration and mobility restrictions. Primary amines were completely converted in all cases due to their high reactivity. Secondary amines only reached full conversion for the Epon 828 system. Epon 1001F was limited as previously mentioned, while the autocatalytic nature of the multifunctional species resulted in up to 25% of secondary amines unreacted, likely a consequence of etherification.

DSC thermograms suggested that the multifunctional epoxies reacted faster than the Epon 828 and Epon 1001F systems due to catalytic effect of the tertiary amine component of the multifunctional epoxies. The increased reaction rates were reflected in the significant cure exotherms that occurred during the scans. Reactions proceeded to reach vitrification limits corresponding to the same duration of cure as the onset of the plateau in NIR analysis, and only

achieved maximum conversion after post-cure. The MY721 sample exhibited an exotherm after post-cure, suggesting incomplete conversion under these conditions. As expected, the increased average functionality resulted in elevated T_gs.

The onset of vitrification was observed by DMA through changes in the onset of softening and changes in rubbery modulus. For difunctional epoxies, reaction proceeded slowly and an increase in the rubbery plateau was observed as functional group concentration limited conversion. Free films were not viable at early stages of cure for the linear epoxies due to insufficient molecular weight development, limited entanglement and minimal crosslinking at low levels of conversion. Multifunctional epoxy films were viable at early stages of conversion due to increased molecular weight and connectivity that developed immediately as a result of increased functionality and reactivity. The autocatalytic nature of the materials was evident by an increase in modulus after the initial softening as well as by the appearance of several maxima in the tan δ. Vitrification limits were very well defined in these systems, each near 160 °C. The T_gs varied based on the molecular weight, functionality and molecular architecture.

Compression testing revealed that Epon 1001F systems exhibited a preference to yield at lower stress and strain. Modulus values trended according to crosslink density. Offset yield values were highest for the MY0610 samples due to increased conformational entropy and cohesive energy density.

Comparison of 3,3'-DDS and 4,4'-DDS systems revealed several trends related to network architecture. Increased density, modulus, and offset yield

strength was reported for 3,3'-DDS systems versus 4,4'-DDS systems, while the latter had higher T_gs. Comparing the 3,3'-DDS/MY0610 and 4,4'-DDS/MY0510 systems highlighted the difference in molecular level architecture while maintaining the same chemical composition. The 3,3'-DDS/MY0610 samples exhibited a small increase in density, a 20% increase in modulus and a 62% increase in offset yield stress while the 4,4'-DDS/MY0510 sample exhibited a 43.6 °C higher T_g.

References

1. Sperling, L. H. *Introduction to Physical Polymer Science, 4th Ed*. John Wiley & Sons, Inc.: New Jersey, 2006.
2. May, C.A. *Epoxy Resins Chemistry and Technology, 2nd Ed*. Marcel Dekker, Inc.: New York, 1988.
3. Dusek, K., Plestil, J., Lednicky, F. & Lunak, S. *Polymer,* **1978**, 19, 393.
4. Ikkai, F. & Shibayama, M. *Journal of Polymer Science Part B Polymer Physics,* **2005**, 43, 617.
5. Prolongo, S.G., Mikes, F., Cabanelas, J.C., Paz-Abuin, S. & Baselga, J. *Journal of Materials Processing Technology,* **2003**, 143, 546.
6. Varley, R.J., Heath, G.R., Hawthorne, D.G. & J.H. Hodgkin *Polymer,* **1995**, 36, 1347.
7. Musto, P., G., Abbate,, Ragosta M. & Scarinzi, G. *Polymer,* **2007**, 48, 703.
8. Liu, H., Uhlherr, A., Varley, R.J., & Bannister, M.K. *Journal of Polymer Science Part A Polymer Chemistry,* **2004**, 47, 3143.
9. Xu, L. & Schlup, J.R. *Journal of Applied Polymer Science,* **1998**, 67, 895.
10. Lee, J. K., Gillham, J. K. *Journal of Applied Polymer Science,* **2003**, 90, 2665.
11. Douglas, E. P. *Journal of Macromolecular Science Part C Polymer Reviews,* **2006**, 46, 127.

12. Calzia, K. J., Lesser, A. J. *Journal of Materials Science,* **2007**, 42, 5229.

13. Vakil, U. M. & Martin, G. C. *Journal of Applied Polymer Science,* **1992**, 46, 2089.

14. Sherman, C. L., Zeigler, R. C., Verghese, N. E. & Marks, M. J. *Polymer*, **2008**, 49, 1164.

15. Marks, M. J. & Snelgrove, R.V. *ACS Applied Materials & Interfaces,* **2009**, 1, 921.

16. Jordan, C., Galy, J., & Pascault, J-P. *Journal of Applied Polymer Science,* **1992**, 46, 859.

17. Guerrero, P., De la Caba, K., Valea, A., Corcuera, M.A. & Mondragon, I. *Polymer,* **1996**, 37, 2195.

18. Roland, C.M., Ngai, K.L. & Plazek, D.J. *Computational and Theoretical Polymer Science*, **1997**, 7, 133.

19. Han, S., Kim, W.G., Yoon, H.G. & Moon, T.J. *Journal of Polymer Science Part A Polymer Chemistry,* **1998**, 36, 773.

20. Yang, G., Fu, S. & Yang, J. *Polymer*, **2007**, 48, 302.

21. Marks, M.J., Verghese, N.E., O'Connell, C. & Mansour, A.S. *Journal of Polymer Science Part B Polymer Physics,* **2009**, 47, 72.

CHAPTER IX

CONCLUSIONS AND RECOMMENDATIONS

Conclusions

Composites rely heavily on the properties of the constituent polymer matrix for performance. Proper development of molecular architecture in polymers is critical for achieving reproducible high strength and toughness. Molecular architecture parameters such as crosslink density, molecular weight between crosslinks, node size/connectivity, and conversion play a key role in composite matrices. The objective of this research is to establish relationships between cure conditions, conversion, connectivity, network architecture and properties in glassy thermosetting matrix resins. Specifically, epoxy and vinyl ester resins were characterized to identify controlling factors in the development of network architecture and understand how they affect the mechanical properties.

The major conclusions of this work are summarized as follows:

1. The reactivity of vinyl ester methacrylates and styrene are heavily dependent upon cure temperature. Methacrylate conversion occurs faster at low temperature, with rapid conversion to ~ 55% before a plateau is reached signifying vitrification as supported by characterization data. Meanwhile, styrene is slowly converted into the greater gel network. Conversion increases upon post-cure at 125 °C, resulting in 99% styrene conversion but only 91% methacrylate conversion. Elevated levels of conversion require increased

temperature, however, this is not always sufficient to ensure complete conversion of the methacrylate species due to topological constraints.

2. Low temperature cure (< 50 °C) of VERs resulted in vitrification points ~ 15 °C above cure temperature using metal catalyzed redox initiation. Network heterogeneity increased at low cure temperatures as supported by the higher M_c values (higher in comparison and versus theoretical). Further thermal treatment of these systems increases degree of conversion, although connectivity (i.e., M_c) may not necessarily be drastically different depending on the topological constraints of the network architecture.
3. Catalyst activity was reduced via *in situ* ligand exchange with cobalt (II) naphthenate. DMA characterization identified a significant reduction in vitrification temperature at higher 2,4-pentanedione loading. Reduced network connectivity was measured by a 30% reduction in rubbery modulus that correlated to a direct increase in M_c.
4. Network architecture is sensitive to the mobility, concentration and rate of radicals within a matrix. These parameters can be altered through changes in temperature or initiating system. Control of the network architecture and ultimately mechanical properties can be achieved by tailoring radical generation and mobility appropriately. Rapid radical production with inadequate mobility increases heterogeneity and reduces mechanical viability through poor connectivity. Radicals must be produced at rates comparable to their mobility to ensure high

conversion and maximize mechanical properties.

5. Molecular weight analysis of the three commercial resins identified subtle changes due to bromination between Derakane 411-350 and Derakane 510A-40, while Derakane 8084 contained nearly 10 wt% of high molecular weight species of ~ 16,000 g/mol. The brominated DGEBA backbone in Derakane 510A-40 resulted in higher density, M_c and fracture toughness over the non-brominated Derakane 411-350 at equivalent styrene content. No significant changes were observed in other properties including modulus and $T_{g.}$ Derakane 8084 exhibited characteristics of a multimodal network architecture attributed to the monomeric components of the resin.
6. POSS species altered initial network development, specifically increasing initial conversion of dimethacrylate and styrene species prior to the vitrification limit. Incorporation of non-reactive POSS in VER systems reduced rubbery modulus by ~ 50% at 5 wt% loading while the inclusion of similar levels of reactive POSS increased rubbery modulus by ~ 50%. Rubbery modulus increased almost by a factor of four and nine when RPOSS was incorporated at 15 wt% and 25 wt%, respectively.
7. Incorporation of reactive POSS species into VER systems did not impact its density or Young's modulus values. For example, density values were 1.332 g/mL for the neat resin and 1.319 g/mL for 25 wt% RPOSS. Young's modulus values were 2.5 MPa and 2.4 MPa for the

neat resin and the resin with 25 wt% RPOSS, respectively.

8. Addition of POSS nanoparticles did not have a beneficial impact on fracture toughness. Fracture toughness of the neat resin (K_{IC}, 1.11 MPa*√m) was unaffected by the addition of 5 wt% NPOSS (1.07 MPa*√m). Addition of 5 wt% RPOSS reduced the fracture toughness to 0.63 MPa*√m while samples containing 15 and 25 wt% RPOSS were too brittle to evaluate. These findings correlated with elimination of the β transition and reduction in tan δ maxima upon addition of POSS.
9. In absence of a catalyst, epoxy-amine reactions proceed within detection limits exclusively through reaction between the epoxy group and primary amines resulting in preferential formation of linear polymer chains in difunctional epoxy systems. Increasing the molecular weight of the diepoxide resulted in reduced epoxy conversion due to mobility and concentration limitations of available functional groups. Vitrification during cure at 125 °C was observed in all polyepoxide systems except Epon 1001F.
10. Comparing the 3,3'-DDS/MY0610 and 4,4'-DDS/MY0510 systems highlighted the difference in molecular level architecture while maintaining the same chemical composition. The 3,3'-DDS/MY0610 samples exhibited a small increase in density, a 20% increase in modulus, and a 62% increase in offset yield stress while the 4,4'-DDS/MY0510 sample exhibited a 43.6°C increase in T_g.

Suggestions for Future Work

While this work primarily focused on neat resin systems, the next step is to correlate these findings to network development and macroscopic properties in the presence of glass and carbon fiber. Ideally, the matrix and fiber would interact synergistically to maximize mechanical performance of composite materials. However, the impact of fibers on radical cure mechanisms is uncertain. Fiber reinforcement may significantly alter initiation resulting in changes to network architecture and connectivity. Impact of the fiber type, sizing and level of defects/contamination requires careful consideration to quantify structure-property relationships between the matrix and fiber reinforcement.

In addition to understanding neat matrix-fiber reinforcement relationships, the investigation of comonomer/copolymer additives to enhance properties between the matrix-filler interphases and interfaces is of significant interest. Understanding critical structure-property relationships at the matrix-filler interphases and interfaces could help gain substantial increases in mechanical properties such as modulus and toughness.

Thiol derivatives of DDS are of interest in imparting improved flexibility and thermo-oxidative stability over amine or ether linkages while simultaneously broadening the available chemical library. Synthesis of the *meta*-substituted bisphenol A type-thiol derivatives is possible in high yield. These materials could then be epoxidized to provide additional unique materials with possibilities for reduced viscosity and improved thermal performance.

Tetraglycidyldiaminodiphenylmethane (TGDDM) is the current standard for high

functionality epoxy resins. Epoxidized derivatives of 3,3'- and 4,4'-DDS would provide alternatives to TGDDM with potential for increased performance. The *para*-substituted tetraglycidyl DDS would provide an epoxy resin with increased thermal stability while the *meta*-substituted alternative would offer potential for reduced viscosity, improved solubility and increased thermo-oxidative stability while maintaining high functionality. Finally, while small changes to network architecture may not manifest significant changes in static testing, it is likely they would play a major role in determining long term viability of composite materials under use conditions. Because of this, fatigue testing and yield modeling is of significant interest. Innovative approaches to reduce time requirements for cyclic measurements must be evaluated. Thorough understanding of the initial network architecture on long term mechanical viability would reduce the current variability in composite materials, ultimately increasing their function, value, longevity and overall performance.